Single-cell lineage tracing identifies hemogenic endothelial cells in the adult mouse bone marrow

Jing-Xin Feng,[1] Mei-Ting Yang,[2, 3] Lili Li,[1] Caiyi C. Li[4], Ferenc Livák[4], Jack Chen[5], Yongmei Zhao[5], Dunrui Wang[1], Avinash Bhandoola[4], Naomi Taylor[6], and Giovanna Tosato[1,7,8*]

[1]Laboratory of Cellular Oncology, Center for Cancer Research, National Cancer Institute (NCI), National Institutes of Health, Bethesda, MD, 20892, USA

[2]School of Life Sciences, Northeast Normal University, Changchun, China

[3]Experimental Immunology Branch, Center for Cancer Research (CCR), National Cancer Institute (NCI), National Institutes of Health, Bethesda, MD, 20892, USA

[4]Laboratory of Genome Integrity, Center for Cancer Research, National Cancer Institute (NCI), National Institutes of Health, Bethesda, MD, 20892, USA

[5]Sequencing Facility Bioinformatics Group, Bioinformatics and Computational Science Directorate, Frederick National Laboratory for Cancer Research, Frederick, MD, 21702, USA

[6]Pediatric Oncology Branch, Center for Cancer Research (CCR), National Cancer Institute (NCI), National Institutes of Health, Bethesda, MD, 20892, USA.

[7]Senior author

[8]Lead contact

*Correspondence: tosatog@mail.nih.gov (G.T.) jing-xin.feng@nih.gov (J.F.)

SUMMARY

During mouse development, hematopoietic stem and progenitor cells (HSPC) originate from hemogenic endothelial cells (ECs) through a process of endothelial-to-hematopoietic transition. These HSPC are thought to fully sustain adult hematopoiesis. However, it remains unknown whether adult ECs retain hemogenic potential. Here we used in vivo genetic lineage tracking at population and single-cell (sc) levels, scRNA sequencing, and bone marrow transplantation to detect hemogenic ECs in adult mice. We identify and characterize bone marrow-resident, adult *Cdh5*/VE-Cadherin^{+} ECs that produce hematopoietic cell-progeny in vitro and in mice. These adult hemogenic ECs and their hematopoietic cell progeny give rise to hematopoietic cells following adoptive transfer into adult mice. Furthermore, blood cells generated from adult and developmental ECs comparably home to peripheral tissues, where they similarly contribute to inflammatory responses. Thus, our results identify previously unrecognized bone marrow-derived adult hemogenic ECs that generate HSPC and functional mature blood cells.

KEYWORDS

Hematopoietic stem and progenitor cells, endothelial cells, hematopoiesis, endothelial to hemogenic transition, mesenchymal cells, blood, *Runx1*, *Col1a2*, single cell lineage tracing, single cell RNA sequencing

39 **INTRODUCTION**

40 During development, hemogenic ECs generate hematopoietic cells through a process of
41 endothelial-to-hematopoietic transition (EHT) at geographically defined anatomical sites[1-9]. At
42 these locations, the hemogenic ECs represent a small fraction of all ECs[10-12], and their
43 competency to produce hematopoietic stem and progenitor cells (HSPC) is temporally restricted
44 to short developmental windows, and the hemogenic potential differs[13-18]. In the dorsal aorta, the
45 hemogenic endothelium produces hematopoietic stem cells (HSC) and other multi-potent
46 progenitors between E10.5 and E11.5[17-19] that persist in the adult and are generally believed to
47 sustain adult hematopoiesis throughout life.

48 Efforts to reliably generate *ex vivo* HSC from Cdh5-expressing ECs identified difficulties
49 in reproducing the microenvironmental clues coming from the inductive niche cells[20-22] and have
50 generally relied on transcription factor-induced reprogramming of the ECs to drive
51 hematopoietic specification[23,24]. The transcription factor RUNX1, which marks the hemogenic
52 endothelium, can confer a hemogenic potential to embryonic ECs lacking such potential[25-28].
53 When transcription factors RUNX1, FOSB, GFI1, and SPI1 were co-expressed in adult murine
54 ECs co-cultured with "vascular niche ECs", EHT was induced in vitro producing HSC with
55 long-term self-renewal capacity[29]. A similar approach was used with human ECs enabling
56 hematopoietic specification[30].

57 An unresolved question is whether hemogenic ECs, thought to be mostly restricted to the
58 early stages of mouse development[12,23], may persist in the adult mouse[2,12,31,32]. Exploiting
59 advances in cell lineage tracking and single cell analyses[33,34], we report the identification of
60 hemogenic ECs in the adult mouse bone marrow (BM) that produce functional hematopoietic
61 progenitors and mature blood cells.

62 **RESULTS**

63 **Evidence that adult bone marrow ECs generate hematopoietic cells**

64 We assessed the hemogenic potential of ECs in adult mice using Cre-reporter-based lineage
65 tracing. Since *Cdh5*, encoding vascular endothelial cadherin (VE-Cadherin), is selectively
66 expressed by ECs, Cdh5-Cre^{ERT2} recombinase activity can allow tracking the hematopoietic cell
67 output from adult hemogenic ECs[35,36]. Therefore, we generated three Cdh5-based lineage-tracing
68 models using inducible Cdh5-Cre^{ERT2}(PAC)[37,38] and Cdh5-Cre^{ERT2}(BAC)[39] mouse lines, in
69 combination with the Cre-reporter lines ZsGreen and mTmG (Figure S1A). We then treated
70 eight- to twelve-week-old mice with three doses of tamoxifen (10 mg·kg^{-1}, gavage) on
71 consecutive days, and four weeks later we evaluated peripheral blood and BM (Figure 1A).
72 Expectedly[36], most BM Endomucin^{+} ECs were ZsGreen^{+} in tamoxifen-treated Cdh5-
73 Cre^{ERT2}(PAC)/ZsGreen and Cdh5-Cre^{ERT2}(BAC)/ZsGreen mice, and virtually no ZsGreen^{+} ECs
74 were present in Cre negative or peanut oil-treated controls (Figures S1B and S1C). By flow
75 cytometry, >90% CD31^{+}VE-Cadherin^{+} BM ECs were tracked by tamoxifen-induced
76 fluorescence in the three mouse lines (Figure 1B; Figure S1D). A low-level tamoxifen-
77 independent reporter fluorescence was also detected in BM ECs, which was low in the mTmG
78 reporter line (Figure 1B), and higher in the ZsGreen reporter lines, previously attributed to
79 "basal" Cre^{ERT2} activity[40] (Figure S1D).

80 To evaluate the hemogenic potential of adult BM ECs, we analyzed the expression of the
81 hematopoietic marker CD45 in Cdh5-tracked cells. Notably, tracked CD45^{+} hematopoietic cells,
82 presumed progeny of VE-Cadherin^{+} ECs, were detected by flow cytometry in BM and blood of
83 mice from all three Cdh5-Cre^{ERT2} mouse lines (Figure 1C and D; Figures S1E and F;
84 representative flow cytometry gating in Figure S1G and H). Moreover, confocal microscopy

85 identified isolated ZsGreen^{+}CD45^{+} cells in BM (Figure S1I) and blood of tamoxifen-induced
86 mice (Figure 1E). Importantly, while a small fraction of fluorescent CD45^{+} cells were detected in
87 EGFP and ZsGreen (Figures 1C and D; and Figure S1D-F) reporter mice without tamoxifen, as
88 reported[40-43], the significant increase of tamoxifen-induced fluorescent CD45^{+} cells (Figure 1C
89 and 1D, Figure S1D-F) indicates the occurrence of Cdh5-Cre recombination in the adult mouse,
90 presumably tracking EHT. This tamoxifen-induced increase in CD45^{+}ZsGreen^{+} peripheral blood
91 mononuclear cells (PBMC) was also observed in individual mice (Figure S1J).

92 We tested the kinetics of tamoxifen-induced ZsGreen expression in BM ECs and PBMC
93 of Cdh5-Cre^{ERT2}(PAC)/ZsGreen mice (Figure 1F). By flow cytometry, virtually all BM ECs
94 were ZsGreen^{+} by day 4 after tamoxifen administration and this level persisted over 50 days.
95 Instead, the percentage of ZsGreen^{+} PBMCs increased more gradually, plateauing around day 30
96 and this level persisted over ~50 days of observation. This gradual increase is likely attributable
97 to tamoxifen-induced ZsGreen expression in hemogenic ECs.

98 Further analysis showed that most BM EGFP^{+}CD45^{+} cells in Cdh5-Cre^{ERT2}(PAC)/mTmG
99 mice were CD11b^{+}Ly6G^{+} granulocytes (48.85%) and CD11b^{+}Ly6G^{-} monocytes (32.06%), while
100 CD19^{+} B (2.46%) and CD3^{+} T (0.84%) lymphocytes were detected at lower frequencies (Figure
101 1G). All EGFP^{+} BM cell populations were significantly induced by tamoxifen administration,
102 including rare LSK (Lin^{-}Sca1^{+}cKit^{+}) progenitors (Figure 1H). Also, the peripheral blood of
103 tamoxifen-induced Cdh5-Cre^{ERT2}(PAC)/mTmG mice contained EGFP^{+} granulocytes and
104 monocytes, and fewer B and T lymphocytes (Figure S1K and L). Similarly, in ZsGreen-reporter
105 mice, tracked LSK progenitors, B lymphocytes, granulocytes, and monocytes were all present in
106 the BM and blood (Figure S2A-D).

107 We further characterized the tracked BM hematopoietic LSK stem/progenitors by flow
108 cytometry (Figure S2E). The results, displayed by Uniform Manifold Approximation and
109 Projection (UMAP) dimensional reduction, showed that the ZsGreen-tracked progenitor cell
110 population includes phenotypic subsets consistent with hematopoietic stem and progenitor cells
111 (HSPC) (Figure 1I). Each ZsGreen^{+} progenitor population represented a similarly small
112 proportion of the corresponding non-tracked progenitor cell population (Figure 1J). These results
113 support the existence of EHT in the adult mouse contributing to generation of hematopoietic
114 progenitors and mature cells.
115
116 **Adult BM ECs cultured ex vivo generate transplantable HSPCs**
117 To investigate whether adult BM ECs can generate hematopoietic cells *ex vivo*, we cultured BM
118 cells isolated from tamoxifen-treated Cdh5-Cre/ZsGreen mice. Initially, BM single-cell (sc)
119 suspensions were cultured under two conditions (Figure 2A): (1) on "Primaria" pro-adhesive
120 flasks, and (2) on OP9 stromal cell[44] monolayers grown on gelatin-coated conventional tissue
121 culture flasks. To attempt recreating BM niches, fresh wild-type (WT) BM cells were added to
122 the ZsGreen-tracked BM cell cultures twice/week throughout the culture period (see Methods for
123 details). By week 8, BM cells cultured on "Primaria" dishes formed a confluent monolayer of
124 ZsGreen-tracked cells with a typical EC morphology, whereas BM cells cultured on OP9
125 monolayers exhibited a fibroblast-like morphology with the ZsGreen^{+} cells clustering in foci,
126 without forming a monolayer (Figure 2A). We visualized some round ZsGreen-tracked
127 (ZsGreen^{+}) cells in cultures of BM cells grown onto OP9 monolayers supplemented with fresh
128 BM cells, but not in cultures of BM cells grown onto "Primaria" surfaces supplemented with

129 fresh BM cells (Figure S2F). This hinted that the OP9 and BM cell culture system may allow
130 hematopoietic cells emergence from Cdh5-Cre/ZsGreen-tracked EC ex vivo.
131 To test this possibility, we generated a pool of BM cells (from 20 adult mice; age 10-18
132 weeks) and used the pool to derive 3 populations: sorted BM CD45^{-}VE-Cadherin^{+}ZsGreen^{+}
133 ECs; sorted CD45^{+}ZsGreen^{+} hematopoietic cells; and unsorted BM cell populations (Figure 2B).
134 We then cultured these 3 cell populations under the same conditions (OP9 monolater and
135 supplementation with fresh BM cells twice/week). After 8-week culture, flow cytometry analysis
136 detected CD45^{+}ZsGreen^{+} cells from the unsorted BM and the sorted CD45^{-}VE-
137 Cadherin^{+}ZsGreen^{+} cell cultures. However, CD45^{+}ZsGreen^{+} were virtually absent from the
138 CD45^{+}ZsGreen^{+} cell cultures (Figure 2C and 2D), likely attributable to the culture conditions not
139 designed to support growth, differentiation or survival of hematopoietic cells. These results show
140 that CD45^{-}VE-Cadherin^{+}ZsGreen^{+} ECs can generate CD45^{+}ZsGreen^{+} *ex vivo*. Notably, most
141 (>80%) CD45^{-}ZsGreen^{+} cells retained expression of VE-Cadherin and Endomucin, thereby
142 confirming their endothelial identity (Figure 2C, most right panel). Importantly, the virtual
143 absence of CD45^{+}ZsGreen^{+} cells in 8-week cultures of sorted CD45^{+}ZsGreen^{+} cells shows that
144 pre-existing CD45^{+}ZsGreen^{+} hematopoietic cells, derived from tamoxifen-dependent and
145 independent processes, are effectively removed during the extended culture. This further
146 suggests that CD45^{+}ZsGreen^{+} hematopoietic cells, potentially contaminating the sorted ECs, are
147 unlikely contributors to EC-derived hematopoiesis. Rather, these results show that the ECs are
148 the likely cell source of hematopoietic cells in this *ex vivo* co-culture model.
149 Next, we tested whether the *ex vivo*-derived CD45^{+}ZsGreen^{+} cells are functional in
150 lethally irradiated recipients (Figure 2E). To this end, we obtained unfractionated BM cells from
151 50 tamoxifen-treated Cdh5-Cre/ZsGreen mice, cultured the cells onto OP9 monolayers with

152 fresh BM supplementation, sorted the ZsGreen$^+$ cells (>95% of which were CD45$^+$ by flow
153 cytometry) at the end of 8-week culture, and transplanted these cells into 8 lethally irradiated WT
154 recipients; 5×10^3 cells; 2.5×10^3 cells; 1.25×10^3 cells; 6.25×10^2 cells, n=2/group (Figure 2E-G).
155 Two mice (recipients of 6.25×10^2 and 1.25×10^3 cells) died on days 4 and 6, but the remaining six
156 mice survived and remain well at the time of manuscript revision (10 months post-transplant).
157 Ten months post-transplant, peripheral blood WBC counts were within normal range in all
158 surviving transplant recipients, indicative of hematopoietic reconstitution (Figure 2H). Flow
159 cytometry revealed that 81.9% of PBMC were ZsGreen$^+$ (Figure 2I-J). Most neutrophils
160 (98.6%), monocytes (98.5%), B cells (74.1%) and T cells (84.3%) were ZsGreen$^+$.
161 These results confirm that BM ECs propagated *ex vivo* onto OP9 monolayers with BM
162 cell supplementation produce hematopoietic cells and show that this output includes HSPC
163 capable of engrafting and generating hematopoietic cell progeny.
164
165 **Adult BM ECs can give rise to hematopoietic cells following transfer into conditioned**
166 **recipients**
167 Next, we examined whether adult BM ECs are hemogenic in transplant recipients. To this end,
168 we FACS-sorted CD45$^-$VE-Cadherin$^+$ZsGreen$^+$ ECs from the BM of tamoxifen-pretreated (4
169 weeks prior to BM harvest) Cdh5-Cre^{ERT2}(PAC)/ZsGreen mice (Figure 3A; Figure S2G and
170 S2H) and transplanted these cells into adult WT C57Bl/6 unconditioned mice (PBS) or
171 conditioned by fluorouracil (5-FU treated) prior to transplant[45]. The choice of 5-FU conditioning
172 rather than lethal irradiation of adult mice was driven by previous experiments showing the
173 difficulties at reconstituting lethally myelo-ablated adult recipients with hemogenic yolk sac
174 cells, which reconstituted conditioned newborns[46]. Four weeks after transplant, we observed a

175 significant increase in the proportion of ZsGreen^{+} ECs in the BM and
176 ZsGreen^{+}CD45^{+}hematopoietic cells in the BM and peripheral blood of the transplant recipients
177 conditioned by 5-FU but not controls (PBS) (Figure 3B and 3C; Figure S2I). These
178 CD45^{+}ZsGreen-tracked cells in BM and blood included granulocytes, monocytes, and
179 lymphocytes (Figure 3D). Thus, BM-derived CD45^{-}VE-Cadherin^{+}ZsGreen^{+} cells transferred into
180 5-FU-conditioned recipients gave rise to detectable CD45^{+}ZsGreen^{+} hematopoietic cells.
181 We further examined the effect of mouse age on the endothelial hemogenic potential by
182 treating the mice with tamoxifen between week 6 and 32 of age. Four weeks later (week 10 to 36
183 of age), we measured the percentage of ZsGreen-tracked CD45^{+} hematopoietic cells in the BM.
184 We observed that tamoxifen inductions beyond week 10 of age resulted in a progressive decrease
185 of the CD45^{+} hematopoietic cell output, and detected an inverse correlation (Pearson's r -0.63,
186 $P<0.0001$) between age and EC hemogenic potential (Figure 3E). This progressive decline of
187 CD45^{+} cell output was not coupled with a loss of BM EC fluorescence, since virtually all BM
188 ECs were ZsGreen^{+} throughout the duration of the experiment (Figure 3F), consistent with the
189 stability of Cre-mediated labeling of Cdh5-expressing cells [36]. These observations suggest an
190 age-related loss of hemogenic capability of BM ECs.
191 Additionally, we examined whether tracked hematopoietic cells from adult BM EC are
192 functional. Since lymphocyte trafficking from the peripheral blood to the peritoneal cavity is
193 critical for their function at this site[47,48], we first evaluated the spontaneous migration of tracked
194 CD45^{+} hematopoietic cells to the peritoneal cavity. Compared to no-tamoxifen controls,
195 tamoxifen-treated Cdh5-Cre^{ERT2}(PAC)/ZsGreen mice displayed a significant increase of
196 CD45^{+}ZsGreen^{+} monocytes, macrophages, and B1, B2, and T lymphocytes in the peritoneal
197 cavity (Figure S2J and S2K).

198 After inducing peritonitis with thioglycolate (TGL, 4 hours) in tamoxifen-treated Cdh5-
199 Cre^{ERT2}(PAC)/ZsGreen mice, the overall number of peritoneal leukocytes increased substantially
200 compared to untreated (PBS) controls (Figure 3G), mostly attributable to neutrophils (Figure
201 3H). In addition, the peritoneal ZsGreen^{+} and ZsGreen^{-} cell populations exhibited a similar cell
202 type distribution in TGL-treated mice (Figure 3I). We further examined *Escherichia coli* (K-12
203 strain) phagocytosis and reactive oxygen species (ROS) production in peritoneal cell exudates in
204 response to TGL (Figure 3J-3O). Both ZsGreen^{+} and ZsGreen^{-} peritoneal neutrophils and
205 macrophages comparably phagocytosed *Escherichia coli* and generated ROS (Figure 3J, 3K, 3M,
206 and 3N), except that the phagocytic and ROS production of ZsGreen^{+} macrophages was
207 somewhat higher than that of ZsGreen^{-} macrophages (Figure 3L and 3O).
208 Thus, Cdh5-tracked mature neutrophils and macrophages are functional at trafficking and
209 homing, and presumably capable of contributing to the host response to tissue inflammation.
210
211 **Adult EHT is independent of preexisting hematopoietic cell progenitors**
212 Faithful Cre-reporter lineage tracing requires that Cre recombinase activity be restricted to the
213 intended cell type[40]. In our system, Cdh5-Cre^{ERT2} is expected to drive recombination specifically
214 in ECs, as *Cdh5* is an established EC-specific marker. However, flow cytometry has occasionally
215 revealed rare VE-Cadherin^{+}CD45^{+} in mouse BM, exemplified in Figure S2G, potentially
216 reflecting double-positive cells. To address the possibility that cells co-expressing VE-
217 Cadherin/*Cdh5* and CD45/*Ptprc* exist in the mouse BM, we analyzed publicly available sc-
218 RNAseq data from adult mouse BM[49]. This analysis showed that only a small subset of
219 plasmacytoid dendritic cells (pDCs) co-express VE-Cadherin and CD45, but not HSPC or other
220 mature blood cells (Figure S3A-S3D). pDCs are terminally differentiated cells and unlikely

221 progenitors of tracked CD45^{+} multilineage progeny in our Cdh5-cre mice. Nonetheless, it is
222 plausible that other, currently unidentified, hematopoietic cells may also co-express *Cdh5*/VE-
223 Cadherin and *Ptprc*/CD45 and possess functional Cre^{ERT2} activity, inducing fluorescence in these
224 cells upon tamoxifen administration.

225 To address these possibilities, we transplanted lethally irradiated (11 Gy) WT C57Bl6
226 mice (n=6) with ZsGreen^{-}Lin^{-}Sca1^{+}cKit^{+} (LSK) progenitors (>99% purity; Figure S3E-G) from
227 tamoxifen untreated Cdh5-Cre^{ERT2}(PAC)/ZsGreen mice and examined whether these ZsGreen^{-}
228 hematopoietic progenitors can become fluorescent after tamoxifen administration (Figure 4A).
229 As a positive control, we also transplanted lethally irradiated WT C57Bl6 mice (n=2) with an
230 LSK population enriched for ZsGreen^{+} cells (45.9% purity, with the remaining 54.1%
231 comprising ZsGreen^{-} LSK cells (Figure 4A and Figure S3F). Four weeks post-transplant, we
232 administered tamoxifen and monitored the peripheral blood for the presence of ZsGreen^{+}
233 hematopoietic cells over six months.

234 Expectedly, all LSK recipients (ZsGreen^{-} LSKs or LSK enriched with ZsGreen^{+} cells)
235 showed successful hematopoietic reconstitution as evidenced by normal blood WBC counts at 10
236 weeks post-transplant (Figure 4B). Importantly, the 6 mice transplanted with ZsGreen^{-} LSKs did
237 not produce ZsGreen^{+} PBMCs post-tamoxifen administration, indicating that the transplanted
238 LSKs and their progeny did not express tamoxifen inducible Cdh5-Cre^{ERT2} recombinase activity
239 (Figure 4C and 4D). Instead, the 2 mice transplanted with ZsGreen^{+}-enriched LSKs displayed a
240 similar percent of ZsGreen^{+} PBMCs prior to and after tamoxifen administration (Figure 4D).
241 Collectively, these results demonstrate that LSK progenitors in adult BM lack of tamoxifen-
242 inducible Cdh5 expression and do not contribute to tamoxifen-induced adult EHT in our Cdh5-

243 reporter mice. Rather, these results strongly support the conclusion that Cdh5^{+}CD45^{-} ECs are a
244 source of hematopoietic cells in the adult mouse.
245 In additional experiments, we took advantage of the relative insensitivity of BM ECs
246 subsets to irradiation relative to BM hematopoietic cells[50] to examine the possibility that EC
247 surviving after lethal irradiation may be hemogenic. As a lethal dose of irradiation effectively
248 eliminates HSPCs and requires hematopoietic reconstitution for survival, we transplanted WT
249 (untracked) BM cells into lethally irradiated Cdh5-Cre/mTmG mice and treated the mice with
250 tamoxifen 4 weeks after transplantation (Figure 4E). Prior to tamoxifen administration, >99% of
251 PBMCs were not fluorescent, indicating that these cells derived from the transplanted WT BM
252 rather than host-derived (Figure 4F). After tamoxifen treatment, a progressive increase in EGFP^{+}
253 PBMCs was observed, reaching ~0.55% by six weeks, which included myeloid cells and B and T
254 lymphocytes (Figure 4F and 4G). Although we cannot exclude the possibility that rare EGFP^{+}
255 hematopoietic progenitor (tracked tamoxifen-dependently or independently) may have survived
256 the irradiation, the presence of EGFP^{+} hematopoietic cells in the circulation of lethally irradiated
257 Cdh5-Cre/mTmG mice suggests their derivation from radioresistant Cdh5^{+} ECs rather than from
258 radiosensitive hematopoietic progenitors. These results further support the view that adult ECs
259 possess hemogenic potential and can produce hematopoietic cells in vivo.
260
261 **Single cell tracking confirms the presence hemogenic ECs in adult BM**
262 To directly trace hematopoietic cell progeny arising from individual adult ECs, we exploited the
263 *PolyloxExpress* sc genetic barcoding system. We generated Cdh5-
264 Cre^{ERT2}/ZsGreen/*PolyloxExpress* mice, in which both the ZsGreen and Polylox transgenes are
265 inserted in the Rosa26 locus, such that individual ZsGreen^{+} cells contain a single Polylox

266 barcode[33,51,52]. To evaluate EC-derived hematopoietic cell output, we harvested BM from
267 tamoxifen-treated Cdh5-Cre^{ERT2}/ZsGreen/*PolyloxExpress* mice (n=3), sorted the ZsGreen^{+}VE-
268 Cadherin^{+}Endomucin^{+} (purity >95%) and the ZsGreen^{+}VE-Cadherin^{-}Endomucin^{-}CD45^{+}
269 hematopoietic cells (purity >98%), mixed these populations (1:1 ratio; total 147,446 cells) and
270 processed for 10x Illumina Sequencing and PacBio sequencing (detailed in Methods). We
271 recovered sc transcriptome from 93,553 cells; of these, 4,069 cells had a barcode (Figure 5A,
272 Figure S5A-B, detailed in Methods).

273 Unsupervised clustering of sc transcriptome data revealed 34 clusters, 31 of which
274 remained after doublet removal (Figure 5B; Figure S4A-S4D). Cell clusters 0, 1, 22, and 13 were
275 annotated as "Endothelial cells" based on expression of the classical EC markers *Cdh5*, *Pecam1*,
276 *Kdr* and *Flt1*, and absence of *Ptprc*/CD45, *Runx1*, and the mesenchymal cell markers *Cxcl12*,
277 *Lepr*, *Pdgfrb*, and *Col1a2* expression (Figure 5B; Figure S4E). Cell cluster 14 was annotated as
278 "Mesenchymal type" based on co-expression of *Cxcl12*, *Lepr*, *Pdgfrb*, *Col1a2*, but expressed
279 *Runx1* and the EC markers *Cdh5* and *Pecam1* (Figure 5B; Figure S4E). The remaining cell
280 clusters included the hematopoietic progenitors and mature blood cells of various lineages
281 (Figure 5B; Figure S4E). Cre^{ERT2} transcripts were detected exclusively in Cdh5-expressing
282 endothelial cell populations and were absent from Ptprc/CD45-expressing hematopoietic cells
283 (Figure S4E). Cre^{ERT2} expression levels in ECs were low but closely tracked with the expression
284 patterns of canonical endothelial markers (*Cdh5*, *Pecam1*, *Emcn*, and *Eng*).

285 Barcode analysis revealed robust *Polylox* barcode diversity among cell populations,
286 including 274 "true" barcodes, defined as barcodes with low generation probability (Figure S5A,
287 $P_{gen} < 1\times10^{-6}$)[51] consistent with rare, unique recombination events (Figure S5A - S5C).

288 Expectedly, “true” barcodes linked HSPC to downstream progenitors and mature hematopoietic
289 cells, validating the system (Figure 5C).
290 Notably, 169 of 828 ECs (from “endothelial” cell clusters 0, 1, 22, and 13) were marked
291 with “true” barcodes. The results detected 19 links between EC and hematopoietic cells based on
292 their shared “true” barcode (Figure 5D). These hematopoietic cells linked to ECs by shared
293 “true” barcodes included HSPC, EPC, GMP, and mature blood cells, encompassing
294 granulocytes, monocytes, dendritic cells, B and T lymphocytes, plasma cells, and pDCs (Figure
295 5D and E). These results provide direct evidence, at sc resolution, that adult mouse BM ECs can
296 generate hematopoietic progenitors and mature blood cells.
297 Additionally, 26 “Mesenchymal type” cells (from cluster 14; co-expressing mesenchymal
298 cell markers, *Runx1*, and the EC markers *Cdh5* and *Pecam1*) were also marked by 11 “true”
299 barcodes, 8 of which were shared with hematopoietic cell progenitors (HSPC and Erythroid) and
300 mature blood cells (Figure 5E and F). Also, 4 “true” barcodes linked “Mesenchymal type” cells
301 to ECs (from clusters 0, 1, 22 and 13), suggesting either a shared precursor or derivation from
302 each other. Although it cannot be excluded that barcoding missed identification of mesenchymal
303 cell links to other ECs or cells, these results raise the possibility that certain BM “Mesenchymal
304 type” cells may produce hematopoietic cell progeny. Despite similarities of sc tracing results
305 linking ECs and “Mesenchymal type” cells to hematopoietic cells, these two cell populations
306 display a distinctive transcriptome profile (Figure 5G; Figure S4E).
307 Additional analysis of all tracked cells showed that several ECs and to a lower extent
308 “Mesenchymal type cells” shared “true” barcodes (Figure S5D-F), indicating clonal expansion.
309 Transcriptome-based sc cell cycle analysis, confirmed the presence of ECs and “Mesenchymal
310 type cells” in the S and G2/M phases, albeit to a much lower degree than HSPC (Figure S5C).

311 Together, these results demonstrate at a sc level that adult BM ECs can generate hematopoietic
312 cell progeny of HSPC and mature blood cells. The results further raise the possibility that
313 "Mesenchymal type" cells, marked by a hybrid endothelial and stromal phenotype, may
314 represent an additional source of hemogenic activity in adult BM.
315
316 **Single cell transcriptome identifies a *Cdh5*$^{+}$*Col1a2*$^{+}$ *Runx1*$^{+}$cell population in the adult BM.**
317 To further characterize adult hemogenic cell populations, we analyzed publicly available
318 scRNAseq datasets comprising BM cells from adult mice (1-16 months of age)[53-59] and
319 embryonic caudal artery ECs (9.5–11.5 days post coitum)[24]. After quality control and
320 dimensional reduction, the remaining 434,810 cells clustered into 71 distinct populations (Figure
321 6A-D). Among the *Cdh5*-expressing endothelial clusters, two clusters, cluster 8 composed
322 predominantly of embryonic cells (98%) and cluster 50 composed largely of adult BM-derived
323 cells (95.5%) (Figure 6E), were notable in comprising cells co-expressing *Cdh5* and *Runx1*, a
324 transcription factor that marks the hemogenic EC identity during development[60] (Figure 6B).
325 We jointly analyzed the transcriptome from the publicly available embryonic cluster 8
326 and adult cluster 50 (Figure 6 A-C), and from our sc Polylox dataset, including adult clusters 14
327 (Mesenchymal type) and adult EC clusters 0, 1, 13 and 22 (Figure 5B). All populations
328 expressed canonical EC markers (*Cdh5*, *Pecam1*, *Kdr*, *Flt1*), though at different levels, but
329 expression of *Runx1* was mostly confined to clusters 8, 50 and Polylox 14 (Figure 6F).
330 Interestingly, adult clusters 50 and Polylox 14 co-expressed the mesenchymal cell-associated
331 genes *Col1a2*, *Lepr*, *Cxcl12*, and *Pdgfrb*, distinguishing these two clusters from the embryonic
332 cluster 8 and adult Polylox clusters 0, 1, 13 and 22 (Figure 6F). Additionally, embryonic cluster
333 8 exhibited higher expression of key EHT-related transcription factors (FLI1, LMO2, TAL1,

334 ERG)[61-64], some of which were variably expressed by the Polylox clusters 0,1,13 and 22 (Figure
335 6F).
336 To explore whether cells expressing *Cdh5*, *Col1a2* and *Runx1* are unique to BM (Figure
337 6G), we looked at other adult mouse tissues. Analysis of public scRNAseq datasets from 11 adult
338 mouse tissues[65] showed that *Cdh5*, *Runx1*, and *Col1a2* expressing ECs are largely restricted to
339 the BM, with only 3 such cells detected out of ~32,000 EC from other tissues (Figure 6H and
340 I)[65]. These observations, together with the Polylox sc tracing experiments, indicate that adult
341 mouse BM harbors a cell population with mixed endothelial and mesenchymal phenotype
342 marked by *Runx1*, *Col1a2* and *Cdh5* expression and raises the possibility that this population has
343 hemogenic potential.
344
345 ***Col1a2* and *Runx1* expression in BM ECs**
346 To evaluate a potential contribution of *Col1a2* expression to EHT in adult BM, we generated the
347 mouse lines Col1a2-Cre^{ERT2}/mTmG and Col1a2-Cre^{ERT2}/ZsGreen to track cells expressing the
348 *Col1a2* gene (Figure S6A). Four weeks after tamoxifen administration, the BM of Col1a2-
349 Cre^{ERT2}/ZsGreen mice contained abundant ZsGreen^{+} cells (Figure S6B). By flow cytometry, a
350 subset of these BM Col1a2-tracked ZsGreen^{+} cells were VE-Cadherin^{+}CD45^{-} and RUNX1^{+}
351 consistent with an endothelial identity and perhaps hemogenic potential (Figure S6C).
352 Noteworthy, a similar subset of VE-Cadherin^{+}CD45^{-}RUNX1^{+} cells was detected in BM of adult
353 WT C57Bl/6 mice (Figure S6D) and in BM of Cdh5-Cre^{ERT2}(PAC)/ZsGreen mice after
354 tamoxifen treatment (Figure S6E).
355 To evaluate hemogenic potential, we looked for Col1a2-tracked CD45^{+} hematopoietic
356 cells in Col1a2-Cre^{ERT2}/mTmG and Col1a2-Cre^{ERT2}/ZsGreen mouse lines after tamoxifen

357 treatment. In both these mouse lines, we detected CD45$^+$ hematopoietic cells tracked by EGFP or
358 ZsGreen fluorescence in BM and blood, which were rare but significantly more abundant than in
359 control mice not treated with tamoxifen (Figure 7A and B; Figure S6F-H). These results
360 indicated that a proportion of the Col1a2-tracked cells in the adult mouse are hemogenic.

361 To further evaluate this possibility, we first sorted VE-Cadherin$^+$CD45$^-$ ZsGreen
362 (Col1a2)$^+$ cells from the BM of tamoxifen-induced adult Col1a2-Cre^{ERT2}/ZsGreen mice (Figure
363 S7A), examined expression of selected genes, and used these cells in transplant experiments. The
364 sorted VE-Cadherin$^+$CD45$^-$ ZsGreen (Col1a2)$^+$ cells expressed *Cdh5*, *Col1a2*, *Cxcl12*, and *Runx1*
365 mRNAs distinctively from other BM cell population (Figure S7B), but resembled the BM
366 hemogenic population annotated as "mesenchymal-type" (cluster 14) identified by Polylox s.c
367 sequencing (Figure 5G; Figure S4E) and subsets of adult BM Cdh5$^+$ cells identified in public
368 adult datasets (Figure 6E and F).

369 We transplanted the BM VE-Cadherin$^+$CD45$^-$ ZsGreen (Col1a2)$^+$ cells (1×10^4
370 cells/mouse) into 5-FU-conditioned adult WT C57Bl/6 recipients and looked for tracked CD45$^+$
371 cells in the BM and blood (Figure 7C). Four weeks after transplantation, BM and peripheral
372 blood of transplant recipients contained ZsGreen$^+$CD45$^+$ cells (Figure 7D; Figure S7C and D),
373 indicating that the transplanted ZsGreen$^+$ (Col1a2)-tracked CD45$^-$ ECs had produced CD45$^+$
374 hematopoietic cell progeny. These ZsGreen$^+$CD45$^+$ cells in the recipient mice comprised mainly
375 granulocytes and monocytes, and few B and T lymphocytes (Figure 7E). These results indicate
376 that Col1a2-tracked ECs, like Cdh5(VE-Cadherin)-tracked ECs, can give rise to hematopoietic
377 progeny in vivo, but display a more restricted multilineage potential compared to ECs from
378 Cdh5-Cre^{ERT2}(PAC)/ZsGreen mice.

379 In additional experiments, we evaluated the role of *Runx1* expression in adult BM
380 hemogenic EC since our analyses identified *Runx1* as a putative marker of adult EHT (Figure 6E
381 and F; Figure S4E). Therefore, we generated a Runx1$^{EC\text{-}KI}$ mouse line (*Cdh5-*
382 *Cre^{ERT2}/ZsGreen/Runx1-Knock-In*), in which Cre-mediated excision of a floxed STOP codon
383 enables co-expression of ZsGreen and *Runx1* in ECs upon tamoxifen induction (Figure S7E)[66].
384 In these Runx1$^{EC\text{-}KI}$ mice, tamoxifen treatment increased significantly the frequency of ZsGreen^{+}
385 cells in PBMC over 60 weeks compared to control tamoxifen-treated (Cdh5-Cre^{ERT2}/ZsGreen)
386 mice (Figure 7F).
387 Since these circulating ZsGreen-tracked cells presumably represent hematopoietic cell
388 progeny of ECs co-expressing ZsGreen and *Runx1*, we tested the hemogenic potential of these
389 tamoxifen-induced BM EC ex vivo. Using the culture system that successfully supported ex vivo
390 hematopoiesis in Cdh5-tracked BM (Figure 2A-H), we now compared the hemogenic potential
391 of BM cells from tamoxifen pretreated Runx1$^{EC\text{-}KI}$ mice to that of BM cells from tamoxifen
392 pretreated Cdh5-Cre^{ERT2}/ZsGreen) mice. We detected a significantly greater number of ZsGreen^{+}
393 clusters in cultures from Runx1$^{EC\text{-}KI}$ BM cells compared to control BM cells (Figure 7G and H),
394 and flow cytometry showed that more CD45^{+}ZsGreen^{+} hematopoietic cells were produced in
395 cultures of Runx1$^{EC\text{-}KI}$ BM cells compared to BM from controls (Figure 7I and J). Although we
396 cannot exclude the possibility that RUNX1 promotes EC proliferation in culture, these results
397 support a role of RUNX1 in promoting adult EHT.

398 **DISCUSSION**

399 Our results provide evidence for the presence of ECs in the adult mouse BM with hemogenic
400 potential. Previously, hemogenic ECs were detected during embryonic development or

401 perinatally but not thereafter[1-9,67]. The current findings argue that EHT is not limited to the
402 prenatal or perinatal development but is present up to 28 weeks after birth, decreasing thereafter.
403 This conclusion is supported by Cdh5-based bulk and Polylox sc lineage tracking, culture of
404 hemogenic ECs, transplant analyses and initial characterization of EC-derived hematopoietic cell
405 progeny, which link features of adult EHT to embryonic EHT[25-28,68].

406 Previous experiments found that EHT, present in the late fetus/neonatal BM, disappears
407 shortly after birth[67]. This contrasts with the current experiments showing persistence of adult
408 EHT well beyond 20 weeks of age. The divergent results likely stem from functional differences
409 of the Cdh5-based tracking systems. In the previous experiments, attempts to activate Cdh5-
410 fluorescence in BM ECs by injecting tamoxifen at different time-points after birth were
411 unsuccessful starting 20 days after birth. Expectedly, the absence of tamoxifen-induced
412 fluorescence in BM ECs was associated with the absence of traced hematopoietic cell output
413 from these cells. In the current experiments and those of others[36], tamoxifen administration after
414 10, 20, and 30 weeks of age consistently induces fluorescence in most BM ECs. We conclude
415 that the absence of adult EHT had not been firmly established.

416 Adult hemogenic ECs identified here express *Cdh5*, *Pecam1*, *Kdr*, and *Flt1*, resembling
417 other BM EC populations and embryonic hemogenic ECs[69]. However, the current studies
418 identify yet another, small hemogenic cell population in the adult BM, distinctive in co-
419 expressing typical EC markers, *Cdh5* and *Pecam1*, and the mesenchymal-type markers *Lepr*,
420 *Col1a2* and *Cxcl12*. These two hemogenic populations are clonally linked, but their relationship
421 is currently unclear.

422 ECs derive from two sources during development: the splanchnic mesoderm that gives
423 rise to the primitive aorta where ECs located on the aortic floor are hemogenic[68], and the somites

424 from the paraxial mesoderm, that produce ECs contributing the endothelial vascular network of
425 the trunk and limb[70,71]. Somite-derived ECs are not hemogenic in situ, but they can transiently
426 acquire a hemogenic potential when variously induced[72] and may also include a cell subset with
427 hemogenic potential[73]. They can also express *Runx1* and trigger aortic hematopoiesis from
428 hemogenic ECs in zebrafish[74] and in the chick[68]. Besides generating hemogenic ECs, blood and
429 other tissues, the mesoderm in conjunction with the neural crest, gives rise to mesenchymal stem
430 cells (MSCs) and perhaps a precursor of both MSCs and ECs[75-77]. However, MSCs do not
431 produce blood cells, although they can differentiate into many other tissues[78], and their potential
432 for endothelial differentiation remains controversial[79-82]. By contrast, endothelial to
433 mesenchymal transition (EndMT) is a well-established process in development and disease
434 states[83].

435 It was suggested that the transient wave of EHT occurring in the BM of the late fetus and
436 perinatally may serve to mitigate the slow HSC colonization of BM from the fetal liver or
437 perhaps prepare the BM niches to accommodate the incoming HSC from the liver, but a function
438 has not yet been firmly established[67]. Similarly, the function of adult BM EHT identified here is
439 currently unclear. We hypothesize that adult EHT plays a functional role under conditions of
440 hematopoietic stress or disease rather than under steady-state conditions, but this will need future
441 investigation. Interestingly, previous studies found that subsets of ECs can regenerate after
442 irradiation that has eliminated HSC[45], and we traced the emergence of some hematopoietic cells
443 from putative ECs that persisted after lethal mouse irradiation. We also found that 5-FU
444 treatment was required for the successful engraftment and function of adult hemogenic ECs,
445 suggesting that this population may require inductive signals from a BM that is recovering from

446 an insult[45,84]. The identification of such inductive factors may enable effective propagation of
447 BM hemogenic ECs ex vivo and motivate a search for hemogenic ECs in human BM.
448 Altogether, our results point to a previously unrecognized capability of ECs in the adult
449 mouse BM to generate blood cells. These results suggest that hematopoiesis in the adult mouse
450 may arise through the contribution of cells and processes beyond the HSCs generated through
451 aortic EHT during development and BM EHT perinatally.
452
453 **Limitations of the study**
454 A limitation of our study is that the function of adult EHT is currently unknown. Under steady-
455 state conditions, the hematopoietic cell output from adult EHT is very low in comparison to that
456 of embryonic EHT, which effectively sustains adult hematopoiesis, and our experiments detected
457 no functional differences between hematopoietic cells from embryonic and adult EHT. To
458 address this limitation, we will examine whether adult EHT is a greater contributor to adult
459 hematopoiesis when stress is imposed on the adult hematopoietic system. In addition, we have
460 not fully characterized the hematopoietic cell population(s) arising from adult EHT or studied the
461 time-course kinetics of hematopoietic cell emergence. A key issue is whether long-term
462 repopulating HSPCs are produced by adult EHT. This will require serial transplantation
463 experiments, including CD45.1/CD45.2 competitive repopulation assays, and kinetic analysis of
464 their emergence from hemogenic ECs. Finally, we could not extend the in vivo single-cell
465 PolyloxExpress genetic lineage tracing to the ex vivo single-cell genetic lineage tracing due to
466 technical limitations of the PolyloxExpress system.

467 **RESOURCE AVAILABILITY**

468 **Lead contact**

469 Further information and requests for resources and reagents should be directed to and will be
470 fulfilled by the lead contact, Giovanna Tosato (tosatog@mail.nih.gov).

471

472 **Materials availability**

473 This study did not generate new unique reagents.

474

475 **Data and code availability**

476 The results of scRNAseq and PacBio SmrtSeq of Polylox barcodes are deposited in NCBI SRA
477 (PRJNA1079369, public at time of publication). A custom script was used to retrieve cell
478 indexes from the PolyloxExpress amplicons (https://github.com/CCRSF-IFX/SF_Polylox-BC).
479 Bash, R, and Python codes are available from the corresponding author upon reasonable request.

480

481 ## ACKNOWLEDGEMENTS

482 This project is supported by the Intramural Program of CCR, NCI, NIH. The findings are those
483 of the authors and do not necessarily represent the official views of the NIH or the Department of
484 Health and Human Services. This work used the computational resources of the NIH High
485 Performance Computing (HPC) Biowulf cluster (*http://hpc.nih.gov*) and Frederick Research
486 Computing Environment (FRCE). Flow cytometry and cell sorting were performed at the CCR
487 Flow Cytometry Core Facility; microscopy analyses at the CCR Microscopy Core Facility in
488 Building 37 of the NCI, NIH. We thank Drs. Ralf Adams and Manfred Boehm for mouse line
489 *Cdh5-Cre^{ERT2}(PAC)*; Drs. Yoshiaki Kubota and Yosuke Mukoyama for mouse line *Cdh5-*

490 *Cre^{ERT2}(BAC)*; Dr. Hans-Reimer Rodewald for the *PolyloxExpress* mouse line. We thank Dr. S.
491 Banerjee, Dr. S. Siddiqui and Ms. K. M. Wolcott for flow cytometry support; Dr. M. Kruhlak
492 and Mr. L. Lim for confocal microscopy support and Mr. A. Abdelmaksoud for bioinformatics
493 assistance. We thank Drs. D. Lowy, R. Yarchoan, M. DiPrima and H. Ohnuki for thoughtfully
494 commenting on aspects of this work.
495

496 AUTHOR CONTRIBUTIONS

497 Concept and design: J-X.F. and G.T. Acquisition, analysis, or interpretation of data: J-X.F., G.T.,
498 C.L., F.L., N.T., A.B., L.L, M-T.Y., D.W., J.C., and Y.Z. G. Drafting of the manuscript: J-X.F.,
499 G.T. Critical revision of the manuscript for important intellectual content: J-X.F., G.T., A.B. and
500 N.T.
501

502 DECLARATION OF INTERESTS

503 The authors declare no competing financial interests.
504

505 SUPPLEMENTAL INFORMATION

506 Document S1. Figures S1–S7

507 FIGURE TITLES AND LEGENDS

508 **Figure 1. Lineage tracking discloses a contribution of endothelial cells to hematopoiesis in**
509 **adult BM**

510 (A) Experimental design: tamoxifen was administered to 8- to12-week-old Cdh5-Cre mice to
511 induce fluorescent labeling of VE-Cadherin^{+} cells and their cell progeny. Four weeks later, BM
512 and blood were analyzed.
513 (B) CD31^{+}EGFP^{+} BM ECs in Cre^{-} mice (n=10) and Cre^{+} mice treated with oil (n=13) or
514 tamoxifen (n=10); flow cytometry results.
515 (C and D) CD45^{+}EGFP^{+} cells in BM and blood from Cre^{-} mice (n=8) and Cre^{+} mice treated with
516 oil (n=6-10) or tamoxifen (n=15-18). Representative flow cytometry gating in Figure S1G.
517 (E) Representative blood smear from a tamoxifen-treated Cdh5-Cre^{ERT2}(PAC)/ZsGreen mouse
518 showing ZsGreen^{+}CD45^{+}DAPI^{+} cells (arrows).
519 (F) Kinetics of ZsGreen^{+} cell detection in BM ECs (CD45^{-}VE-Cadherin^{+}) and blood white blood
520 cells (WBC) post-tamoxifen; mouse n=8-10/group).
521 (G) EGFP^{+} B and T-lymphocytes, granulocytes, and monocytes in BM of tamoxifen-treated mice
522 (n=14) as percent of total EGFP^{+} cells; 3 experiments.
523 (H) EGFP^{+} BM LSK, lymphocytes, granulocytes, and monocytes as percent of total EGFP$^{+/-}$ cell
524 type; Cdh5-Cre^{ERT2}(PAC)/mTmG mice (oil n=10; tamoxifen n=15), 3 experiments.
525 (I) UMAP plots of Lin^{-} BM HSPC from tamoxifen-treated Cdh5-Cre^{ERT2}(PAC)/ZsGreen mice
526 (n=26; 1 femur/mouse) showing FlowSOM clustering of all (ZsGreen^{+}/-) and ZsGreen^{+}
527 populations.
528 (J) Violin plots showing ZsGreen^{+} cell distribution across HSPC subsets from (I).
529 Dots represent individual mice; data shown as mean±SD except shown as median in (G). *$p <$
530 0.05, **$p < 0.01$, ***$p < 0.001$ by Student's t test.
531

532 **Figure 2. BM ECs generate engraftable hematopoietic cells ex vivo**

533 (A) BM cells from tamoxifen-treated mice were cultured on high-attachment Primaria flasks or
534 OP9 cell monolayers. Representative images show ZsGreen$^+$ cells at weeks 1, 3, and 8.

535 (B) Workflow for culturing unsorted and sorted BM cell populations. Post-sort purity of
536 ZsGreen$^+$ ECs is shown in the bottom left panel. All cells were cultured (8 weeks) on OP9 cell
537 monolayers supplemented with WT BM cells. Culture medium and floating cells were removed
538 twice/week for 7 weeks. At the start of week 8, one final WT BM and medium supplementation
539 was implemented prior to harvest at the end of week 8.

540 (C and D) Representative flow cytometry plots (C) and quantification (D) of CD45$^+$ZsGreen$^+$
541 cells from each of the 8-week cultures (n=5).

542 (E) Floating/loosely adherent ZsGreen$^+$ cells from unsorted BM 8-week cell cultures were sorted
543 and transplanted (5×10^4, 2.5×10^4,1.25×10^4 or 6.25×10^3 cells) into lethally irradiated (11 Gy) WT
544 mice (n=2/group).

545 (F and G) Representative flow cytometry image (F) and quantification (G) of low-adherent cells
546 harvested after 8 weeks of culture, showing that >95% (group average) of ZsGreen$^+$ low-
547 adherent cells are CD45$^+$. These ZsGreen$^+$CD45$^+$ cells were sorted for transplantation.

548 (H - J) WBC counts from 5 control mice (no irradiation or transplant) (H) and percent ZsGreen$^+$,
549 ZsGreen dim and ZsGreen$^-$ cells (I-J) in blood of transplant recipients 10 months post-transplant
550 (n=6).

551 Dots represent individual mice. Data are shown as mean ± SD. ns, not significant by Student's *t*
552 test.

553

554 **Figure 3. Adult BM endothelial cells give rise to hematopoietic cells following transfer into**
555 **conditioned recipients**
556 (A) Transplant experiment: donor ECs from BM of tamoxifen-treated mice were FACS-sorted
557 and transplanted into WT C57Bl/6 recipients conditioned with 5-FU or PBS.
558 (B) ZsGreen^{+} ECs detected in BM of 5-FU-conditioned (n=5) or PBS-conditioned (n=15)
559 recipients of ECs 4 weeks post-transplant.
560 (C and D) ZsGreen^{+}CD45^{+} cells (C) and cell type distribution (D) in the BM and blood of 5-FU-
561 conditioned transplant recipients of BM ECs or no cell controls (n=5/group).
562 (E and F) Age-dependent decline of ZsGreen^{+}CD45^{+} cells (E) but not ZsGreen^{+}VE-Cadhenin^{+}
563 cells (F) in the BM of Cdh5-Cre^{ERT2}(BAC)/ZsGreen mice (n=35) treated with tamoxifen 4-weeks
564 prior to harvest.
565 (G and H) Cell number (G; mouse n=8-12) and cell type distribution (H; mouse n=6) in the
566 peritoneal cavity (PerC) of PBS- or thioglycolate (TGL)-pretreated (4 hours) mice.
567 (I) ZsGreen^{+} and ZsGreen^{-} PerC cell types in TGL-pretreated mice (n=12).
568 (J) Representative histograms depicting pHrodo Red fluorescence detection of E-Coli
569 phagocytosis.
570 (K and L) E. coli^{+} phagocytosis by ZsGreen^{+} and ZsGreen^{-} PerC neutrophils (K) and
571 macrophages (L) in TGL-pretreated mice (n=4).
572 (M) Representative histograms depicting CellRox Orange fluorescence for cell-associated ROS
573 detection.
574 (N and O) CellRox mean fluorescence intensity (MFI) in ZsGreen^{+} and ZsGreen^{-} PerC
575 neutrophils (N) and macrophages (O) in TGL-pretreated mice (n=4).

576 Dots represent individual mice. Data are shown as mean ± SD. *p < 0.05, ***p < 0.001, ns, not
577 significant by Student's *t* test.
578
579 **Figure 4. Independence of adult EHT from preexisting HSPC**
580 (A) Transplantation experiment: donor LSK sorting, recipient irradiation, transplantation,
581 tamoxifen treatment, and analysis (top). Tabular representation of possible outcomes of the
582 experiment designed to address the question "Do HSPCs/other hematopoietic cells in
583 Cdh5Cre^{ERT2}/ZsGreen mice express Cdh5-Cre^{ERT2}?" (bottom).
584 (B-D) Blood WBC counts (B), percent ZsGreen^{+} PBMC (C), and time course of ZsGreen^{+}
585 PBMC detection (D) in transplant recipients of ZsGreen^{-} LSK (5×10^4 or 2.5×10^4 cells/mouse;
586 n=3/group) and ZsGreen-enriched LSKs (2.8×10^3 cells/mouse; n=2). Results in B and C are from
587 week 24 post-tamoxifen.
588 (E) Experiment: WT BM transplantation (BMTP) into lethally irradiated Cdh5-Cre/mTmG mice
589 (n=9). Four weeks later, tamoxifen was administered; blood was monitored for 16 weeks.
590 (F and G) EGFP^{+} PBMC detection before and after tamoxifen or peanut oil administration (F)
591 and cell type distribution of EGFP^{+} and EGFP^{-} PBMCs at week 12 post-tamoxifen or peanut oil
592 (G) in Cdh5-Cre/mTmG recipients (n=9) of WT BM (5×10^6 cells). Statistical significance
593 reflects comparisons between EGFP^{+} and EGFP^{-} cells in the tamoxifen vs peanut oil groups.
594 Dots represent individual mice. Data are shown as mean ± SD. ***p < 0.001, ns, not significant
595 by Student's *t* test.
596
597 **Figure 5. Polylox sc lineage tracing links adult BM ECs to hematopoietic progenitors and**
598 **mature blood cell progeny**

599 (A) Schematic of Polylox barcode and transcriptome profiling. FACS-enriched ECs
600 (ZsGreen^{+}VE-Cadherin^{+}Endomucin^{+}) and EC-depleted (ZsGreen^{-}VE-Cadherin^{-}Endomucin^{-}) BM
601 cells from tamoxifen-treated Cdh5-Cre^{ERT2}/ZsGreen/PolyloxExpress mice (n=3, 10-week-old at
602 the time of tamoxifen treatment) were mixed (1:1), and encapsulated (147,446 cells loaded;
603 93,553 processed). Indexed cDNA was used for scRNA-seq and barcode detection by PacBio
604 sequencing after nested PCR enrichment; barcode-transcriptome integration was accomplished
605 via shared cell indices.
606 (B) UMAP clustering and cell type annotation. Clusters 0, 1, 13, and 22 comprise ECs; cluster 14
607 comprises Mesenchymal-type cells.
608 (C – E) Heatmaps showing "true" Polylox barcodes (pGen < 1×10^{-6}) linking HSPCs to
609 hematopoietic cells (C), ECs to hematopoietic and other cells (D), and Mesenchymal-type cells
610 to other cells (E). The numbers within the colored boxes identify cell number; the labels at the
611 bottom of each column denote the barcode shared by all cells in that column; the number on the
612 right side the heatmaps reflects the total number of cells in each row.
613 (F) UpSet plot showing cells (identified by colored dots) sharing the same "true" barcode
614 (identified by lines connecting the colored dots); bar graph at the top of the plot reflects (height
615 and number on each bar) the number of "true" barcodes. Colors of dots: EC (red), Mesenchymal-
616 type (orange), ECs connecting with Mesenchymal-type cells (blue), cells other than ECs and
617 Mesenchymal-type cells (black).
618 (G) Violin plots showing selected gene expression profile in Mesenchymal-type cells (cluster 14)
619 and ECs (clusters 0, 1, 13, 22 combined).
620
621 **Figure 6. Sc transcriptomic analysis of prospective hemogenic ECs**

622 (A) UMAP clustering of 434,810 cells from eight public scRNA-seq datasets.

623 (B) Dot plot showing relative Cdh5 and Runx1 co-expression across clusters; clusters 8 and 50

624 co-express both genes.

625 (C) UMAP highlighting clusters 8 and 50; all other clusters shown in grey.

626 (D) Violin plots of doublet scores across Leiden clusters. Clusters 50 and 8 show no evidence of

627 doublet enrichment.

628 (E) Datasets proportional contribution to clusters 50 and 8; each dataset is color-coded.

629 (F) Dot plot showing expression of selected marker genes in clusters 50 and 8 (from the public sc

630 RNA-seq datasets listed in Figure 7D) and from clusters 0, 1, 13, 22 and 14 (from Polylox

631 scRNA-seq; Figure 5B). Results reflect mean expression and fraction of cells in group.

632 (G) Cdh5, Runx1 and Col1a2 co-expression in the indicated clusters as a fraction of cells in the

633 cluster.

634 (H and I) t-SNE plot of ECs from 11 murine tissues (G) and Venn diagram (H) showing rare co-

635 expression of Cdh5, Runx1, and Col1a2 in these tissues.

636

637 **Figure 7. Contribution of *Col1a2* and *Runx1* expression to ECs hemogenic activity**

638 (A and B) Percent $EGFP^{+}CD45^{+}$ cells in BM and blood of tamoxifen-treated (n=6) or oil-treated

639 (n=5) Col1a2-Cre^{ERT2}/mTmG mice (A) and tamoxifen-treated (n=4) or oil-treated (n=3) Col1a2-

640 Cre^{ERT2}/ZsGreen mice (B). Cre-control mice (n=5 in A, and n=2 in B).

641 (C) Transplant experiment: sorted VE-$Cadherin^{+}CD45^{-}ZsGreen^{+}$/$Col1a2^{+}$ cells from tamoxifen-

642 treated Col1a2-Cre^{ERT2}/ZsGreen mice are transplanted into 5-FU-conditioned WT recipients.

643 (D and E) Detection (D) and characterization (E) of $ZsGreen^{+}CD45^{+}$ cells in BM and blood of

644 WT 5-FU-conditioned mice (n=5), 4 weeks post-transplant of VE-

645 Cadherin^{+}CD45^{-}ZsGreen^{+}/Col1a2^{+} cells. Control FU-conditioned WT mice (n=4) received no

646 cell transplant (D).

647 (F) Time course of ZsGreen^{+} PBMC detection in control (Cdh5-Cre^{+}/ZsGreen^{+}) and Runx1$^{EC\text{-}KI}$

648 (Cdh5-Cre^{+}/ZsGreen^{+}/Runx1-KI) mice (n=10 per group).

649 (G and H) Representative images (G) and quantification (H) of ZsGreen^{+} cells from OP9 cell-

650 supported cultures of BM cells from tamoxifen-treated Cdh5-Cre^{+}/ZsGreen^{+} (n=11) and

651 Runx1$^{EC\text{-}KI}$ mice (n=5).

652 (I and J) Representative flow cytometry plots (I) and quantification (J) of CD45^{+}ZsGreen^{+} cells

653 from OP9 cell-supported BM cell cultures (n=5/group).

654 Dots represent individual mice. Data are shown as mean ± SD. **$p<0.01$, ***$p < 0.001$ by

655 Student's t test.

656

657 **REFERENCES**

658 1. Jaffredo, T., Gautier, R., Eichmann, A., and Dieterlen-Lievre, F. (1998). Intraaortic

659 hemopoietic cells are derived from endothelial cells during ontogeny. Development *125*,

660 4575-4583. 10.1242/dev.125.22.4575.

661 2. Zovein, A.C., Hofmann, J.J., Lynch, M., French, W.J., Turlo, K.A., Yang, Y., Becker,

662 M.S., Zanetta, L., Dejana, E., Gasson, J.C., et al. (2008). Fate tracing reveals the

663 endothelial origin of hematopoietic stem cells. Cell Stem Cell *3*, 625-636.

664 10.1016/j.stem.2008.09.018.

665 3. Bertrand, J.Y., Chi, N.C., Santoso, B., Teng, S., Stainier, D.Y., and Traver, D. (2010).
666 Haematopoietic stem cells derive directly from aortic endothelium during development.
667 Nature *464*, 108-111. 10.1038/nature08738.
668 4. Boisset, J.C., van Cappellen, W., Andrieu-Soler, C., Galjart, N., Dzierzak, E., and Robin,
669 C. (2010). In vivo imaging of haematopoietic cells emerging from the mouse aortic
670 endothelium. Nature *464*, 116-120. 10.1038/nature08764.
671 5. Yokomizo, T., and Dzierzak, E. (2010). Three-dimensional cartography of hematopoietic
672 clusters in the vasculature of whole mouse embryos. Development *137*, 3651-3661.
673 10.1242/dev.051094.
674 6. Chen, M.J., Li, Y., De Obaldia, M.E., Yang, Q., Yzaguirre, A.D., Yamada-Inagawa, T.,
675 Vink, C.S., Bhandoola, A., Dzierzak, E., and Speck, N.A. (2011). Erythroid/myeloid
676 progenitors and hematopoietic stem cells originate from distinct populations of
677 endothelial cells. Cell Stem Cell *9*, 541-552. 10.1016/j.stem.2011.10.003.
678 7. Frame, J.M., Fegan, K.H., Conway, S.J., McGrath, K.E., and Palis, J. (2016). Definitive
679 Hematopoiesis in the Yolk Sac Emerges from Wnt-Responsive Hemogenic Endothelium
680 Independently of Circulation and Arterial Identity. Stem Cells *34*, 431-444.
681 10.1002/stem.2213.
682 8. Rhodes, K.E., Gekas, C., Wang, Y., Lux, C.T., Francis, C.S., Chan, D.N., Conway, S.,
683 Orkin, S.H., Yoder, M.C., and Mikkola, H.K. (2008). The emergence of hematopoietic
684 stem cells is initiated in the placental vasculature in the absence of circulation. Cell Stem
685 Cell *2*, 252-263. 10.1016/j.stem.2008.01.001.
686 9. Nakano, H., Liu, X., Arshi, A., Nakashima, Y., van Handel, B., Sasidharan, R., Harmon,
687 A.W., Shin, J.H., Schwartz, R.J., Conway, S.J., et al. (2013). Haemogenic endocardium

688 contributes to transient definitive haematopoiesis. Nat Commun *4*, 1564.
689 10.1038/ncomms2569.
690 10. Goldie, L.C., Lucitti, J.L., Dickinson, M.E., and Hirschi, K.K. (2008). Cell signaling
691 directing the formation and function of hemogenic endothelium during murine
692 embryogenesis. Blood *112*, 3194-3204. 10.1182/blood-2008-02-139055.
693 11. Marcelo, K.L., Goldie, L.C., and Hirschi, K.K. (2013). Regulation of endothelial cell
694 differentiation and specification. Circ Res *112*, 1272-1287.
695 10.1161/CIRCRESAHA.113.300506.
696 12. Hirschi, K.K. (2012). Hemogenic endothelium during development and beyond. Blood
697 *119*, 4823-4827. 10.1182/blood-2011-12-353466.
698 13. Yoshimoto, M., Porayette, P., Glosson, N.L., Conway, S.J., Carlesso, N., Cardoso, A.A.,
699 Kaplan, M.H., and Yoder, M.C. (2012). Autonomous murine T-cell progenitor
700 production in the extra-embryonic yolk sac before HSC emergence. Blood *119*, 5706-
701 5714. 10.1182/blood-2011-12-397489.
702 14. Lin, Y., Yoder, M.C., and Yoshimoto, M. (2014). Lymphoid progenitor emergence in the
703 murine embryo and yolk sac precedes stem cell detection. Stem Cells Dev *23*, 1168-1177.
704 10.1089/scd.2013.0536.
705 15. Iturri, L., Freyer, L., Biton, A., Dardenne, P., Lallemand, Y., and Gomez Perdiguero, E.
706 (2021). Megakaryocyte production is sustained by direct differentiation from
707 erythromyeloid progenitors in the yolk sac until midgestation. Immunity *54*, 1433-1446
708 e1435. 10.1016/j.immuni.2021.04.026.
709 16. Soares-da-Silva, F., Freyer, L., Elsaid, R., Burlen-Defranoux, O., Iturri, L., Sismeiro, O.,
710 Pinto-do, O.P., Gomez-Perdiguero, E., and Cumano, A. (2021). Yolk sac, but not

711 hematopoietic stem cell-derived progenitors, sustain erythropoiesis throughout murine
712 embryonic life. J Exp Med *218*. 10.1084/jem.20201729.
713 17. de Bruijn, M.F., Ma, X., Robin, C., Ottersbach, K., Sanchez, M.J., and Dzierzak, E.
714 (2002). Hematopoietic stem cells localize to the endothelial cell layer in the midgestation
715 mouse aorta. Immunity *16*, 673-683. 10.1016/s1074-7613(02)00313-8.
716 18. Hadland, B.K., Varnum-Finney, B., Poulos, M.G., Moon, R.T., Butler, J.M., Rafii, S.,
717 and Bernstein, I.D. (2015). Endothelium and NOTCH specify and amplify aorta-gonad-
718 mesonephros-derived hematopoietic stem cells. J Clin Invest *125*, 2032-2045.
719 10.1172/JCI80137.
720 19. Patel, S.H., Christodoulou, C., Weinreb, C., Yu, Q., da Rocha, E.L., Pepe-Mooney, B.J.,
721 Bowling, S., Li, L., Osorio, F.G., Daley, G.Q., and Camargo, F.D. (2022). Lifelong
722 multilineage contribution by embryonic-born blood progenitors. Nature *606*, 747-753.
723 10.1038/s41586-022-04804-z.
724 20. Ding, B.S., Nolan, D.J., Butler, J.M., James, D., Babazadeh, A.O., Rosenwaks, Z., Mittal,
725 V., Kobayashi, H., Shido, K., Lyden, D., et al. (2010). Inductive angiocrine signals from
726 sinusoidal endothelium are required for liver regeneration. Nature *468*, 310-315.
727 10.1038/nature09493.
728 21. Kobayashi, H., Butler, J.M., O'Donnell, R., Kobayashi, M., Ding, B.S., Bonner, B., Chiu,
729 V.K., Nolan, D.J., Shido, K., Benjamin, L., and Rafii, S. (2010). Angiocrine factors from
730 Akt-activated endothelial cells balance self-renewal and differentiation of haematopoietic
731 stem cells. Nat Cell Biol *12*, 1046-1056. 10.1038/ncb2108.

732 22. Butler, J.M., Gars, E.J., James, D.J., Nolan, D.J., Scandura, J.M., and Rafii, S. (2012).
733 Development of a vascular niche platform for expansion of repopulating human cord
734 blood stem and progenitor cells. Blood *120*, 1344-1347. 10.1182/blood-2011-12-398115.
735 23. Yzaguirre, A.D., and Speck, N.A. (2016). Insights into blood cell formation from
736 hemogenic endothelium in lesser-known anatomic sites. Dev Dyn *245*, 1011-1028.
737 10.1002/dvdy.24430.
738 24. Zhu, Q., Gao, P., Tober, J., Bennett, L., Chen, C., Uzun, Y., Li, Y., Howell, E.D.,
739 Mumau, M., Yu, W., et al. (2020). Developmental trajectory of prehematopoietic stem
740 cell formation from endothelium. Blood *136*, 845-856. 10.1182/blood.2020004801.
741 25. North, T., Gu, T.L., Stacy, T., Wang, Q., Howard, L., Binder, M., Marin-Padilla, M., and
742 Speck, N.A. (1999). Cbfa2 is required for the formation of intra-aortic hematopoietic
743 clusters. Development *126*, 2563-2575. 10.1242/dev.126.11.2563.
744 26. Chen, M.J., Yokomizo, T., Zeigler, B.M., Dzierzak, E., and Speck, N.A. (2009). Runx1 is
745 required for the endothelial to haematopoietic cell transition but not thereafter. Nature
746 *457*, 887-891. 10.1038/nature07619.
747 27. Eliades, A., Wareing, S., Marinopoulou, E., Fadlullah, M.Z.H., Patel, R., Grabarek, J.B.,
748 Plusa, B., Lacaud, G., and Kouskoff, V. (2016). The Hemogenic Competence of
749 Endothelial Progenitors Is Restricted by Runx1 Silencing during Embryonic
750 Development. Cell Rep *15*, 2185-2199. 10.1016/j.celrep.2016.05.001.
751 28. Yzaguirre, A.D., Howell, E.D., Li, Y., Liu, Z., and Speck, N.A. (2018). Runx1 is
752 sufficient for blood cell formation from non-hemogenic endothelial cells in vivo only
753 during early embryogenesis. Development *145*, dev158162. 10.1242/dev.158162.

754 29. Lis, R., Karrasch, C.C., Poulos, M.G., Kunar, B., Redmond, D., Duran, J.G.B., Badwe,
755 C.R., Schachterle, W., Ginsberg, M., Xiang, J., et al. (2017). Conversion of adult
756 endothelium to immunocompetent haematopoietic stem cells. Nature *545*, 439-445.
757 10.1038/nature22326.
758 30. Sandler, V.M., Lis, R., Liu, Y., Kedem, A., James, D., Elemento, O., Butler, J.M.,
759 Scandura, J.M., and Rafii, S. (2014). Reprogramming human endothelial cells to
760 haematopoietic cells requires vascular induction. Nature *511*, 312-318.
761 10.1038/nature13547.
762 31. Pelosi, E., Castelli, G., Martin-Padura, I., Bordoni, V., Santoro, S., Conigliaro, A., Cerio,
763 A.M., De Santis Puzzonia, M., Marighetti, P., Biffoni, M., et al. (2012). Human haemato-
764 endothelial precursors: cord blood CD34+ cells produce haemogenic endothelium. PLoS
765 One *7*, e51109. 10.1371/journal.pone.0051109.
766 32. Kilani, B., Gourdou-Latyszenok, V., Guy, A., Bats, M.L., Peghaire, C., Parrens, M.,
767 Renault, M.A., Duplaa, C., Villeval, J.L., Rautou, P.E., et al. (2019). Comparison of
768 endothelial promoter efficiency and specificity in mice reveals a subset of Pdgfb-positive
769 hematopoietic cells. J Thromb Haemost *17*, 827-840. 10.1111/jth.14417.
770 33. Pei, W., Shang, F., Wang, X., Fanti, A.K., Greco, A., Busch, K., Klapproth, K., Zhang,
771 Q., Quedenau, C., Sauer, S., et al. (2020). Resolving Fates and Single-Cell
772 Transcriptomes of Hematopoietic Stem Cell Clones by PolyloxExpress Barcoding. Cell
773 Stem Cell *27*, 383-395 e388. 10.1016/j.stem.2020.07.018.
774 34. Hernandez, G.E., Ma, F., Martinez, G., Firozabadi, N.B., Salvador, J., Juang, L.J., Leung,
775 J., Zhao, P., Lopez, D.A., Ardehali, R., et al. (2022). Aortic intimal resident macrophages

776 are essential for maintenance of the non-thrombogenic intravascular state. Nat
777 Cardiovasc Res *1*, 67-84. 10.1038/s44161-021-00006-4.
778 35. Gentek, R., Ghigo, C., Hoeffel, G., Bulle, M.J., Msallam, R., Gautier, G., Launay, P.,
779 Chen, J., Ginhoux, F., and Bajenoff, M. (2018). Hemogenic Endothelial Fate Mapping
780 Reveals Dual Developmental Origin of Mast Cells. Immunity *48*, 1160-1171 e1165.
781 10.1016/j.immuni.2018.04.025.
782 36. Wang, L., Benedito, R., Bixel, M.G., Zeuschner, D., Stehling, M., Savendahl, L., Haigh,
783 J.J., Snippert, H., Clevers, H., Breier, G., et al. (2013). Identification of a clonally
784 expanding haematopoietic compartment in bone marrow. EMBO J *32*, 219-230.
785 10.1038/emboj.2012.308.
786 37. Sorensen, I., Adams, R.H., and Gossler, A. (2009). DLL1-mediated Notch activation
787 regulates endothelial identity in mouse fetal arteries. Blood *113*, 5680-5688.
788 10.1182/blood-2008-08-174508.
789 38. Pitulescu, M.E., Schmidt, I., Benedito, R., and Adams, R.H. (2010). Inducible gene
790 targeting in the neonatal vasculature and analysis of retinal angiogenesis in mice. Nat
791 Protoc *5*, 1518-1534. 10.1038/nprot.2010.113.
792 39. Okabe, K., Kobayashi, S., Yamada, T., Kurihara, T., Tai-Nagara, I., Miyamoto, T.,
793 Mukouyama, Y.S., Sato, T.N., Suda, T., Ema, M., and Kubota, Y. (2014). Neurons limit
794 angiogenesis by titrating VEGF in retina. Cell *159*, 584-596. 10.1016/j.cell.2014.09.025.
795 40. Alvarez-Aznar, A., Martinez-Corral, I., Daubel, N., Betsholtz, C., Makinen, T., and
796 Gaengel, K. (2020). Tamoxifen-independent recombination of reporter genes limits
797 lineage tracing and mosaic analysis using CreER(T2) lines. Transgenic Res *29*, 53-68.
798 10.1007/s11248-019-00177-8.

799 41. Stifter, S.A., and Greter, M. (2020). STOP floxing around: Specificity and leakiness of
800 inducible Cre/loxP systems. Eur J Immunol *50*, 338-341. 10.1002/eji.202048546.
801 42. Liu, Y., Suckale, J., Masjkur, J., Magro, M.G., Steffen, A., Anastassiadis, K., and
802 Solimena, M. (2010). Tamoxifen-independent recombination in the RIP-CreER mouse.
803 PLoS One *5*, e13533. 10.1371/journal.pone.0013533.
804 43. Vooijs, M., Jonkers, J., and Berns, A. (2001). A highly efficient ligand-regulated Cre
805 recombinase mouse line shows that recombination is position dependent. Embo Reports
806 *2*, 292-297. 10.1093/embo-reports/kve064.
807 44. Nakano, T. (1996). In vitro development of hematopoietic system from mouse embryonic
808 stem cells: a new approach for embryonic hematopoiesis. Int J Hematol *65*, 1-8.
809 10.1016/s0925-5710(96)00531-2.
810 45. Xu, C., Gao, X., Wei, Q., Nakahara, F., Zimmerman, S.E., Mar, J., and Frenette, P.S.
811 (2018). Stem cell factor is selectively secreted by arterial endothelial cells in bone
812 marrow. Nat Commun *9*, 2449. 10.1038/s41467-018-04726-3.
813 46. Yoder, M.C., Hiatt, K., Dutt, P., Mukherjee, P., Bodine, D.M., and Orlic, D. (1997).
814 Characterization of definitive lymphohematopoietic stem cells in the day 9 murine yolk
815 sac. Immunity *7*, 335-344. 10.1016/s1074-7613(00)80355-6.
816 47. Auffray, C., Sieweke, M.H., and Geissmann, F. (2009). Blood monocytes: development,
817 heterogeneity, and relationship with dendritic cells. Annu Rev Immunol *27*, 669-692.
818 10.1146/annurev.immunol.021908.132557.
819 48. Ghosn, E.E., Cassado, A.A., Govoni, G.R., Fukuhara, T., Yang, Y., Monack, D.M.,
820 Bortoluci, K.R., Almeida, S.R., Herzenberg, L.A., and Herzenberg, L.A. (2010). Two

821 physically, functionally, and developmentally distinct peritoneal macrophage subsets.
822 Proc Natl Acad Sci U S A *107*, 2568-2573. 10.1073/pnas.0915000107.
823 49. Kucinski, I., Campos, J., Barile, M., Severi, F., Bohin, N., Moreira, P.N., Allen, L.,
824 Lawson, H., Haltalli, M.L.R., Kinston, S.J., et al. (2024). A time- and single-cell-resolved
825 model of murine bone marrow hematopoiesis. Cell Stem Cell *31*, 244-259 e210.
826 10.1016/j.stem.2023.12.001.
827 50. Skulimowska, I., Morys, J., Sosniak, J., Gonka, M., Gulati, G., Sinha, R., Kowalski, K.,
828 Mosiolek, S., Weissman, I.L., Jozkowicz, A., et al. (2024). Polyclonal regeneration of
829 mouse bone marrow endothelial cells after irradiative conditioning. Cell Rep *43*, 114779.
830 10.1016/j.celrep.2024.114779.
831 51. Pei, W., Feyerabend, T.B., Rossler, J., Wang, X., Postrach, D., Busch, K., Rode, I.,
832 Klapproth, K., Dietlein, N., Quedenau, C., et al. (2017). Polylox barcoding reveals
833 haematopoietic stem cell fates realized in vivo. Nature *548*, 456-460.
834 10.1038/nature23653.
835 52. Pei, W., Wang, X., Rossler, J., Feyerabend, T.B., Hofer, T., and Rodewald, H.R. (2019).
836 Using Cre-recombinase-driven Polylox barcoding for in vivo fate mapping in mice. Nat
837 Protoc *14*, 1820-1840. 10.1038/s41596-019-0163-5.
838 53. Baryawno, N., Przybylski, D., Kowalczyk, M.S., Kfoury, Y., Severe, N., Gustafsson, K.,
839 Kokkaliaris, K.D., Mercier, F., Tabaka, M., Hofree, M., et al. (2019). A Cellular
840 Taxonomy of the Bone Marrow Stroma in Homeostasis and Leukemia. Cell *177*, 1915-
841 1932 e1916. 10.1016/j.cell.2019.04.040.
842 54. Tikhonova, A.N., Dolgalev, I., Hu, H., Sivaraj, K.K., Hoxha, E., Cuesta-Dominguez, A.,
843 Pinho, S., Akhmetzyanova, I., Gao, J., Witkowski, M., et al. (2019). The bone marrow

844 microenvironment at single-cell resolution. Nature *569*, 222-228. 10.1038/s41586-019-
845 1104-8.
846 55. Baccin, C., Al-Sabah, J., Velten, L., Helbling, P.M., Grunschlager, F., Hernandez-
847 Malmierca, P., Nombela-Arrieta, C., Steinmetz, L.M., Trumpp, A., and Haas, S. (2020).
848 Combined single-cell and spatial transcriptomics reveal the molecular, cellular and
849 spatial bone marrow niche organization. Nat Cell Biol *22*, 38-48. 10.1038/s41556-019-
850 0439-6.
851 56. Sivaraj, K.K., Jeong, H.W., Dharmalingam, B., Zeuschner, D., Adams, S., Potente, M.,
852 and Adams, R.H. (2021). Regional specialization and fate specification of bone stromal
853 cells in skeletal development. Cell Rep *36*, 109352. 10.1016/j.celrep.2021.109352.
854 57. Zhong, L., Yao, L., Tower, R.J., Wei, Y., Miao, Z., Park, J., Shrestha, R., Wang, L., Yu,
855 W., Holdreith, N., et al. (2020). Single cell transcriptomics identifies a unique adipose
856 lineage cell population that regulates bone marrow environment. Elife *9*, e54695.
857 10.7554/eLife.54695.
858 58. Lang, A., Collins, J.M., Nijsure, M.P., Belali, S., Khan, M.P., Moharrer, Y., Schipani, E.,
859 Yien, Y.Y., Fan, Y., Gelinsky, M., et al. (2025). Local erythropoiesis directs oxygen
860 availability in bone fracture repair. bioRxiv, 2025.2001. 2010.632440.
861 10.1101/2025.01.10.632440.
862 59. Smith, N.P., Janton, C., Alcantara, A.C.M., George, M., Mankongtreecheep, K., Mao, G.,
863 Villani, A.-C., and Kronenberg, H.M. (2025). Single cell RNA sequencing shows that
864 cells expressing Sox9 postnatally populate most skeletal lineages in mouse bone. Journal
865 of Bone and Mineral Research, zjaf043.

866 60. Howell, E.D., Yzaguirre, A.D., Gao, P., Lis, R., He, B., Lakadamyali, M., Rafii, S., Tan,
867 K., and Speck, N.A. (2021). Efficient hemogenic endothelial cell specification by
868 RUNX1 is dependent on baseline chromatin accessibility of RUNX1-regulated TGFβ
869 target genes. Genes & Development *35*, 1475-1489. 10.1101/gad.348738.121.
870 61. Serina Secanechia, Y.N., Bergiers, I., Rogon, M., Arnold, C., Descostes, N., Le, S.,
871 Lopez-Anguita, N., Ganter, K., Kapsali, C., Bouilleau, L., et al. (2022). Identifying a
872 novel role for the master regulator Tal1 in the Endothelial to Hematopoietic Transition.
873 Sci Rep *12*, 16974. 10.1038/s41598-022-20906-0.
874 62. Bergiers, I., Andrews, T., Vargel Bolukbasi, O., Buness, A., Janosz, E., Lopez-Anguita,
875 N., Ganter, K., Kosim, K., Celen, C., Itir Percin, G., et al. (2018). Single-cell
876 transcriptomics reveals a new dynamical function of transcription factors during
877 embryonic hematopoiesis. Elife *7*, e29312. 10.7554/eLife.29312.
878 63. Guibentif, C., Ronn, R.E., Boiers, C., Lang, S., Saxena, S., Soneji, S., Enver, T.,
879 Karlsson, G., and Woods, N.B. (2017). Single-Cell Analysis Identifies Distinct Stages of
880 Human Endothelial-to-Hematopoietic Transition. Cell Rep *19*, 10-19.
881 10.1016/j.celrep.2017.03.023.
882 64. Wilson, N.K., Foster, S.D., Wang, X., Knezevic, K., Schutte, J., Kaimakis, P., Chilarska,
883 P.M., Kinston, S., Ouwehand, W.H., Dzierzak, E., et al. (2010). Combinatorial
884 transcriptional control in blood stem/progenitor cells: genome-wide analysis of ten major
885 transcriptional regulators. Cell Stem Cell *7*, 532-544. 10.1016/j.stem.2010.07.016.
886 65. Kalucka, J., de Rooij, L., Goveia, J., Rohlenova, K., Dumas, S.J., Meta, E., Conchinha,
887 N.V., Taverna, F., Teuwen, L.A., Veys, K., et al. (2020). Single-Cell Transcriptome Atlas
888 of Murine Endothelial Cells. Cell *180*, 764-779 e720. 10.1016/j.cell.2020.01.015.

889 66. Qi, L., Huang, C., Wu, X., Tao, Y., Yan, J., Shi, T., Cao, C., Han, L., Qiu, M., Ma, Q., et
890 al. (2017). Hierarchical Specification of Pruriceptors by Runt-Domain Transcription
891 Factor Runx1. J Neurosci *37*, 5549-5561. 10.1523/JNEUROSCI.0094-17.2017.
892 67. Yvernogeau, L., Gautier, R., Petit, L., Khoury, H., Relaix, F., Ribes, V., Sang, H.,
893 Charbord, P., Souyri, M., Robin, C., and Jaffredo, T. (2019). In vivo generation of
894 haematopoietic stem/progenitor cells from bone marrow-derived haemogenic
895 endothelium. Nat Cell Biol *21*, 1334-1345. 10.1038/s41556-019-0410-6.
896 68. Richard, C., Drevon, C., Canto, P.Y., Villain, G., Bollerot, K., Lempereur, A., Teillet,
897 M.A., Vincent, C., Rossello Castillo, C., Torres, M., et al. (2013). Endothelio-
898 mesenchymal interaction controls runx1 expression and modulates the notch pathway to
899 initiate aortic hematopoiesis. Dev Cell *24*, 600-611. 10.1016/j.devcel.2013.02.011.
900 69. Dignum, T., Varnum-Finney, B., Srivatsan, S.R., Dozono, S., Waltner, O., Heck, A.M.,
901 Ishida, T., Nourigat-McKay, C., Jackson, D.L., Rafii, S., et al. (2021). Multipotent
902 progenitors and hematopoietic stem cells arise independently from hemogenic
903 endothelium in the mouse embryo. Cell Rep *36*, 109675. 10.1016/j.celrep.2021.109675.
904 70. Ambler, C.A., Nowicki, J.L., Burke, A.C., and Bautch, V.L. (2001). Assembly of trunk
905 and limb blood vessels involves extensive migration and vasculogenesis of somite-
906 derived angioblasts. Dev Biol *234*, 352-364. 10.1006/dbio.2001.0267.
907 71. Pudliszewski, M., and Pardanaud, L. (2005). Vasculogenesis and angiogenesis in the
908 mouse embryo studied using quail/mouse chimeras. Int J Dev Biol *49*, 355-361.
909 10.1387/ijdb.041956mp.

910 72. Pardanaud, L., and Dieterlen-Lievre, F. (1999). Manipulation of the
911 angiopoietic/hemangiopoietic commitment in the avian embryo. Development *126*, 617-
912 627. 10.1242/dev.126.4.617.
913 73. Qiu, J., Fan, X., Wang, Y., Jin, H., Song, Y., Han, Y., Huang, S., Meng, Y., Tang, F., and
914 Meng, A. (2016). Embryonic hematopoiesis in vertebrate somites gives rise to definitive
915 hematopoietic stem cells. J Mol Cell Biol *8*, 288-301. 10.1093/jmcb/mjw024.
916 74. Nguyen, P.D., Hollway, G.E., Sonntag, C., Miles, L.B., Hall, T.E., Berger, S., Fernandez,
917 K.J., Gurevich, D.B., Cole, N.J., Alaei, S., et al. (2014). Haematopoietic stem cell
918 induction by somite-derived endothelial cells controlled by meox1. Nature *512*, 314-318.
919 10.1038/nature13678.
920 75. Morikawa, S., Mabuchi, Y., Niibe, K., Suzuki, S., Nagoshi, N., Sunabori, T., Shimmura,
921 S., Nagai, Y., Nakagawa, T., Okano, H., and Matsuzaki, Y. (2009). Development of
922 mesenchymal stem cells partially originate from the neural crest. Biochem Biophys Res
923 Commun *379*, 1114-1119. 10.1016/j.bbrc.2009.01.031.
924 76. Takashima, Y., Era, T., Nakao, K., Kondo, S., Kasuga, M., Smith, A.G., and Nishikawa,
925 S. (2007). Neuroepithelial cells supply an initial transient wave of MSC differentiation.
926 Cell *129*, 1377-1388. 10.1016/j.cell.2007.04.028.
927 77. Vodyanik, M.A., Yu, J., Zhang, X., Tian, S., Stewart, R., Thomson, J.A., and Slukvin, II
928 (2010). A mesoderm-derived precursor for mesenchymal stem and endothelial cells. Cell
929 Stem Cell *7*, 718-729. 10.1016/j.stem.2010.11.011.
930 78. Bianco, P., Robey, P.G., and Simmons, P.J. (2008). Mesenchymal stem cells: revisiting
931 history, concepts, and assays. Cell Stem Cell *2*, 313-319. 10.1016/j.stem.2008.03.002.

932 79. Oswald, J., Boxberger, S., Jorgensen, B., Feldmann, S., Ehninger, G., Bornhauser, M.,
933 and Werner, C. (2004). Mesenchymal stem cells can be differentiated into endothelial
934 cells in vitro. Stem Cells *22*, 377-384. 10.1634/stemcells.22-3-377.
935 80. Conrad, C., Niess, H., Huss, R., Huber, S., von Luettichau, I., Nelson, P.J., Ott, H.C.,
936 Jauch, K.W., and Bruns, C.J. (2009). Multipotent mesenchymal stem cells acquire a
937 lymphendothelial phenotype and enhance lymphatic regeneration in vivo. Circulation
938 *119*, 281-289. 10.1161/CIRCULATIONAHA.108.793208.
939 81. Ubil, E., Duan, J., Pillai, I.C., Rosa-Garrido, M., Wu, Y., Bargiacchi, F., Lu, Y.,
940 Stanbouly, S., Huang, J., Rojas, M., et al. (2014). Mesenchymal-endothelial transition
941 contributes to cardiac neovascularization. Nature *514*, 585-590. 10.1038/nature13839.
942 82. Crisan, M. (2013). Transition of mesenchymal stem/stromal cells to endothelial cells.
943 Stem Cell Res Ther *4*, 95. 10.1186/scrt306.
944 83. Xu, Y., and Kovacic, J.C. (2023). Endothelial to Mesenchymal Transition in Health and
945 Disease. Annu Rev Physiol *85*, 245-267. 10.1146/annurev-physiol-032222-080806.
946 84. Termini, C.M., Pang, A., Fang, T., Roos, M., Chang, V.Y., Zhang, Y., Setiawan, N.J.,
947 Signaevskaia, L., Li, M., Kim, M.M., et al. (2021). Neuropilin 1 regulates bone marrow
948 vascular regeneration and hematopoietic reconstitution. Nat Commun *12*, 6990.
949 10.1038/s41467-021-27263-y.
950 85. Zheng, B., Zhang, Z., Black, C.M., de Crombrugghe, B., and Denton, C.P. (2002).
951 Ligand-dependent genetic recombination in fibroblasts : a potentially powerful technique
952 for investigating gene function in fibrosis. Am J Pathol *160*, 1609-1617. 10.1016/S0002-
953 9440(10)61108-X.

954 86. Madisen, L., Zwingman, T.A., Sunkin, S.M., Oh, S.W., Zariwala, H.A., Gu, H., Ng, L.L.,
955 Palmiter, R.D., Hawrylycz, M.J., Jones, A.R., et al. (2010). A robust and high-throughput
956 Cre reporting and characterization system for the whole mouse brain. Nat Neurosci *13*,
957 133-140. 10.1038/nn.2467.
958 87. Muzumdar, M.D., Tasic, B., Miyamichi, K., Li, L., and Luo, L. (2007). A global double-
959 fluorescent Cre reporter mouse. Genesis *45*, 593-605. 10.1002/dvg.20335.
960 88. Happerfield, L., Saward, R., Grimwade, L., Bloxham, D., and Erber, W. (2008).
961 Automated immunostaining of cell smears: an alternative to flow cytometry8.
962 International Journal of Laboratory Hematology *30*, 8.
963

964 **METHODS**

965 **RESOURCES TABLE**

REAGENT or RESOURCE	SOURCE	IDENTIFIER
Antibodies		
BD Horizon™ BV786 Rat Anti-Mouse CD117	BD Biosciences	564012; RRID:AB_2732005
Brilliant Violet 421™ anti-mouse CD117 (c-Kit) Antibody	BioLegend	105828; RRID:AB_11204256
Brilliant Violet 785™ anti-mouse CD117 (c-Kit) Antibody	BioLegend	105841; RRID:AB_2629799
BD Pharmingen™ APC Rat Anti-CD11b	BD Biosciences	553312; RRID:AB_398535
PerCP/Cyanine5.5 anti-mouse CD150 (SLAM) Antibody	BioLegend	115922; RRID:AB_2303663
APC/Fire™ 750 anti-mouse CD150 (SLAM) Antibody	BioLegend	115940; RRID:AB_2629587
BD Pharmingen™ APC-Cy™7 Rat Anti-Mouse CD19	BD Biosciences	557655; RRID:AB_396770
BD Horizon™ BUV737 Rat Anti-Mouse CD19	BD Biosciences	612781; RRID:AB_2870110

Brilliant Violet 510™ anti-mouse CD3 Antibody	BioLegend	100234; RRID:AB_2562555
BD Pharmingen™ Purified Rat Anti-Mouse CD31	BD Biosciences	553370; RRID:AB_394816
BV421 anti-mouse Cd31	BD Biosciences	563356; RRID:AB_2738154
Brilliant Violet 421™ anti-mouse CD31 Antibody	BioLegend	102424; RRID:AB_2650892
Brilliant Violet 605™ anti-mouse CD31 Antibody	BioLegend	102427; RRID:AB_2563982
BD Pharmingen™ Alexa Fluor® 700 Rat Anti-Mouse CD45	BD Biosciences	560510; RRID:AB_1645208
BD OptiBuild™ BUV615 Rat Anti-Mouse CD45	BD Biosciences	751170; RRID:AB_2875194
PE anti-mouse CD45 Antibody	BioLegend	103106; RRID:AB_312971
PerCP/Cyanine5.5 anti-mouse CD45 Antibody	BioLegend	103131; RRID:AB_893344 103132; RRID:AB_893340
BD Horizon™ BV510 Hamster Anti-Mouse CD48	BD Biosciences	563536; RRID:AB_2738266
APC/Cyanine7 anti-mouse CD48 Antibody	BioLegend	103432; RRID:AB_2561463
Brilliant Violet 510™ anti-mouse CD48 Antibody	BioLegend	103443; RRID:AB_2650826
Collagen I Polyclonal Antibody, Biotin	Invitrogen	PA1-28530; RRID: AB_1956957
Endomucin Monoclonal Antibody (eBioV.7C7 (V.7C7)), eFluor™ 660	Invitrogen	50-5851-82; RRID:AB_11220465
Anti-Endomucin Antibody (V.7C7) AF546	Santa Cruz Biotechnology	sc-65495 AF546; RRID:AB_2100037
BD Pharmingen™ PE-Cy™7 Rat Anti-Mouse Ly-6G	BD Biosciences	560601; RRID:AB_1727562
BD Horizon™ BUV395 Rat Anti-Mouse Ly-6G	BD Biosciences	563978; RRID:AB_2716852
BD Pharmingen™ APC Mouse Lineage Antibody Cocktail, with Isotype Control	BD Biosciences	558074; RRID:AB_1645213
Goat anti-Rat IgG (H+L) Highly Cross-Adsorbed Secondary Antibody, Alexa Fluor™ Plus 594	Invitrogen	A48264; RRID:AB_2896333
RUNX1 Monoclonal Antibody (RXDMC), PE, eBioscience™	Invitrogen	12-9816-80; RRID:AB_11151519
BD Pharmingen™ PE-Cy™7 Rat Anti-Mouse Ly-6A/E	BD Biosciences	561021; RRID:AB_2034021
PE/Cy7 anti-mouse Ly-6A/E (Sca-1)	BioLegend	108114; RRID:AB_493596
PerCP/Cyanine5.5 anti-mouse TER-119/Erythroid Cells Antibody	BioLegend	116228; RRID:AB_893636
Brilliant Violet 605™ anti-mouse TER-119/Erythroid Cells Antibody	BioLegend	116239; RRID:AB_2562447

BD Pharmingen™ Alexa Fluor® 647 Rat Anti-Mouse CD144	BD Biosciences	562242; RRID:AB_2737608
BD Pharmingen™ PE Rat Anti-Mouse CD144	BD Biosciences	562243; RRID:AB_2737609
BUV737 Rat Anti-Mouse CD144	BD Biosciences	741792; RRID:AB_2871138
Alexa Fluor® 647 anti-mouse CD144 (VE-cadherin) Antibody	BioLegend	138006; RRID:AB_10569114
BD OptiBuild™ RB780 Rat Anti-Mouse CD144	BD Biosciences	755945; RRID:AB_3683567
PE anti-mouse CD144 (VE-cadherin) Antibody	BioLegend	138010; RRID:AB_10641139
PE/Cyanine7 anti-mouse CD144 (VE-cadherin) Antibody	BioLegend	138015; RRID:AB_2562885 138016; RRID:AB_2562886
PE anti-mouse CD144 (VE-cadherin) Antibody	BioLegend	138105; RRID:AB_2077941
Chemicals, peptides, and recombinant proteins		
5-FLUOROURACIL	Sigma-Aldrich	F6627
7-AAD Viability Stain SOLN	Life Technologies Corp.	00-6993-50
7-Aminoactinomycin D	Sigma-Aldrich	A9400
ACETONE	MALLINCKRODT	2440
ACK lysing Buffer	Lonza	10-548E
Acrylamide/Bis 19:1, 40% (w/v) solution	Invitrogen	AM9024
Acrylamide/Bis-acrylamide 19:1	Sigma-Aldrich	A2917
Acridine Orange / Propidium Iodide Stain	Logos Biosystems	F23001
AMPure beads	Beckman Coulter	A63881
Antibiotic-Antimycotic	Gibco	15240062
Anti-Rat Ig, κ/Negative Control (BSA) Compensation Plus (7.5 μm) Particles Set	BD Biosciences	560499
Anti-Rat Ig, κ/Negative Control Compensation Particles Set	BD Biosciences	552844
APC/Fire™ 750 Streptavidin	BioLegend	405250
Azide-Free Fc Receptor Blocker	INNOVEX	NB335-60
Bovine Serum Albumin solution	MP Biomedicals	160069
CellROX Orange Flow Cytometry Assay Kit	Invitrogen	C10493
Collagenase Type 2	Worthington Biochemical Corporation	LS004176
Dispase	Worthington Biomedical	LS02109

Deoxyribonuclease	Worthington Biomedical	LS006344
DAPI (4',6-Diamidino-2-Phenylindole, Dilactate)	BioLegend	422801
Dihydroethidium (Hydroethidine)	Invitrogen	D1168
Donkey serum	Sigma-Aldrich	D9663
DRAQ5	Biostatus	DR50200
EDTA (0.5M, pH 8.0)	KD Medical	RGF3130
ETHYL ALCOHOL (200 PROOF ANHYDROUS)	Warner-Graham Co.	201096
Ethylenediamine-N,N,N′,N′-tetra-2-propanol	Sigma-Aldrich	8219401000
Fetal Bovine Serum	Millipore Sigma	F2442-500ML (Lot 24G002)
Fc Receptor Blocker	Innovex	NB309-30
Formalin solution, neutral buffered, 10%	Sigma-Aldrich	HT501128-4L
Gelatin	Sigma-Aldrich	G9391
Goldenrod™ Animal Lancet	Braintree Scientific Inc.	GR-3MM
HBSS	Gibco	14025075
HEPES	Gibco	15630080
Immu-Mount™ mountant	Epredia	9990402
Isoflurane	Baxter	10019036040
Mag-Bind® TotalPure NGS	Omega Bio-tek	M1378-01
Methanol, HPLC Grade	Avantor	JT-9093-03
MojoSort™ Mouse CD45 Nanobeads	BioLegend	480028
Kwik Stop® Stypic Power	Miracle Care	SKU 423615
Lineage Cell Depletion Kit, mouse	MiltenyiBiotec	130-090-858
Lipopolysaccharides	Sigma Aldrich	L2880-25MG
Microscope Slides	MATSUNAMI GLASS IND.	SUMGP12
Neutral Protease, Partially Purified, Animal Free/AF	Worthington Biochemical Corporation	LS02109
Paraformaldehyde (formaldehyde) aqueous solution (20%)	Electron Microscopy Sciences	15713-S
Penicillin-Streptomycin	Gibco	15140-122
Peanut oil	Sigma-Aldrich	P2144
Phusion Green Hot Start II High-Fidelity PCR Master Mix	Thermo Scientific	F566L
pHrodo™ Red E. coli BioParticles	Invitrogen	P35361
Polyvinylpyrrolidone	Sigma-Aldrich	P5288

Propidium iodide	Sigma-Aldrich	P4170
Q5 Hot Start High-Fidelity 2X Master Mix	NEB	M0494S
Richard-Allan Scientific™ Cover glass	Epredia	102424
RNeasy® Micro Kit	QIAGEN	74004
Saponin	Sigma-Aldrich	47036
SPRIselect Beads	Beckman Coulter	B23318
Sucrose	Sigma-Aldrich	S8501
SuperScript™ IV First-Strand Synthesis System	Invitrogen	18091050
Tamoxifen	Sigma-Aldrich	T5648
TaqMan™ Fast Advanced Master Mix	ThermoFisher Scientific	4444557
Thioglycollate Broth	Sigma Aldrich	70157
Tissue-Tek® O.C.T. Compound	SAKURA	4583
Triton™ X-100	Sigma-Aldrich	T9284
Trypsin-EDTA (0.25%), phenol red	Gibco	25200056
TruBond™ 380 Adhesion Slide	Electron Microscopy Sciences	63700-Y10
UNI-TRIEVE	INNOVEX	NB325
VA-044 (Water soluble Azo initiators)	FUJIFILM Labchem Wako	VA-044
VECTASHIELD Vibrance Antifade Mounting Medium	Vector Laboratories	H-1700-10
Zombie Aqua™ Fixable Viability Kit	BioLegend	423101
Zombie NIR™ Fixable Viability Kit	BioLegend	423105
Zombie UV™ Fixable Viability Kit	BioLegend	423107
Zombie Yellow™ Fixable Viability Kit	BioLegend	423103
Zymosan A from Saccharomyces cerevisiae	Sigma Aldrich	Z4250
Critical commercial assays		
Chromium GEM-X Single Cell 3' Kit	10× Genomics	1000686
Chromium GEM-X Single Cell 3' Chip Kit v4	10× Genomics	1000690
Chromium Next GEM Chip G Single Cell Kit	10× Genomics	1000127
Chromium Next GEM Single Cell 3' Kit v3.1	10× Genomics	1000269
Dual Index Kit TT Set	10× Genomics	1000215
NextSeq 2000 P4 Reagents (100 Cycles)	Illumina	20100994

NextSeq 2000 P3 Reagents (100 Cycles)	Illumina	20040559
Deposited data		
Polylox PacBio long-read sequencing data	This Study	PRJNA1079369
Single cell RNA seq data	This Study	PRJNA1079369
Experimental models: Cell lines		
OP9 cells	Dr. Nakano; same line deposited in ATCC	ATCC # CRL-2749; RRID:CVCL_4398
Experimental models: Organisms/strains		
Cdh5-Cre(PAC)^{ERT2}	Drs. R. Adams and M. Boehm; also available from Taconic Biosciences	MGI:3848982 Taconic # 13073
Cdh5-Cre(BAC)^{ERT2}	Drs. Y. Kubota and Y. Mukoyama	MGI:5705396
Col1a2-CreERT	JAX, #029567	MGI:3785760
ZsGreen (Ai6)	JAX, #007906	MGI:3809522
mTmG	JAX, #007676	MGI:3716464
PolyloxExpress	Drs. H. Rodewald and A. Bhandoola	MGI:6470648
Runx1Knock-In	Drs. Q. Ma and N. Speck	MGI:7490340
Oligonucleotides		
mTmG mouse strain genotyping primers (5' – 3')	CTT TAA GCC TGC CCA GAA GA TAG AGC TTG CGG AAC CCT TC AGG GAG CTG CAG TGG AGT AG	JAX: 007676
ZsGreen mouse strain genotyping primers (5' – 3')	AAG GGA GCT GCA GTG GAG TA CCG AAA ATC TGT GGG AAG TC GGC ATT AAA GCA GCG TAT CC AAC CAG AAG TGG CAC CTG AC	JAX: 007906
Cdh5-Cre^{ERT2}(PAC) mouse strain genotyping primers (5' – 3')	TCC TGA TGG TGC CTA TCC TC CCT GTT TTG CAC GTT CAC CG CAC CCT GTT CTT TGC CTC CT	This study.

Cdh5-Cre^{ERT2}(BAC) mouse strain genotyping primers (5' – 3')	ATA CCG GAG ATC ATG CAA GC ATG TGA ACC AGC TCC CTG TC CTA GGC CAC AGA ATT GAA AGA TCT GTA GGT GGA AAT TCT AGC ATC ATC C	JAX: Protocol 029211
Col1a2-Cre^{ERT} mouse strain genotyping primers (5' – 3')	CAT GTC CAT CAG GTT CTT GC TGA AAA AGT CCA CTA ATT AAA ACC A CTA ACA ACC CTT TCT CTC AAG GT CAG GAG GTT TCG ACT AAG TTG G	JAX: Protocol 19893
Runx1 Knock-In mouse strain genotyping primers (5' – 3')	GAG TTC TCT GCT GCC TCC TGG CGA GGG CAG CCA TAG CAA CTC CGA GGC GGA TCA CAA GCA ATA	Qi, et al., 2017
PolyloxExpress mouse strain genotyping primers (5' – 3')	AAG GGA GCT GCA GTG GAG TA TAA GCC TGC CCA GAA GAC TCC AAG ACC GCG AAG AGT TTG TCC	Pei, et al., 2020
Software and algorithms		
FlowJo v10	BD	https://www.flowjo.com RRID:SCR_008520
GraphPad Prism 10	Dotmatics	www.graphpad.com RRID:SCR_002798
Snakemake	Köster et al.	https://snakemake.github.io/ RRID:SCR_003475
Lima	PacBio	https://lima.how/ RRID:SCR_025520
Iso-Seq	PacBio	https://isoseq.how/ RRID:SCR_025481
Minimap2	Li, et al (2021)	https://github.com/lh3/minimap2 RRID:SCR_018550
Cell Ranger	10x Genomics	V8.0.1, RRID:SCR_017344

Polylox barcode recovery	This study	https://github.com/CCRSF-IFX/SF_Polylox-BC
pGen calculation	Pei, et al. (2020)	https://github.com/hoefer-lab/polylox
Scanpy	Scanpy Community	https://scanpy.readthedocs.io RRID:SCR_018139
rapids-singlecell	Rapids-SingleCell	https://rapids-singlecell.readthedocs.io
decoupler	Badia-i-Mompel et al. (2022)	https://decoupler-py.readthedocs.io
scANVI	Gayoso et al. (2022)	https://github.com/scverse/scvi-tools
CellTypist	Xu et al. (2021)	https://celltypist.readthedocs.io/
Other		
Primaria™ dishes/flasks	Corning	353808; 353810; 353846
Regular Cell Culture Flask	Corning	430641U

EXPERIMENTAL MODEL AND STUDY PARTICIPANT DETAILS

Mouse strains

All animal studies were approved by the Institutional Animal Care and Use Committee of the CCR (Bethesda, MD), National Cancer Institute (NCI), NIH and conducted in adherence to the NIH Guide for the Care and Use of Laboratory Animals (National Academies Press, 2011) and approved protocols. *Cdh5-Cre^{ERT2}(PAC)* mice [37] (MGI:3848982) were a gift from Dr. R. Adams and *Cdh5-Cre^{ERT2}(BAC)* mice [39] (MGI:5705396) were a gift from Dr. Kubota. *Col1a2-CreER* mice [85] were purchased from the Jackson Laboratory (JAX#029567). Cre-dependent *Ai6-ZsGreen* [86] (JAX#007906) and *mTmG* [87] (JAX#007676) fluorescent reporter mice were purchased from the Jackson Laboratory. In *ZsGreen* reporter mice, Cre activity leads to

976 constitutive expression of ZsGreen1 in cell bodies. In *mTmG* reporter mice, Cre activity leads to
977 an irreversible switch from cell membrane-localized tdTomato (mT) to membrane-localized
978 EGFP (mG). *PolyloxExpress* mice [33] were a kind gift of Drs. Hans-Reimer Rodewald and
979 Avinash Bhandoola. The Cdh5-Cre^{ERT2}/ZsGreen/*PolyloxExpress* mouse line was generated in
980 house. Runx1 conditional knock-in mice[66] (Gt(ROSA)26Sor$^{tm1(CAG-Runx1)Lzjg}$, MGI:7490340)
981 were generously provided by Drs. Qiufu Ma and Nancy Speck. Runx1 endothelial-specific
982 knock-in (*Runx1^{EC-KI}*) mice were generated by crossing *Runx1$^{Ki/+}$* mice with *Cdh5-*
983 *Cre^{ERT2}(PAC)/ZsGreen$^{Tg/Tg}$* mice. Upon tamoxifen treatment, Cre-mediated excision of the two
984 floxed STOP codons enables co-expression of Runx1 and ZsGreen in ECs.
985
986 All animals were bred in the animal facilities of CCR/NCI (Bethesda, MD). The mice were
987 maintained in a C57BL/6J background. Mice were identified with ear tags and routinely
988 genotyped by PCR. No mouse was excluded from the experiments, unless assessed as sick by the
989 veterinarians or fight wounds were observed at harvest. Tamoxifen (Sigma-Aldrich, #T5648)
990 dissolved in peanut oil (Sigma-Aldrich, #P2144) (10 mg·mL^{-1}) was administered orally (via
991 gavage using 22g feeding needles) at 100 mg·kg^{-1}. Unless otherwise specified, three doses on
992 consecutive days were administered. Unless indicated otherwise, 8- to 12-week-old male and
993 female mice were used when tamoxifen was administrated. No randomization or blinding was
994 used to allocate experimental groups. Mice were typically sacrificed between 9 AM and 11 AM
995 local time.

996 **METHOD DETAILS**

997 **OP9 cell culture**

998 OP9 cells, a gift from Dr. T. Nakano[44] (also available from ATCC, #CRL-2749), were
999 maintained in α-MEM (Gibco #12561056; without ribonucleosides and deoxyribonucleosides,
1000 with 2.2 g/L sodium bicarbonate) supplemented with 20% fetal bovine serum (FBS; Sigma-
1001 Aldrich #2442). Culture dishes and flasks (Corning #353003, #430641U) were precoated with
1002 gelatin (Sigma-Aldrich #G9391; ~100 µL/cm², 60 minutes at 37°C). Cells were incubated at
1003 37°C in a humidified atmosphere of 95% air and 5% CO_2.
1004
1005 **Bone marrow cell harvesting, culture and terminal harvest for analysis**
1006 To harvest BM cells to be cultured, mice were euthanized by cervical dislocation and soaked in
1007 70% ethanol for 5 minutes. Long bones (femurs and tibiae) were dissected, and surrounding skin,
1008 muscle, and connective tissue were carefully removed. Cleaned bones were immediately
1009 transferred into ice-cold sterile PBS and kept on ice. Once all bones were harvested, they were
1010 soaked in 70% ethanol for 1 minute and rinsed three times with ice-cold PBS.
1011 Each bone was cut into two pieces using sterile scissors and placed--with the open end facing
1012 downward-- into a sterile 500 µL microcentrifuge tube pre-perforated with a 16G needle
1013 (sterilized in advance). Each 500 µL tube was loaded with two femurs and two tibiae. To each
1014 tube, 200 µL of DMEM supplemented with 1 mM EDTA was added. The 500 µL tubes were
1015 then placed inside sterile 1.5 mL microcentrifuge tubes, sealed with Parafilm, and centrifuged at
1016 12,000 rpm for 20 seconds. The inner tubes were discarded, and the BM pellet collected in the
1017 1.5 mL tubes was resuspended in 1 mL DMEM + 1 mM EDTA.
1018 Cells were filtered through 70 µm cell strainers, centrifuged at 350 × g for 5 minutes at 4°C, and
1019 resuspended in complete DMEM (DMEM containing 15% FBS (Sigma-Aldrich #2442-500ML,

1020 LOT:24G002), Penicillin-Streptomycin [Gibco #15140-122], and Anti-Anti [Gibco #15240-
1021 062]). A single-cell suspension was prepared by pipetting 30 times with a 1 mL pipette.
1022 Bone marrow cells were cultured either on Corning Primaria™ dishes/flasks (Corning #353808,
1023 #353810, #353846) or on OP9 stromal cell monolayers in standard tissue culture dishes/flasks
1024 (Corning #353003, #430641U) precoated with gelatin (Sigma-Aldrich #G9391; ~100 µL/cm²,
1025 incubated 60 min at 37°C).
1026 Cells were seeded at a density equivalent to BM cells from two femurs and two tibiae per ~75
1027 cm² culture surface (e.g., T75 flask) in 15 mL complete DMEM. After ~32 hours, non-adherent
1028 cells and medium were removed, and adherent cells were gently washed three times with PBS.
1029 For Primaria cultures, 15 mL fresh complete DMEM was replenished twice weekly. For OP9 co-
1030 cultures, non-adherent cells and medium were removed twice weekly and replaced with fresh
1031 complete DMEM supplemented with freshly isolated unfractionated WT BM cells (from two
1032 femurs and two tibiae per ~75 cm² surface, using the same BM isolation method mentioned
1033 above).
1034 For terminal collection, at the start of the final culture week, all non-adherent cells were
1035 removed, and adherent cells were washed three times with PBS. Fresh complete DMEM (15 mL)
1036 was added. After three days, a second 15 mL complete DMEM addition was made. No further
1037 medium changes occurred before harvest. For final collection, non-adherent cells and
1038 supernatant were collected first. Adherent cells were washed with PBS, and the wash was pooled
1039 with the supernatant. Remaining adherent cells (including OP9 and BM-derived cells) were
1040 detached using 0.25% Trypsin-EDTA (Gibco #25200-056) for 5 minutes at 37°C and added to
1041 the pooled suspension. After another PBS wash, a second trypsinization (10 minutes at 37°C)
1042 was performed. All collected material from each step was combined for downstream flow

1043 cytometric analysis. For transplantation experiments, only non-adherent cells (with supernatant)
1044 and loosely adherent cells recovered after the initial 5-minute Trypsin-EDTA incubation were
1045 pooled and subjected to FACS sorting to isolate ZsGreen^{+} cells for injection.
1046
1047 **Blood collection**
1048 For terminal collection, blood was obtained from the mouse abdominal aorta with BD
1049 Vacutainer™ EDTA tubes (BD #367856) and Vaculet™ blood collection needles (23G,
1050 EXELINT #26766). Blood smears were prepared with 10 µL of collected blood. For flow
1051 cytometry analysis, ACK buffer (Lonza, #BP10-548E) was added to the blood to lyse red blood
1052 cells before Fc receptor blocking and antibody staining. For non-terminal blood collection, ~20-
1053 50µL blood was collected by submandibular blood sampling, using a 3mm animal lancet
1054 (BRAINTREE SCI., GR-3MM) and a 250µL BD Microtainer® K2EDTA tube (BD #365974).
1055 Kwik Stop® Styptic Powder was applied to stop the bleeding (Miracle Corp. #423615). For long-
1056 term, repeated blood collection, 2 drops of blood were collected from the tail vein with
1057 Microhematocrit Capillary Tubes (Fisherbrand # 22-362574). White blood cell (WBC) counts
1058 were determined using acridine orange/propidium iodide (AO/PI, Logos Biosystems, #F23001)
1059 staining and quantified with a LUNA-FL™ fluorescence cell counter (Logos Biosystems). For
1060 flow cytometry detection of ZsGreen/EGFP positive PBMCs, blood was collected with one of
1061 the methods above. For flow cytometric detection of ZsGreen^{+}/EGFP^{+} PBMCs, blood was
1062 collected using one of the three methods described above. Red blood cells were lysed with ACK
1063 buffer, and DAPI and DRAQ5 were used to exclude dead cells and to identify nucleated PBMCs.
1064
1065 **Bone marrow harvest for flow cytometry analysis**

1066 For flow cytometry analysis, bone marrow was harvested using one of the two methods
1067 described below. For hematopoietic cell isolation, bone marrow was harvested by flushing
1068 femurs and tibiae with ice-cold Sort Buffer (1× PBS [Gibco, #10010-031] supplemented with 5
1069 mM EDTA, 25 mM HEPES, and 2% FBS [Sigma-Aldrich, #F2442]). Red blood cells were then
1070 lysed using ACK lysing buffer (Lonza, #10-548E) according to the manufacturer's instructions.
1071 Cells were then washed with Sort Buffer and passed through a 40μm cell strainer (GREINER
1072 BIO-ONE, #542040, #542140). For greater preservation of endothelial cells, bone marrows were
1073 harvested by gently crushing mouse femurs and tibiae in Sort Buffer (5mM EDTA, 25mM
1074 HEPES, 2% FBS in 1× PBS). Red cell lysis was performed using ACK buffer. Bone marrow
1075 cells were then incubated with $0.1U \cdot mL^{-1}$ Collagenase (Worthington Biomedical Corp.,
1076 #LS004176), $0.8U \cdot mL^{-1}$ Dispase (Worthington Biomedical Corp., #LS02109), and $0.5mg \cdot mL^{-1}$
1077 DNase (Worthington Biomedical Corp., #LS006344) in 1x Hanks' Balanced Salt Solution
1078 (HBSS) with Ca^{2+} and Mg^{2+} (Gibco, # 14065056) at 37°C for 30 min on a rotating mixer. Cells
1079 were then washed with Sort Buffer and passed through a 40μm cell strainer.
1080
1081 **Endothelial cell transplantation experiments**
1082 Four days prior to transplant, recipient mice received one dose of 5-FU ($150\ mg \cdot kg^{-1}$ in PBS,
1083 Sigma-Aldrich, #F6627) intraperitoneally under isoflurane anesthesia. Sorted bone marrow cells
1084 (Col1a2-Cre/ZsGreen: 5,000 cells; Cdh5-Cre/ZsGreen: 20,000 cells in 100μL PBS) were
1085 inoculated retro-orbitally under isoflurane anesthesia. Bone marrows and blood were harvested
1086 from transplant recipients four weeks after the transplant unless otherwise specified.
1087
1088 **Bone marrow ablation and transplantation**

1089 Recipient mice were lethally irradiated (11 Gy) using a Cesium-137 (^{137}Cs) gamma irradiator
1090 three days prior to transplantation.
1091 For whole BM cell transplantation into *mTmG* recipients, BM cells were harvested from WT
1092 donor mice by flushing (as described above); 5×10^6 cells were transplanted per recipient via tail
1093 vein. No rescue bone marrow cells were infused.
1094 For LSK transplantation into WT recipients, BM from Cdh5-Cre^{ERT2}(PAC)/ZsGreen mice (not
1095 treated with tamoxifen) was harvested by flushing, followed by red blood cell lysis with ACK
1096 buffer. Fc receptor blocking was performed using Azide-Free Fc Receptor Blocker (Innovex,
1097 #NB335-60) per manufacturer's instructions. Cells were stained with antibodies to Lineage
1098 cocktail, Sca-1, and c-Kit. DAPI was used to exclude dead cells. LSK populations were sorted
1099 using Sony SH800S and its Ultra Purity mode. Transplanted cell numbers were as follows:
1100 ZsGreen$^-$ LSKs (5×10^4, n = 3; 2.5×10^4, n = 3) and ZsGreen$^+$-enriched LSKs (2,800 cells, n =
1101 2). No rescue bone marrow cells were infused.
1102 For transplantation of ex vivo–cultured BM cells, non-adherent and loosely adherent ZsGreen$^+$
1103 cells were collected from 8-week OP9 co-cultures (as described above), sorted by FACS for live
1104 (DAPI$^-$) ZsGreen$^+$ cells, and transplanted into irradiated recipients at 5×10^4, 2.5×10^4, or $1.25 \times$
1105 10^4 cells per mouse (n = 2 per group). No rescue bone marrow cells were infused.
1106

1107 **Flow cytometry and cell sorting**

1108 For intracellular antigen detection, single cell suspensions of bone marrow and blood were first
1109 incubated with Azide-Free Fc Receptor Blocker (Innovex, #NB335-60), following the
1110 manufacturer's instructions. After washing, cells were first stained with surface marker
1111 antibodies at the concentration of 2μg per 1×10^7 cells in Sort Buffer for 30 minutes at 4°C and

1112 then stained with live/dead cell discriminating BioLegend Zombie Dyes (UV, NIR, Violet, or
1113 Yellow, BioLegend #423108, #423106, #423114, and # 423104) following the manufacturer's
1114 instructions. After washing, cells were fixed in 4% paraformaldehyde for 10 minutes at 37°C,
1115 and then permeabilized with 1% saponin (Sigma-Aldrich, # 47036) /Sort Buffer for 30min on
1116 ice. Subsequently, the cells were stained with rat monoclonal primary RUNX1-PE Ab
1117 (Invitrogen, # 12-9816-80) in 0.1% saponin/Sort Buffer overnight. After washing and
1118 resuspension, propidium iodide (PI, 0.5μM, Millipore Sigma, # P4170), 7-AAD (1μg·mL^{-1},
1119 Millipore Sigma, #A9400) or DAPI (0.5μg·mL^{-1}, BioLegend, #422801) was added as a nuclear
1120 counterstain. For live cell staining without cell permeabilization, after cell surface antibody
1121 staining, cells were washed and suspended in Sort buffer containing propidium iodide (PI,
1122 0.5μM, Millipore Sigma, # P4170), 7-AAD (1μg·mL^{-1}, Millipore Sigma, #A9400) or DAPI
1123 (0.5μg·mL^{-1}, BioLegend, # 422801), to distinguish dead cells from the live cells. For FACS
1124 sorting of live endothelial cells, after Fc receptor blocking, bone marrow cells were first depleted
1125 of CD45^{+} cells with MojoSort mouse CD45 nanobeads (BioLegend #480028) following the
1126 manufacturer's protocol and then stained with specific antibodies. For flow cytometry analysis,
1127 compensation beads (BD Biosciences, #552844) were used for flow cytometer compensation.
1128 Flow cytometric data were acquired with BD FACSCanto-II, BD LSRFortessa, BD
1129 FACSymphony A5 (BD Biosciences), Sony SA3800 or Sony ID7000 cell analyzers. Cell sorting
1130 was performed with BD FACS Aria III, BD FACS Aria Fusion or Sony SH800S cell sorters.
1131 FSC and SSC profiles were used for excluding dead cells and debris. 7-AAD, PI, DAPI or
1132 BioLegend Zombie Dye was used for excluding dead cells. FSC-W versus FSC-H and SSC-W
1133 versus SSC-H were used to gate on single cells. Unless otherwise specified, fluorescence minus
1134 one (FMO) controls are used for negative gating reference. For BM HSPC analysis, BM cells

1135 were harvested followed by lineage positive cell depletion (Biolegend #480004). Data were
1136 analyzed with FlowJo (BD, v10.8.1), SONY ID7000 Software (Version 1.2.0.28212) or FACS
1137 Diva (BD, v6.1 and v9.0). Flowjo Plugins UMAP_R (v4.0.4) and FlowSOM (v4.1.0) were used
1138 for UMAP dimensional reduction and unsupervised clustering of flow cytometry data. Following
1139 sorting, a small aliquot of collected events were re-run on the sorter to assess purity. Analysis
1140 was performed using the identical gating hierarchy (FSC/SSC → singlets → live cells → target
1141 population).
1142
1143 **Bone marrow cryosections**
1144 Deeply anesthetized mice were transcardially perfused with 20mL ice-cold 1x PBS, followed by
1145 perfusion with 15mL ice-cold hydrogel solution (5% acrylamide/bis-acrylamide 19:1 (Sigma-
1146 Aldrich, #A2917), 2.5mg/mL polymerization initiator VA-044 (FUJIFILM, Wako, VA-044,
1147 Water soluble Azo initiators), 4% PFA in 1× PBS, 5mL/min flow speed). Femurs and tibiae were
1148 collected in tubes containing 5mL hydrogel solution and incubated at 4°C for 4 hours. The bones
1149 were then washed with PBS and incubated at 37°C for 2 hours. Bone decalcification was
1150 performed by incubating the bones in 40mL 0.5M EDTA pH 8.0 (KD Medical, #RGF-3130) for
1151 3 days on a rotate mixer, with daily refreshed 0.5M EDTA solution. The bones were then
1152 dehydrated in 20% sucrose and 2% polyvinylpyrrolidone in PBS overnight. Dehydrated bones
1153 were then embedded in OCT (SAKURA, #4583) blocks using Precision Cryoembedding System
1154 (IHC WORLD, #IW-P101). Cryosections (10µm) for immunofluorescence staining were
1155 prepared from OCT frozen bone blocks using Leica CM3050S microtome, low-profile
1156 microtome blades (Leica 819, #14035838925), and TruBond™ 380 adhesion slides (Electron
1157 Microscopy Sciences, # 63701-W10).

1158

1159 **Immunofluorescence staining and imaging**

1160 Tissue sections were rehydrated with 1× PBS (15 minutes), permeabilized in 0.3% Triton X-100
1161 (Sigma-Aldrich, #T9284)/PBS (15 minutes), washed in 1× PBS, and incubated (2 hours) with
1162 blocking solution (2% BSA, 5% donkey serum (SIGMA, #D9663), and 0.3% Triton X-
1163 100/PBS). Samples were then washed 3 times with PBS and incubated with primary antibodies
1164 (5ng/mL; 4°C overnight). When secondary antibodies were used, 3 PBS washes were performed
1165 before incubating with fluorescent-labeled secondary antibodies (2ng/mL, room temperature, 2
1166 hours). After washing (3x, 10 minutes each with 1× PBS), DAPI was added (300nM in PBS, 10
1167 min). After 3 washes (5 min each with 1× PBS), coverslips were mounted (EPREDIA,
1168 #9990402), dried and sealed with nail polish. For blood smear staining, slides were first soaked
1169 in acetone/methanol/PFA (19:19:2 for 90 seconds) before rehydration [88]. Confocal imaging was
1170 performed with Zeiss LSM 780, Zeiss LSM 880 NLO Two Photon, or Nikon *ECLIPSE* Ti2-E
1171 SoRa systems, according to the experimental specific needs (resolution, speed, wavelength
1172 capabilities). Images were processed with Zen (Zen Black v2.3, release Version 14.0.12.201, Zen
1173 Blue Lite v2.5, Carl Zeiss), Bitplane Imaris (v9.7.0, Oxford instruments), and Photoshop
1174 (v23.3.0, Adobe, for whole image contrast and brightness adjustments).

1175

1176 **Isolation of peritoneal cavity cells**

1177 To isolate peritoneal cavity cells, mice were euthanized by cervical dislocation, injected
1178 intraperitoneally (i.p.) with cold FACS sort buffer (5 mL), massaged and flicked gently on the
1179 abdomen. Peritoneal fluid was then withdrawn slowly and transferred into a polypropylene
1180 centrifuge tube on ice prior to centrifugation (350×g, 10min, at 4°C) and analysis.

1181

1182 **Thioglycolate induced sterile peritonitis**

1183 Mice were injected i.p. with 1 mL PBS or 4% thioglycolate (Sigma-Aldrich, #70157). Peritoneal
1184 cavity cells were harvested 4 hours after injection for further analysis.

1185

1186 **Phagocytosis assay**

1187 Phagocytosis assay was performed using pHrodo™ Red *Escherichia coli* BioParticles
1188 (Invitrogen, # P35361) following the manufacturer's instructions. Briefly, mice were first treated
1189 with thioglycolate (as described). Peritoneal cavity cells were incubated with the fluorescent
1190 *Escherichia coli* particles for 60 min at 37°C. Cells were then stained with surface marker
1191 antibodies and analyzed by flow cytometry.

1192

1193 **ROS assay**

1194 ROS assay was performed using CellROX™ Orange Flow Cytometry Assay Kit (Invitrogen, #
1195 C10493) following the manufacturer's instructions. Briefly, mice were first treated with
1196 thioglycolate (as described). CellROX detection reagent was added to peritoneal cavity cells
1197 (final concentration of 500nM) prior to incubation for 60 min at 37°C. Cells were then stained
1198 with the surface marker antibodies and analyzed by flow cytometry.

1199

1200 **PolyloxExpress single cell lineage tracing**

1201 These experiments essentially followed published procedures [33]. Briefly, BM cells from
1202 tamoxifen treated Cdh5-Cre/ZsGreen/Polylox mice (treated at 10 weeks old and harvested at 16
1203 weeks old) were enriched for ZsGreen positive cells by FACS. Single cell capturing was

1204 performed with 10x Genomics Chromium Single Cell 3′ Reagent Kits, following manufacturer's
1205 protocols. After reverse transcription (RT) in droplets, pooled cDNA was amplified and split into
1206 two aliquots for parallel transcriptome library preparation and barcode enrichment. Initial library
1207 quality control was performed with Agilent TapeStation D5000. For transcriptome analysis, 10
1208 µL (25%) of a 10x cDNA library was fragmented and a gene expression library, generated
1209 following protocols in Single Cell 3' Reagent Kits v3 and v4, was sequenced with Illumina
1210 NextSeq 2000 P3/P4 Reagents (28+74 bp read length). For Polylox barcode amplification,
1211 targeted amplification of barcodes from a 5-10 ng aliquot of a 10x cDNA library was performed
1212 by nested PCR. In the first round, primers #2,652 (5′-GCATGGACGAGCTGTACAAG-3′,
1213 annealing at the 5′ end of Polylox) and #2,674 (5′-
1214 AATGATACGGCGACCACCGAGATCTACACTCTTTCCCTACACGACGCTC-3′, annealing
1215 at the adaptor site (read 1) were used for amplification for 5 min at 95°C; (30 s at 95°C, 30 s at
1216 57°C, 3 min at 72°C) 12 times; 10 min at 72°C. PCR products purified with 0.7x AMPure beads
1217 were used for the second round of PCR using primers #2,426 (5′-
1218 CGACGACACTGCCAAAGATTTC-3′, annealing at the 5′ end of Polylox) and #2,676 (5′-
1219 AATGATACGGCGACCACCGA-3′, annealing at the 5′ end of primer #2,674), for 5 min at
1220 95°C; (30 s at 95°C, 30 s at 60°C, 3 min at 72°C) 18 times; 10 min at 72°C. The PCR products
1221 were purified with AMPure PB beads according to the manufacturer's protocol. Long read
1222 amplicon-seq libraries were sequenced by PacBio Sequel II with PacBio Amplicons Library
1223 Preparation using SMRTbell prep kit 3.0. A custom transcriptome reference was built from
1224 mouse reference MM10 to include ZsGreen1.
1225 A snakemake workflow with custom python script was used to retrieve cell indexes and Polylox
1226 barcodes from the PolyloxExpress amplicons (https://github.com/CCRSF-IFX/SF_Polylox-BC).

1227 Single cell transcriptome and single cell barcodes were linked using the 10x 3' kit cell index and
1228 group information. Further analysis and illustrations were generated using Scanpy
1229 (https://github.com/scverse/scanpy). Doublet detection was performed using Scrublet, with the
1230 predicted doublet rate calculated based on 10x Genomics guidance about the cell numbers loaded
1231 to the microfluidic chips. Batch correction was done using BBKNN method
1232 (https://github.com/Teichlab/bbknn). Cell types were manually annotated based on canonical
1233 marker gene expression, guided by results from three automated annotation tools: (1) decoupleR
1234 ((https://saezlab.github.io/decoupleR/), using PangLaoDB (https://panglaodb.se/) as reference;
1235 (2) scANVI (https://github.com/scverse/scvi-tools) using ImmGne (https://www.immgen.org/) as
1236 reference; (3) CellTypist, using the embedded Immune_All_Low model. The rare barcodes and
1237 their pGen were identified using the MatLab script from the Höefer's Lab
1238 (https://github.com/hoefer-lab/polylox). True barcodes are defined as pGen < 1×10^{-4}, such that
1239 the expectation of a True barcode in detected 4,072 cells is 0.407. This work utilized the
1240 computational resources of the NIH HPC Biowulf cluster (*http://hpc.nih.gov*) and Frederick
1241 Research Computing Environment (FRCE). Python version: 3.10.; R version 4.5.0.
1242
1243 **Public single-cell RNA-seq data analysis**
1244 Raw FASTQ and BAM files were downloaded from publicly available datasets (GSE108885 [54],
1245 GSE108891 [54], GSE118436 [54], GSE123078 [54], GSE122465 [55], GSE128423 [53], GSE145477 [65],
1246 GSE156635 [56], GSE137116 [24], E-MTAB-8077 [65], GSE230260[58], GSE259382[59]). The BAM files
1247 were first converted to FASTQ files with bamtofastq (10x Genomics, v2.0.1). All FASTQ files
1248 were then processed by the count function of Cell Ranger (10x Genomics, v8.0.1) and aligned to

1249 the mouse genome (mm10, version 2020-A), to generate read matrixes. Further analysis and
1250 illustrations were generated using Scanpy as described above.
1251
1252 **Definition of cultured fluorescent BM cell clusters and quantification**
1253 A cluster was defined as (1) a spatially distinct group of ZsGreen^{+} cells not contiguous with other
1254 fluorescent cells, (2) containing a central core with at least five extending branches, and (3)
1255 exhibiting a roughly radial organization, with projections spreading outward in multiple
1256 directions, and (4) extending at least ~200 µm in one direction. Isolated or irregularly scattered
1257 fluorescent cells were not counted. Due to their large size, clusters were counted manually across
1258 the culture dish using a tally counter under fluorescence microscopy.
1259
1260 **RNA isolation and quantitative RT PCR**
1261 RNA was extracted using RNeasy® Micro Kit (QIAGEN, #74004), following the manufacturer's
1262 protocol. Cells were sorted directly into RNA lysis buffer (Buffer RTL of RNeasy® Micro Kit).
1263 cDNA samples were prepared with SuperScript IV Reverse Transcriptase (Invitrogen,
1264 #18091050), following manufacturer's instructions. Real Time PCR was performed using
1265 Applied Biosystems™ TaqMan™ Fast Advanced Master Mix (4444557) and Applied
1266 Biosystem™ QuantStudio™ 5 Real-Time PCR System. TaqMan™ probes used were purchased
1267 from Applied Biosystems™: Spp1 (Mm00436767_m1); Cxcl12 (Mm00445553_m1); Col1a2
1268 (Mm00483888_m1); Cdh5 (Mm00486938_m1); Runx1 (Mm01213404_m1); Ptprc
1269 (Mm01293577_m1); Gapdh (Mm99999915_g1); Actb (Mm02619580_g1). The reaction
1270 condition was set as follows: 50°C 2 minutes, 95°C 20 seconds, 45 cycles of 95°C 1 second,
1271 60°C 20 seconds. Ct values were determined using the ABI QuantStudio™ Design & Analysis

1272 Software (v1.5.2). Relative gene expression was assessed using the $2^{-\Delta\Delta Ct}$ method, normalized to
1273 Gapdh expression level for each sample. The data was further normalized to gene expression
1274 levels in the unsorted bone marrow sample to calculate relative gene expression levels in each
1275 sample. Data reflect triplicates real-time PRC experiments.
1276

1277 QUANTIFICATION AND STATISTICAL ANALYSIS

1278 No statistical method was used to predetermine sample size. No data were excluded from the
1279 analyses. Mice with the correct genotypes were randomly assigned to control or treated groups.
1280 Unless otherwise specified, data are represented as mean ± S.D, and individual dots in the graphs
1281 indicate individual mice. Comparisons between two groups were performed using two-tailed
1282 unpaired Student's *t*-tests (except for Figure S1-H, which used a paired *t*-test). Spearman rank
1283 correlation test was used for Figure 3E. Statistical analyses were performed with GraphPad
1284 Prism (v9.0.1). A statistical difference of $P<0.05$ was considered significant: ns, not significant,
1285 * $P < 0.05$, ** $P < 0.01$, *** $P< 0.001$.

Figure 1

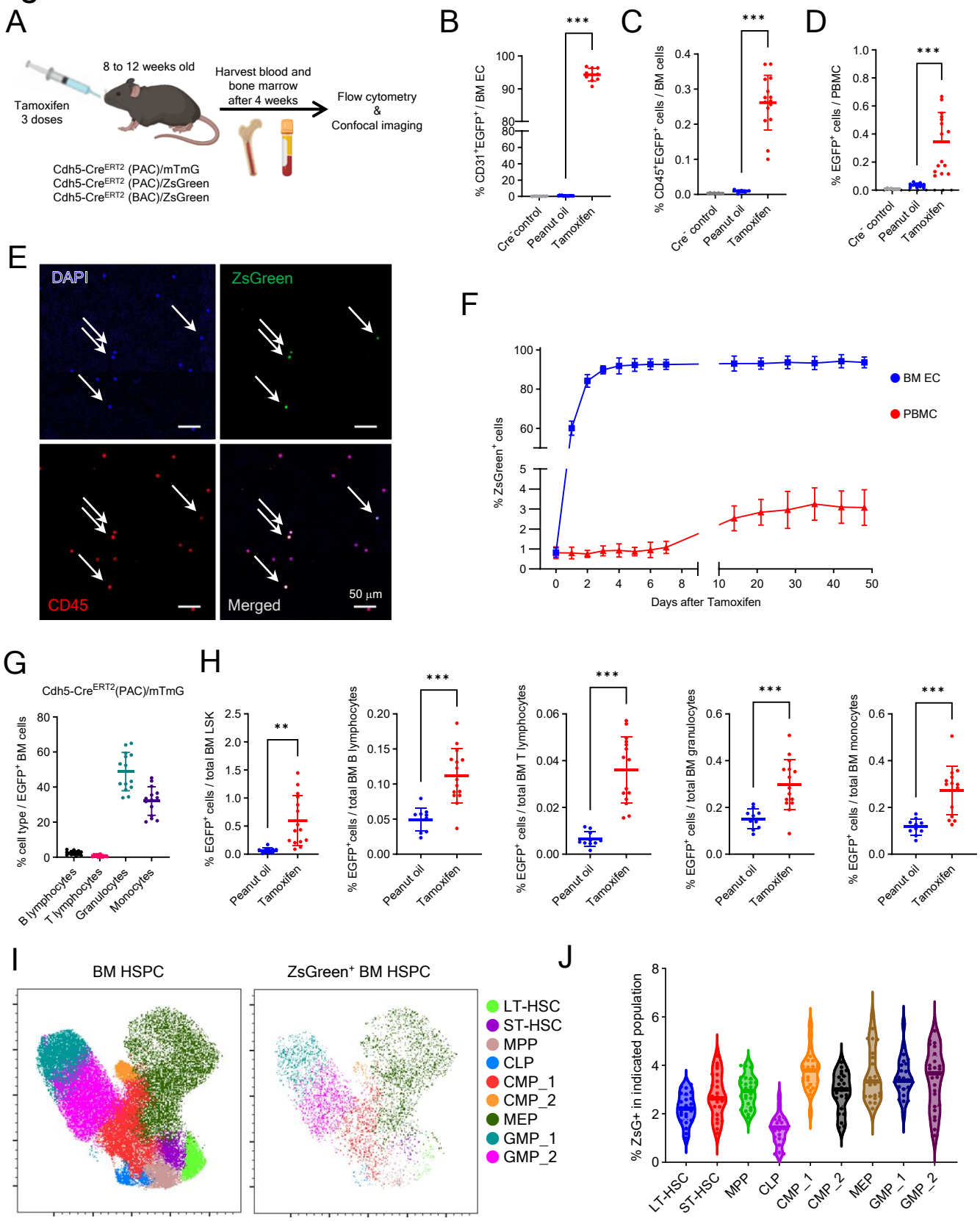
A
8 to 12 weeks old
Tamoxifen
3 doses
Harvest blood and
bone marrow
after 4 weeks
Flow cytometry
&
Confocal imaging
Cdh5-CreERT2 (PAC)/mTmG
Cdh5-CreERT2 (PAC)/ZsGreen
Cdh5-CreERT2 (BAC)/ZsGreen
B
% CD31+EGFP+ / BM EC
Cre- control
Peanut oil
Tamoxifen
C
% CD45+EGFP+ cells / BM cells
D
% EGFP+ cells / PBMC
E
DAPI
ZsGreen
CD45
Merged
50 µm
F
% ZsGreen+ cells
BM EC
PBMC
Days after Tamoxifen
G
Cdh5-CreERT2(PAC)/mTmG
% cell type / EGFP+ BM cells
B lymphocytes
T lymphocytes
Granulocytes
Monocytes
H
% EGFP+ cells / total BM LSK
% EGFP+ cells / total BM B lymphocytes
% EGFP+ cells / total BM T lymphocytes
% EGFP+ cells / total BM granulocytes
% EGFP+ cells / total BM monocytes
I
BM HSPC
ZsGreen+ BM HSPC
LT-HSC
ST-HSC
MPP
CLP
CMP_1
CMP_2
MEP
GMP_1
GMP_2
J
% ZsG+ in indicated population

Figure 2

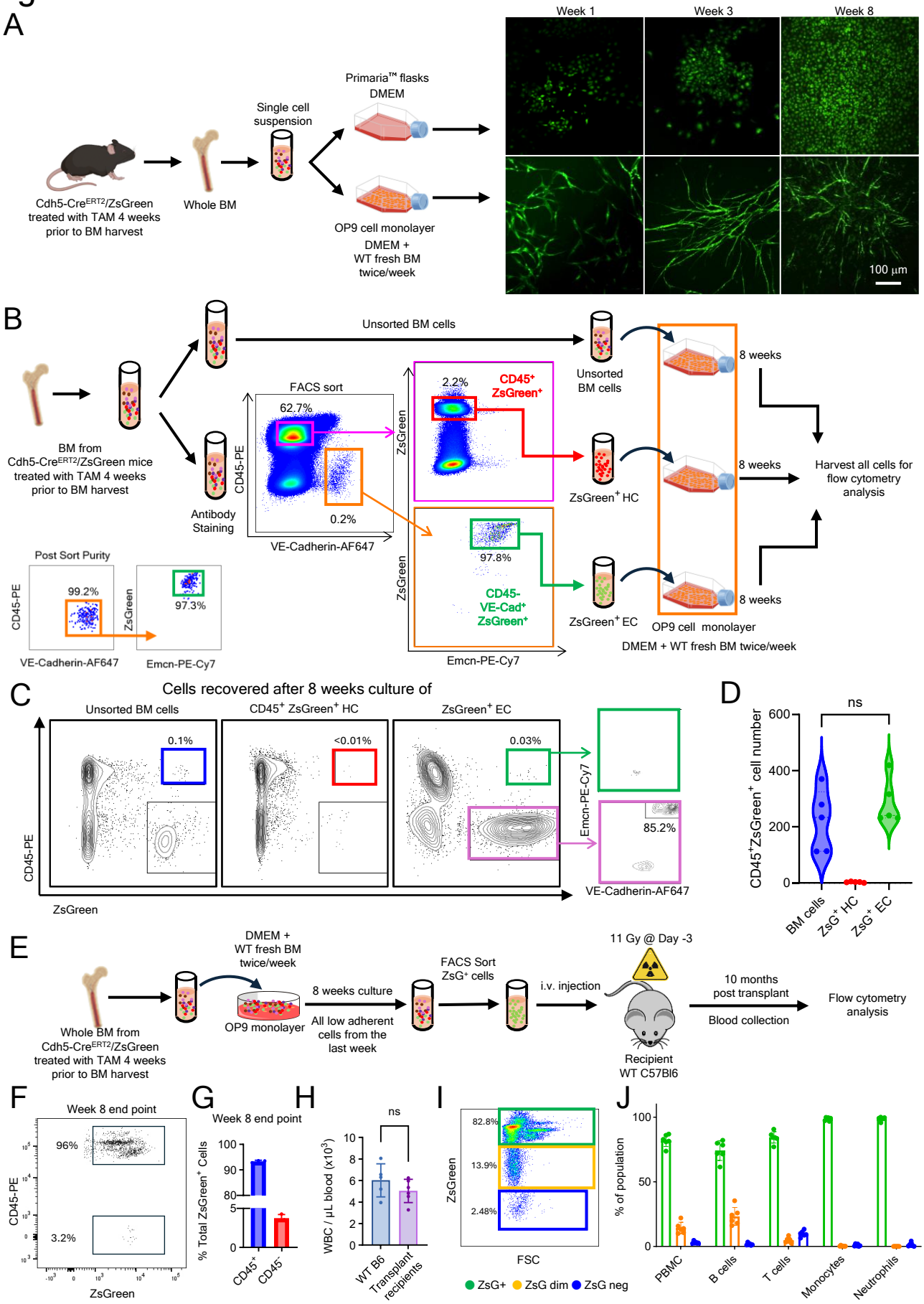
A
Week 1
Week 3
Week 8
Primaria™ flasks
DMEM
Single cell suspension
Cdh5-CreERT2/ZsGreen treated with TAM 4 weeks prior to BM harvest
Whole BM
OP9 cell monolayer
DMEM + WT fresh BM twice/week
100 µm
B
Unsorted BM cells
BM from Cdh5-CreERT2/ZsGreen mice treated with TAM 4 weeks prior to BM harvest
Antibody Staining
FACS sort
62.7%
0.2%
CD45-PE
VE-Cadherin-AF647
2.2%
CD45+ ZsGreen+
97.8%
CD45- VE-Cad+ ZsGreen+
ZsGreen
Emcn-PE-Cy7
Unsorted BM cells
ZsGreen+ HC
ZsGreen+ EC
8 weeks
OP9 cell monolayer
DMEM + WT fresh BM twice/week
Harvest all cells for flow cytometry analysis
Post Sort Purity
99.2%
97.3%
C
Cells recovered after 8 weeks culture of
Unsorted BM cells
CD45+ ZsGreen+ HC
ZsGreen+ EC
0.1%
<0.01%
0.03%
85.2%
CD45-PE
ZsGreen
Emcn-PE-Cy7
VE-Cadherin-AF647
D
ns
CD45+ZsGreen+ cell number
600
400
200
0
BM cells
ZsG+ HC
ZsG+ EC
E
Whole BM from Cdh5-CreERT2/ZsGreen treated with TAM 4 weeks prior to BM harvest
DMEM + WT fresh BM twice/week
OP9 monolayer
8 weeks culture
All low adherent cells from the last week
FACS Sort ZsG+ cells
i.v. injection
11 Gy @ Day -3
Recipient WT C57Bl6
10 months post transplant
Blood collection
Flow cytometry analysis
F
Week 8 end point
96%
3.2%
CD45-PE
ZsGreen
G
Week 8 end point
% Total ZsGreen+ Cells
100
90
80
5
0
CD45+
CD45-
H
ns
WBC / µL blood (x10³)
10
8
6
4
2
0
WT B6
Transplant recipients
I
82.8%
13.9%
2.48%
ZsGreen
FSC
ZsG+
ZsG dim
ZsG neg
J
% of population
100
50
0
PBMC
B cells
T cells
Monocytes
Neutrophils

Figure 3

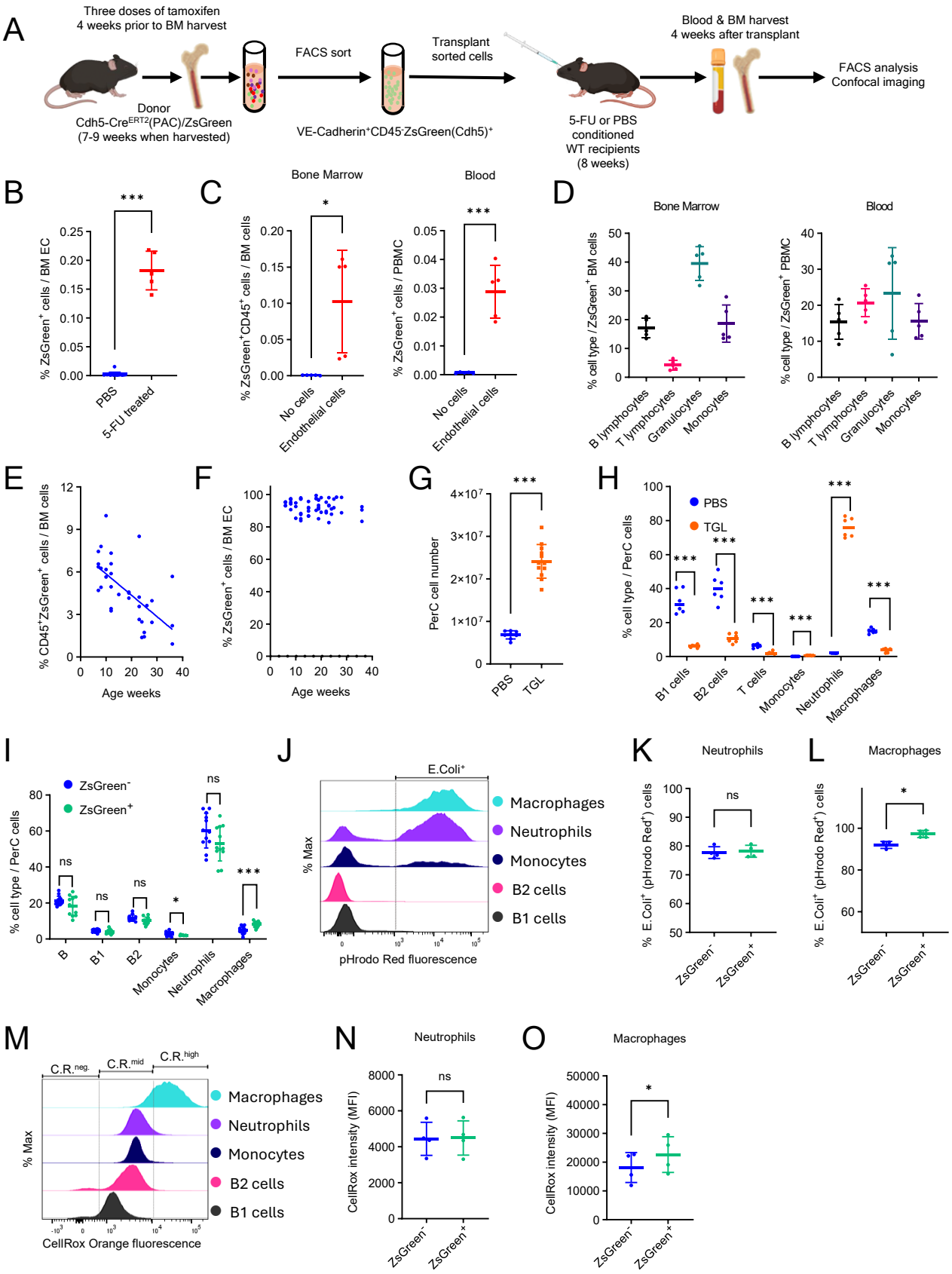
A
Three doses of tamoxifen
4 weeks prior to BM harvest
Donor
Cdh5-Cre^ERT2(PAC)/ZsGreen
(7-9 weeks when harvested)
FACS sort
VE-Cadherin+CD45-ZsGreen(Cdh5)+
Transplant
sorted cells
5-FU or PBS
conditioned
WT recipients
(8 weeks)
Blood & BM harvest
4 weeks after transplant
FACS analysis
Confocal imaging
B
% ZsGreen+ cells / BM EC
PBS
5-FU treated
C
Bone Marrow
Blood
% ZsGreen+CD45+ cells / BM cells
% ZsGreen+ cells / PBMC
No cells
Endothelial cells
D
Bone Marrow
Blood
% cell type / ZsGreen+ BM cells
% cell type / ZsGreen+ PBMC
B lymphocytes
T lymphocytes
Granulocytes
Monocytes
E
% CD45+ZsGreen+ cells / BM cells
Age weeks
F
% ZsGreen+ cells / BM EC
Age weeks
G
PerC cell number
PBS
TGL
H
PBS
TGL
% cell type / PerC cells
B1 cells
B2 cells
T cells
Monocytes
Neutrophils
Macrophages
I
ZsGreen-
ZsGreen+
% cell type / PerC cells
B
B1
B2
Monocytes
Neutrophils
Macrophages
J
E.Coli+
% Max
Macrophages
Neutrophils
Monocytes
B2 cells
B1 cells
pHrodo Red fluorescence
K
Neutrophils
% E.Coli+ (pHrodo Red+) cells
ZsGreen-
ZsGreen+
L
Macrophages
% E.Coli+ (pHrodo Red+) cells
ZsGreen-
ZsGreen+
M
C.R.neg.
C.R.mid
C.R.high
% Max
Macrophages
Neutrophils
Monocytes
B2 cells
B1 cells
CellRox Orange fluorescence
N
Neutrophils
CellRox intensity (MFI)
ZsGreen-
ZsGreen+
O
Macrophages
CellRox intensity (MFI)
ZsGreen-
ZsGreen+

Figure 4

A

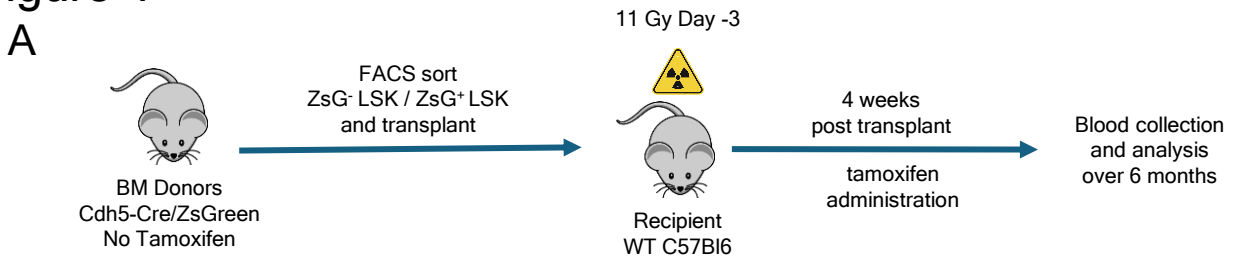

Do HSPCs / other hematopoietic cells in Cdh5-Cre^{ERT2}/ZsGreen mice express Cdh5-Cre^{ERT2}?	Donor LSK from Cdh5-Cre^{ERT2}/ ZsGreen mice, transplanted into WT recipients	Predicted detection pattern of ZsGreen^{+} PBMCs in WT recipients prior to and/or after TAM
Yes	~50:50 mix (ZsGreen^{+} / ZsGreen^{-})	ZsGreen^{+} PBMCs are present prior to TAM and increase after TAM.
	ZsGreen^{-} LSK only (>99% purity)	ZsGreen^{+} PBMCs become detectable after TAM and increase over time.
No	~50:50 mix (ZsGreen^{+} / ZsGreen^{-})	ZsGreen^{+} PBMCs are present at baseline but show no increase after TAM.
	ZsGreen^{-} LSK only (>99% purity)	No ZsGreen^{+} PBMCs prior to or after TAM.

B

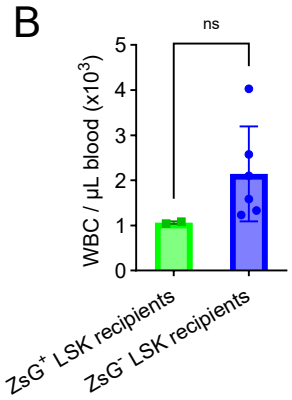

C

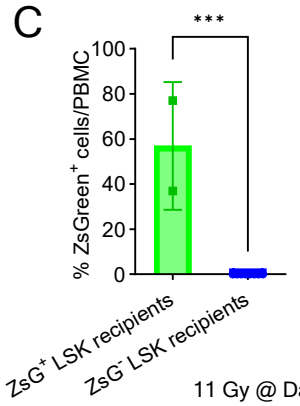

D

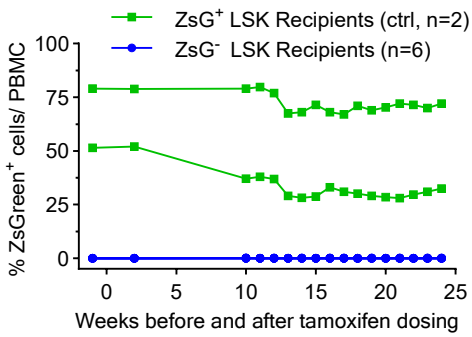

E

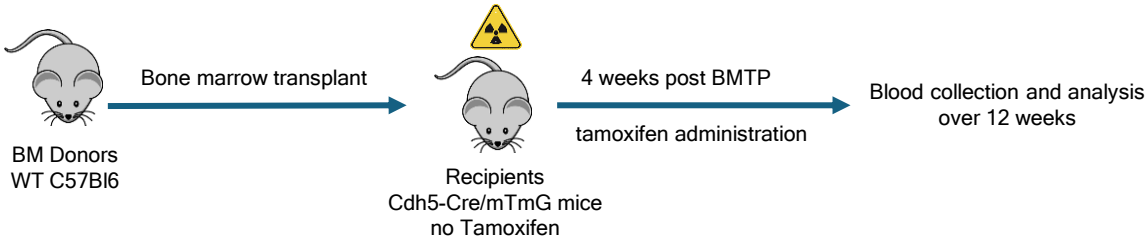

F

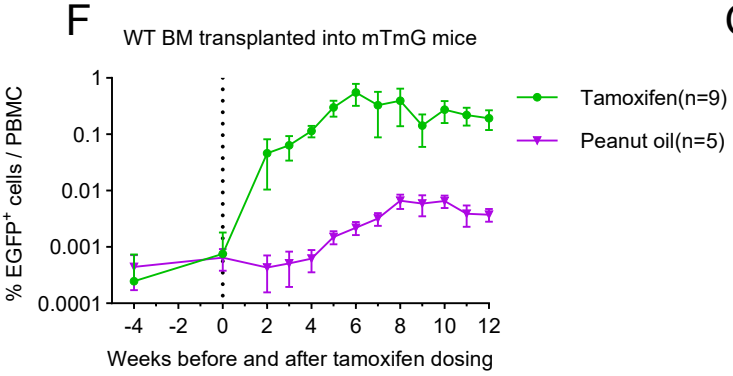

G

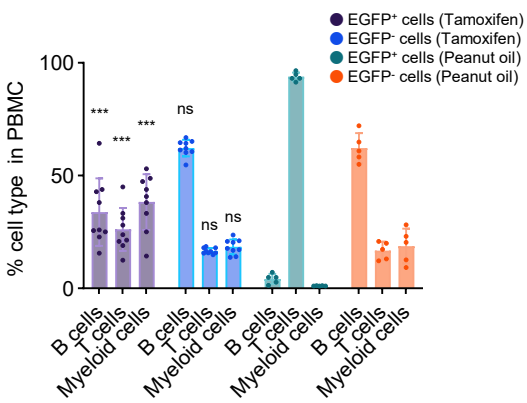

Figure 5

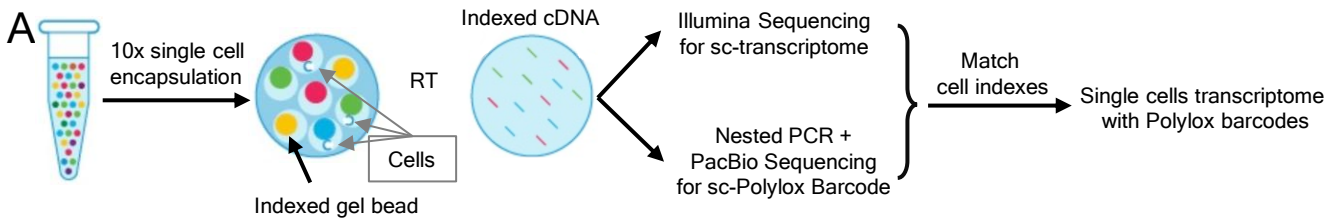
A
10x single cell encapsulation
RT
Cells
Indexed gel bead
Indexed cDNA
Illumina Sequencing for sc-transcriptome
Nested PCR + PacBio Sequencing for sc-Polylox Barcode
Match cell indexes
Single cells transcriptome with Polylox barcodes

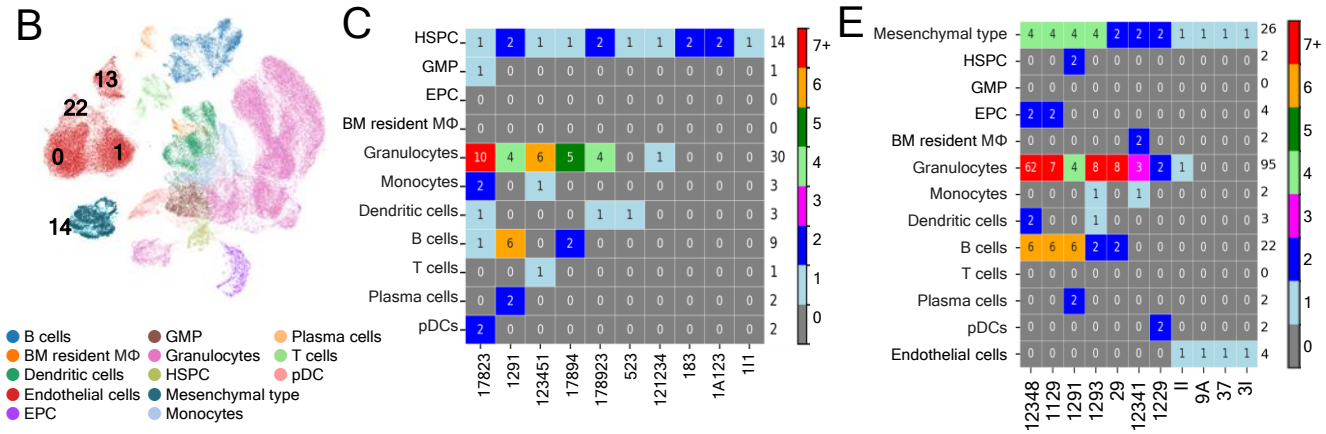
B
13
22
0
1
14
B cells
BM resident MΦ
Dendritic cells
Endothelial cells
EPC
GMP
Granulocytes
HSPC
Mesenchymal type
Monocytes
Plasma cells
T cells
pDC
C
HSPC
GMP
EPC
BM resident MΦ
Granulocytes
Monocytes
Dendritic cells
B cells
T cells
Plasma cells
pDCs
17823
1291
123451
17894
178923
523
121234
183
1A123
111
E
Mesenchymal type
HSPC
GMP
EPC
BM resident MΦ
Granulocytes
Monocytes
Dendritic cells
B cells
T cells
Plasma cells
pDCs
Endothelial cells
12348
1129
1291
1293
29
12341
1229
II
9A
37
3I

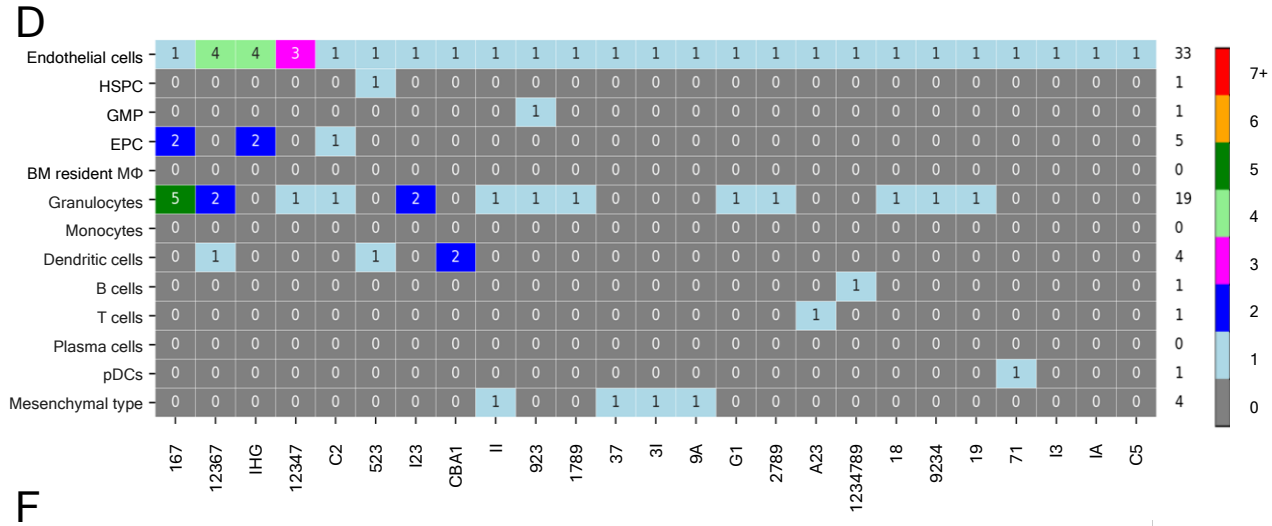
D
Endothelial cells
HSPC
GMP
EPC
BM resident MΦ
Granulocytes
Monocytes
Dendritic cells
B cells
T cells
Plasma cells
pDCs
Mesenchymal type
167
12367
IHG
12347
C2
523
I23
CBA1
II
923
1789
37
3I
9A
G1
2789
A23
1234789
18
9234
19
71
I3
IA
C5

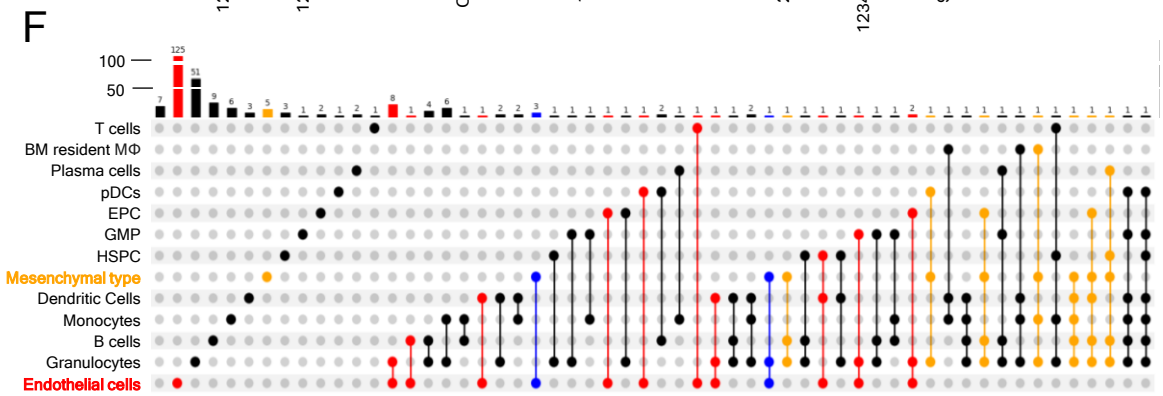
F
T cells
BM resident MΦ
Plasma cells
pDCs
EPC
GMP
HSPC
Mesenchymal type
Dendritic Cells
Monocytes
B cells
Granulocytes
Endothelial cells

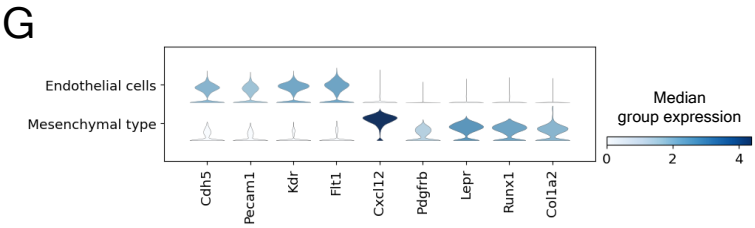
G
Endothelial cells
Mesenchymal type
Cdh5
Pecam1
Kdr
Flt1
Cxcl12
Pdgfrb
Lepr
Runx1
Col1a2
Median group expression
0
2
4

Figure 6

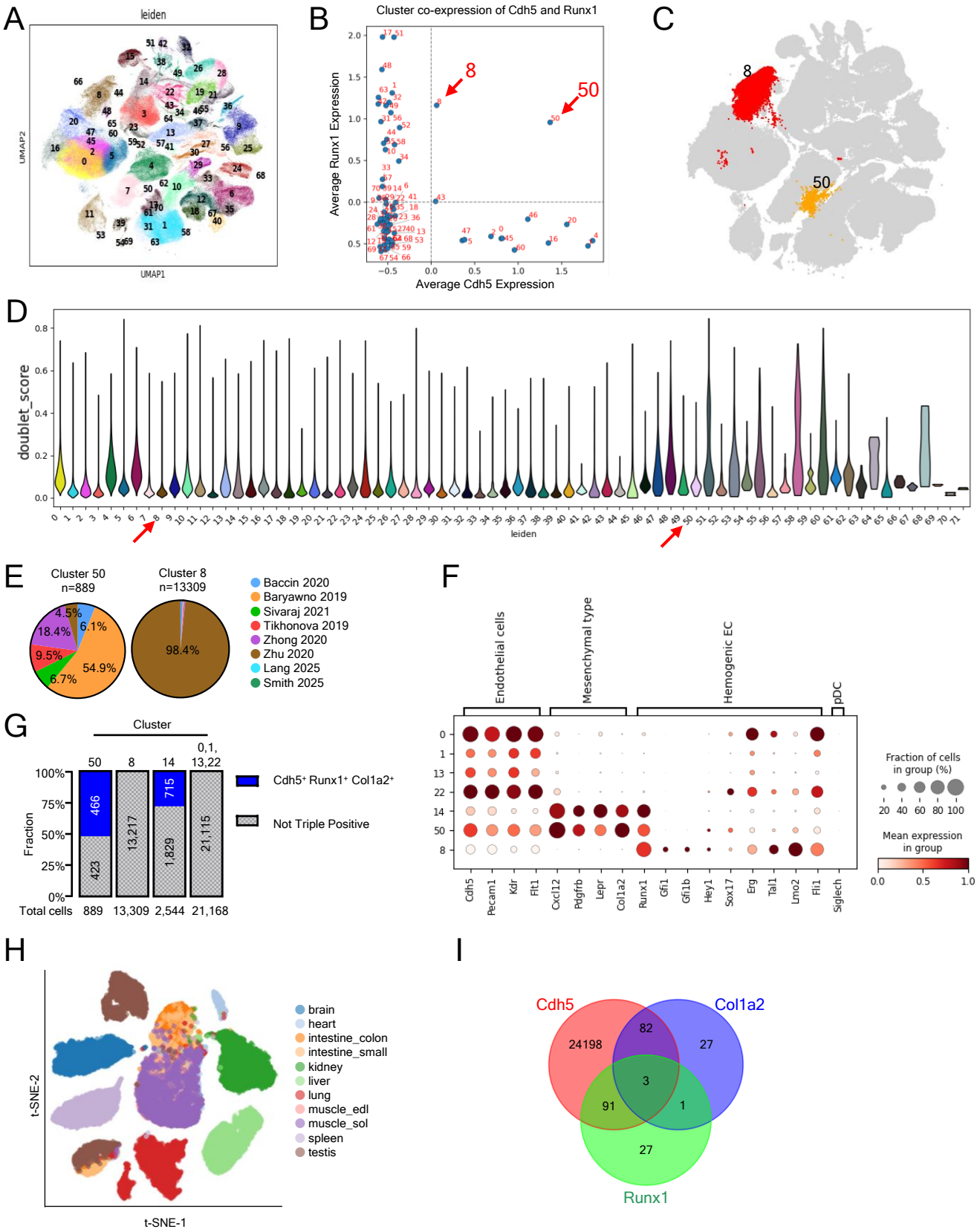
A
leiden
UMAP2
UMAP1
B
Cluster co-expression of Cdh5 and Runx1
Average Runx1 Expression
Average Cdh5 Expression
8
50
C
8
50
D
doublet_score
leiden
E
Cluster 50
n=889
Cluster 8
n=13309
4.5%
6.1%
18.4%
9.5%
54.9%
6.7%
98.4%
Baccin 2020
Baryawno 2019
Sivaraj 2021
Tikhonova 2019
Zhong 2020
Zhu 2020
Lang 2025
Smith 2025
F
Endothelial cells
Mesenchymal type
Hemogenic EC
pDC
Cdh5
Pecam1
Kdr
Flt1
Cxcl12
Pdgfrb
Lepr
Col1a2
Runx1
Gfi1
Gfi1b
Hey1
Sox17
Erg
Tal1
Lmo2
Fli1
Siglech
Fraction of cells in group (%)
Mean expression in group
G
Cluster
50
8
14
0,1, 13,22
Fraction
466
423
13,217
715
1,829
21,115
Cdh5+ Runx1+ Col1a2+
Not Triple Positive
Total cells
889
13,309
2,544
21,168
H
t-SNE-2
t-SNE-1
brain
heart
intestine_colon
intestine_small
kidney
liver
lung
muscle_edl
muscle_sol
spleen
testis
I
Cdh5
Col1a2
Runx1
24198
82
27
3
91
1
27

Figure 7

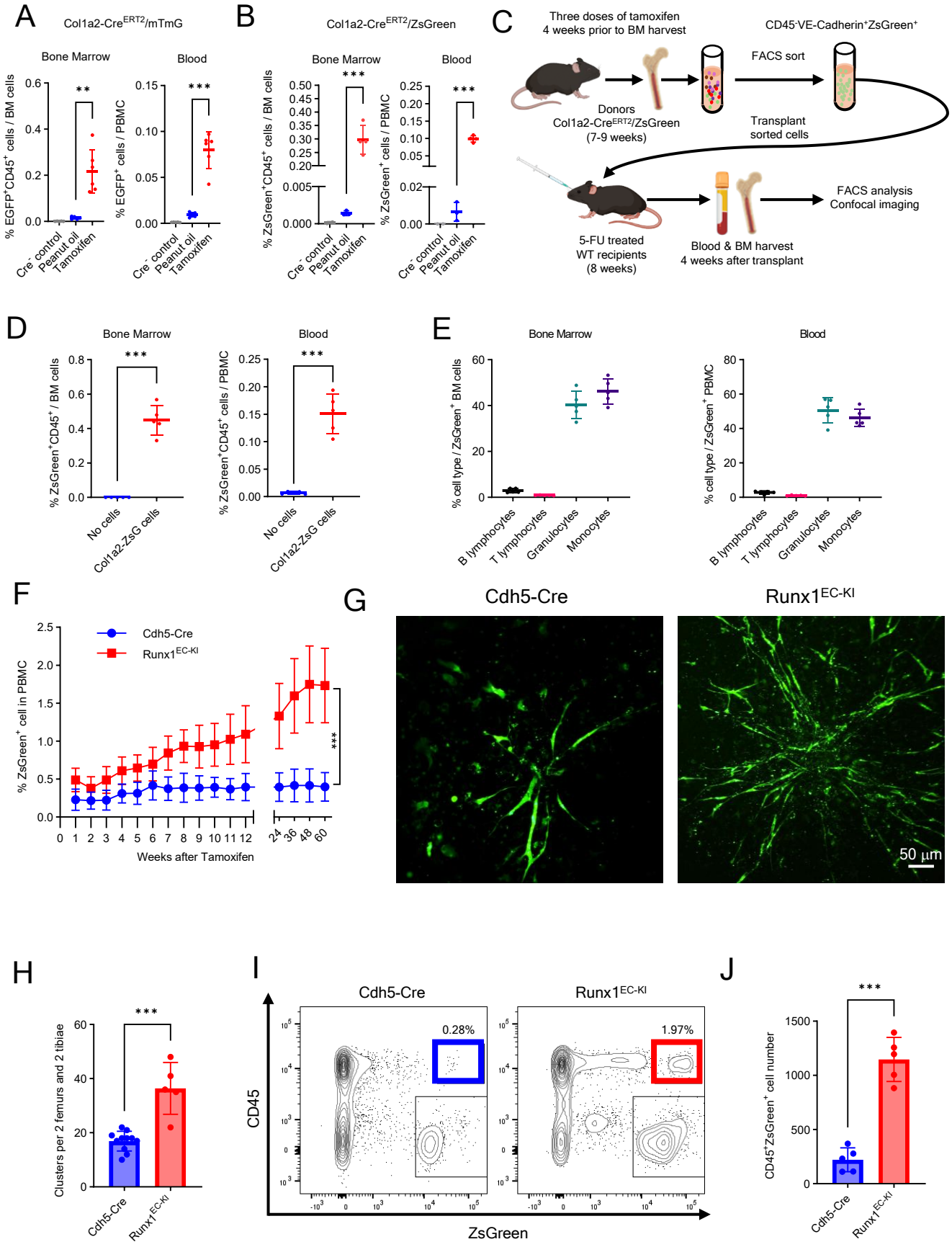
A
Col1a2-CreERT2/mTmG
Bone Marrow
Blood
% EGFP+CD45+ cells / BM cells
% EGFP+ cells / PBMC
Cre- control
Peanut oil
Tamoxifen
B
Col1a2-CreERT2/ZsGreen
% ZsGreen+CD45+ cells / BM cells
% ZsGreen+ cells / PBMC
C
Three doses of tamoxifen
4 weeks prior to BM harvest
CD45-VE-Cadherin+ZsGreen+
FACS sort
Donors
Col1a2-CreERT2/ZsGreen
(7-9 weeks)
Transplant
sorted cells
5-FU treated
WT recipients
(8 weeks)
Blood & BM harvest
4 weeks after transplant
FACS analysis
Confocal imaging
D
% ZsGreen+CD45+ / BM cells
% ZsGreen+CD45+ cells / PBMC
No cells
Col1a2-ZsG cells
E
% cell type / ZsGreen+ BM cells
% cell type / ZsGreen+ PBMC
B lymphocytes
T lymphocytes
Granulocytes
Monocytes
F
Cdh5-Cre
Runx1EC-KI
% ZsGreen+ cell in PBMC
Weeks after Tamoxifen
G
Cdh5-Cre
Runx1EC-KI
50 µm
H
Clusters per 2 femurs and 2 tibiae
I
Cdh5-Cre
Runx1EC-KI
0.28%
1.97%
CD45
ZsGreen
J
CD45+ZsGreen+ cell number

Figure S1

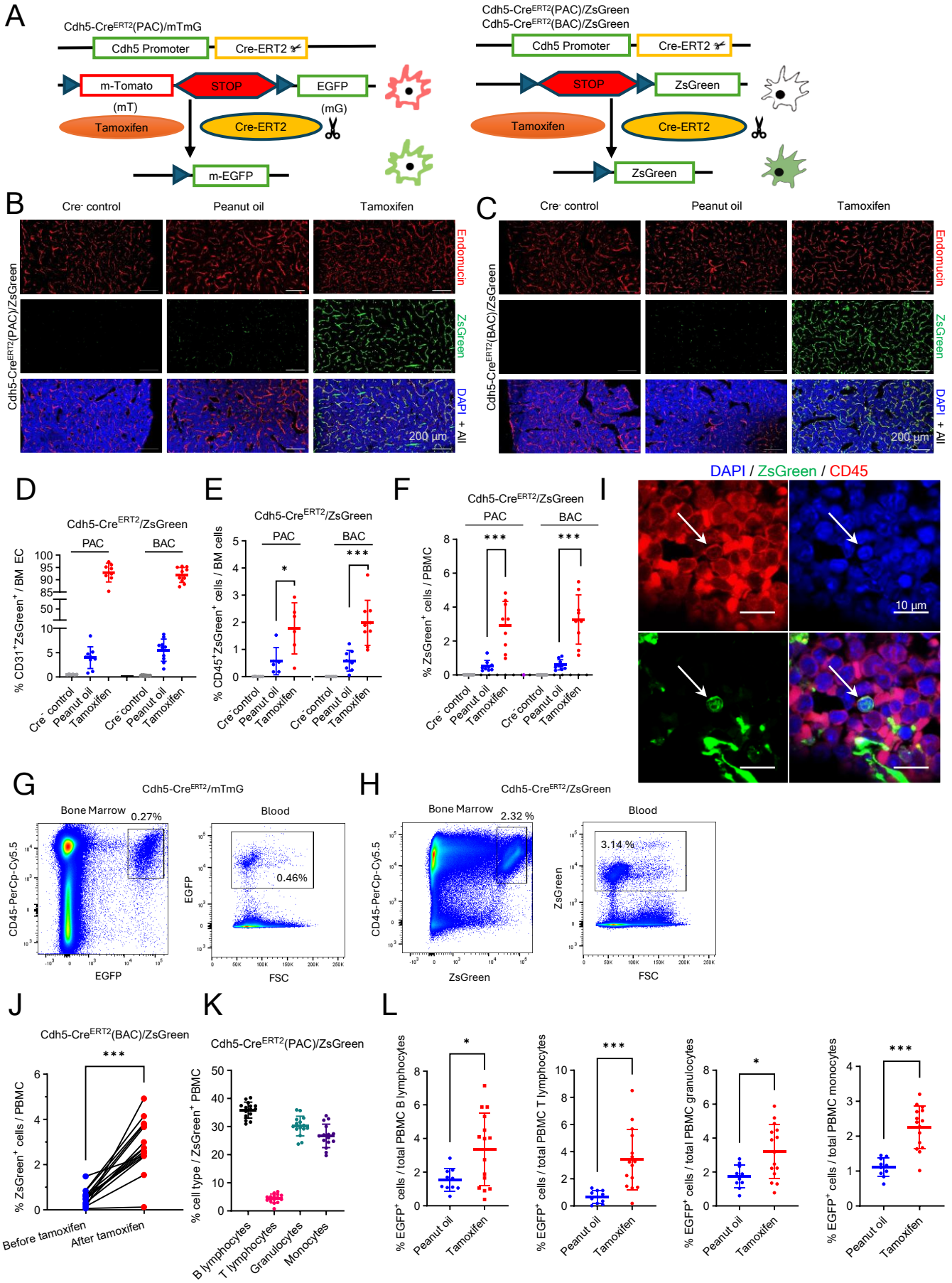
A
Cdh5-CreERT2(PAC)/mTmG
Cdh5 Promoter
Cre-ERT2
m-Tomato
STOP
EGFP
(mT)
(mG)
Tamoxifen
Cre-ERT2
m-EGFP
Cdh5-CreERT2(PAC)/ZsGreen
Cdh5-CreERT2(BAC)/ZsGreen
Cdh5 Promoter
Cre-ERT2
STOP
ZsGreen
Tamoxifen
Cre-ERT2
ZsGreen
B
Cre- control
Peanut oil
Tamoxifen
Cdh5-CreERT2(PAC)/ZsGreen
Endomucin
ZsGreen
DAPI + All
200 µm
C
Cre- control
Peanut oil
Tamoxifen
Cdh5-CreERT2(BAC)/ZsGreen
Endomucin
ZsGreen
DAPI + All
200 µm
D
Cdh5-CreERT2/ZsGreen
PAC
BAC
% CD31+ZsGreen+ / BM EC
Cre- control
Peanut oil
Tamoxifen
E
Cdh5-CreERT2/ZsGreen
PAC
BAC
% CD45+ZsGreen+ cells / BM cells
*
***
Cre- control
Peanut oil
Tamoxifen
F
Cdh5-CreERT2/ZsGreen
PAC
BAC
% ZsGreen+ cells / PBMC
***
***
Cre- control
Peanut oil
Tamoxifen
I
DAPI / ZsGreen / CD45
10 µm
G
Cdh5-CreERT2/mTmG
Bone Marrow
0.27%
CD45-PerCp-Cy5.5
EGFP
Blood
0.46%
EGFP
FSC
H
Cdh5-CreERT2/ZsGreen
Bone Marrow
2.32 %
CD45-PerCp-Cy5.5
ZsGreen
Blood
3.14 %
ZsGreen
FSC
J
Cdh5-CreERT2(BAC)/ZsGreen
***
% ZsGreen+ cells / PBMC
Before tamoxifen
After tamoxifen
K
Cdh5-CreERT2(PAC)/ZsGreen
% cell type / ZsGreen+ PBMC
B lymphocytes
T lymphocytes
Granulocytes
Monocytes
L
% EGFP+ cells / total PBMC B lymphocytes
*
% EGFP+ cells / total PBMC T lymphocytes
***
% EGFP+ cells / total PBMC granulocytes
*
% EGFP+ cells / total PBMC monocytes
***
Peanut oil
Tamoxifen

Figure S2

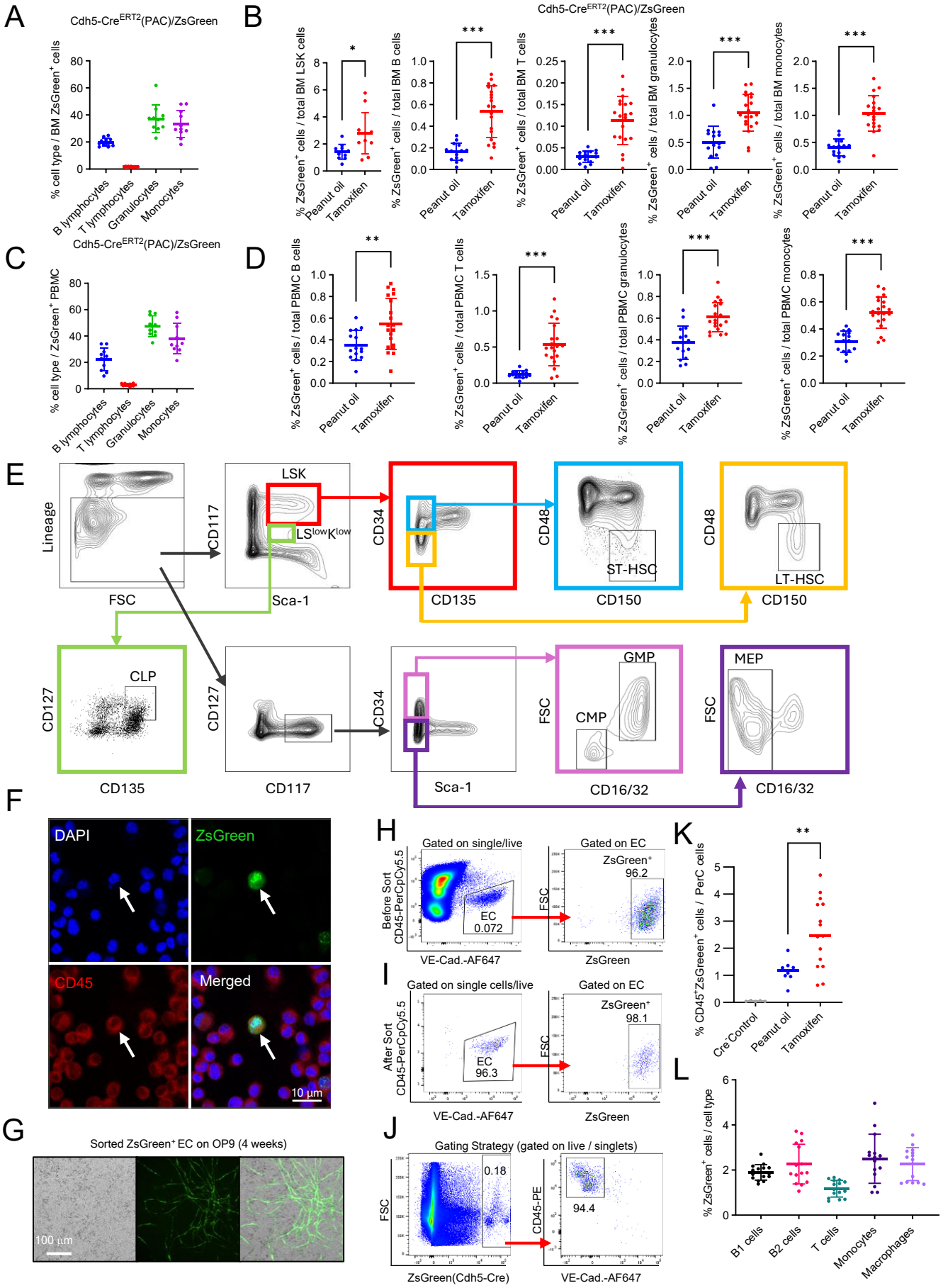
A
Cdh5-CreERT2(PAC)/ZsGreen
% cell type / BM ZsGreen+ cells
B lymphocytes
T lymphocytes
Granulocytes
Monocytes
B
Cdh5-CreERT2(PAC)/ZsGreen
% ZsGreen+ cells / total BM LSK cells
% ZsGreen+ cells / total BM B cells
% ZsGreen+ cells / total BM T cells
% ZsGreen+ cells / total BM granulocytes
% ZsGreen+ cells / total BM monocytes
Peanut oil
Tamoxifen
C
Cdh5-CreERT2(PAC)/ZsGreen
% cell type / ZsGreen+ PBMC
D
% ZsGreen+ cells / total PBMC B cells
% ZsGreen+ cells / total PBMC T cells
% ZsGreen+ cells / total PBMC granulocytes
% ZsGreen+ cells / total PBMC monocytes
E
Lineage
FSC
CD117
LSK
LSlowKlow
Sca-1
CD34
CD135
CD48
ST-HSC
CD150
LT-HSC
CD127
CLP
GMP
CMP
FSC
CD16/32
MEP
F
DAPI
ZsGreen
CD45
Merged
10 µm
G
Sorted ZsGreen+ EC on OP9 (4 weeks)
100 µm
H
Gated on single/live
Before Sort
CD45-PerCpCy5.5
EC
0.072
VE-Cad.-AF647
Gated on EC
ZsGreen+
96.2
ZsGreen
I
Gated on single cells/live
After Sort
EC
96.3
Gated on EC
ZsGreen+
98.1
J
Gating Strategy (gated on live / singlets)
FSC
0.18
ZsGreen(Cdh5-Cre)
CD45-PE
94.4
VE-Cad.-AF647
K
% CD45+ZsGreen+ cells / PerC cells
Cre Control
Peanut oil
Tamoxifen
L
% ZsGreen+ cells / cell type
B1 cells
B2 cells
T cells
Monocytes
Macrophages

Figure S3

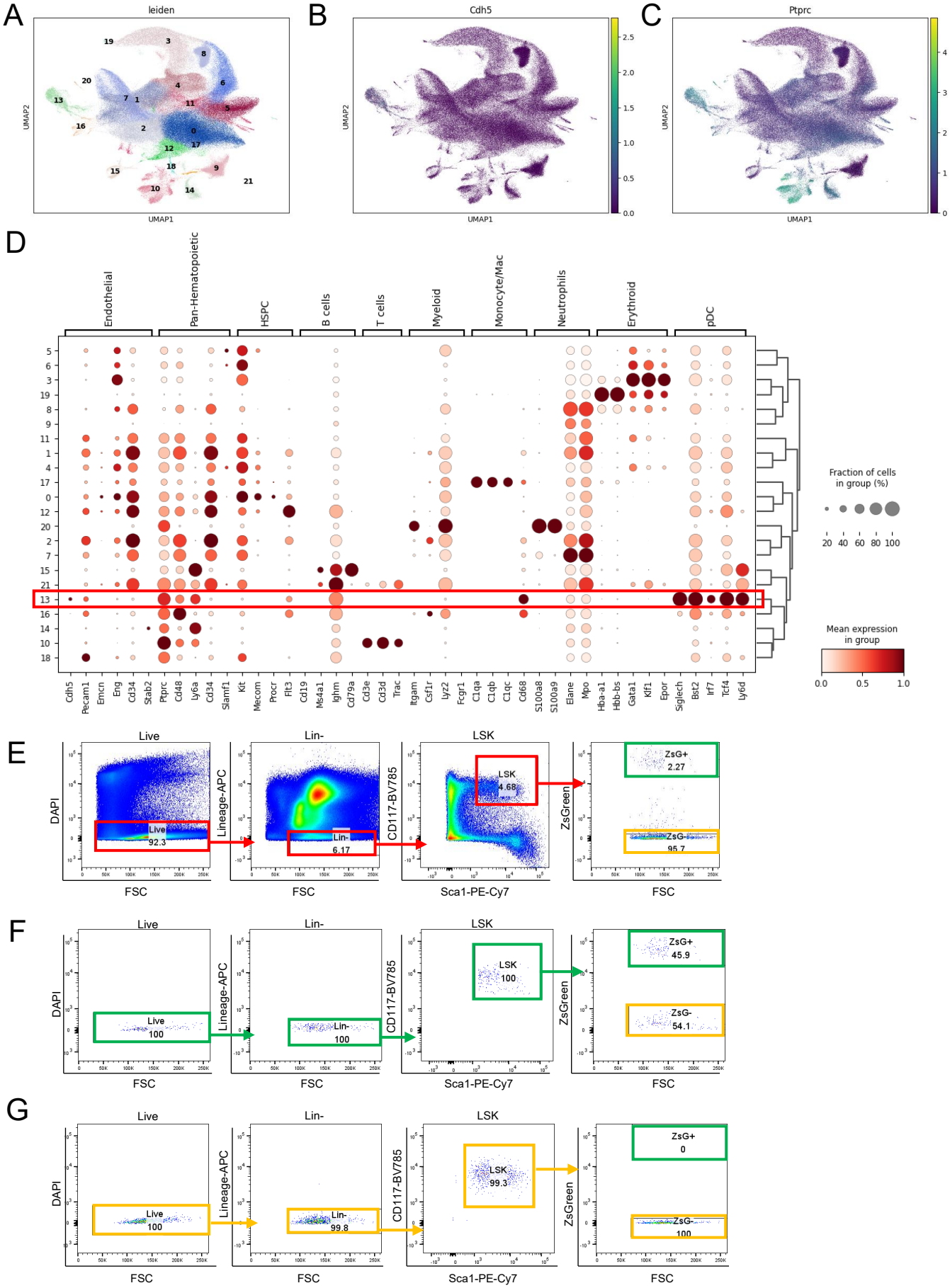
A
leiden
UMAP2
UMAP1
B
Cdh5
C
Ptprc
D
Endothelial
Pan-Hematopoietic
HSPC
B cells
T cells
Myeloid
Monocyte/Mac
Neutrophils
Erythroid
pDC
Cdh5
Pecam1
Emcn
Eng
Cd34
Stab2
Ptprc
Cd48
Ly6a
Cd34
Slamf1
Kit
Mecom
Procr
Flt3
Cd19
Ms4a1
Ighm
Cd79a
Cd3e
Cd3d
Trac
Itgam
Csf1r
Lyz2
Fcgr1
C1qa
C1qb
C1qc
Cd68
S100a8
S100a9
Elane
Mpo
Hba-a1
Hbb-bs
Gata1
Klf1
Epor
Siglech
Bst2
Irf7
Tcf4
Ly6d
Fraction of cells in group (%)
20 40 60 80 100
Mean expression in group
0.0 0.5 1.0
E
Live
Lin-
LSK
DAPI
Lineage-APC
CD117-BV785
ZsGreen
Live 92.3
Lin- 6.17
LSK 4.68
ZsG+ 2.27
ZsG- 95.7
FSC
Sca1-PE-Cy7
F
Live 100
Lin- 100
LSK 100
ZsG+ 45.9
ZsG- 54.1
G
Live 100
Lin- 99.8
LSK 99.3
ZsG+ 0
ZsG- 100

Figure S4

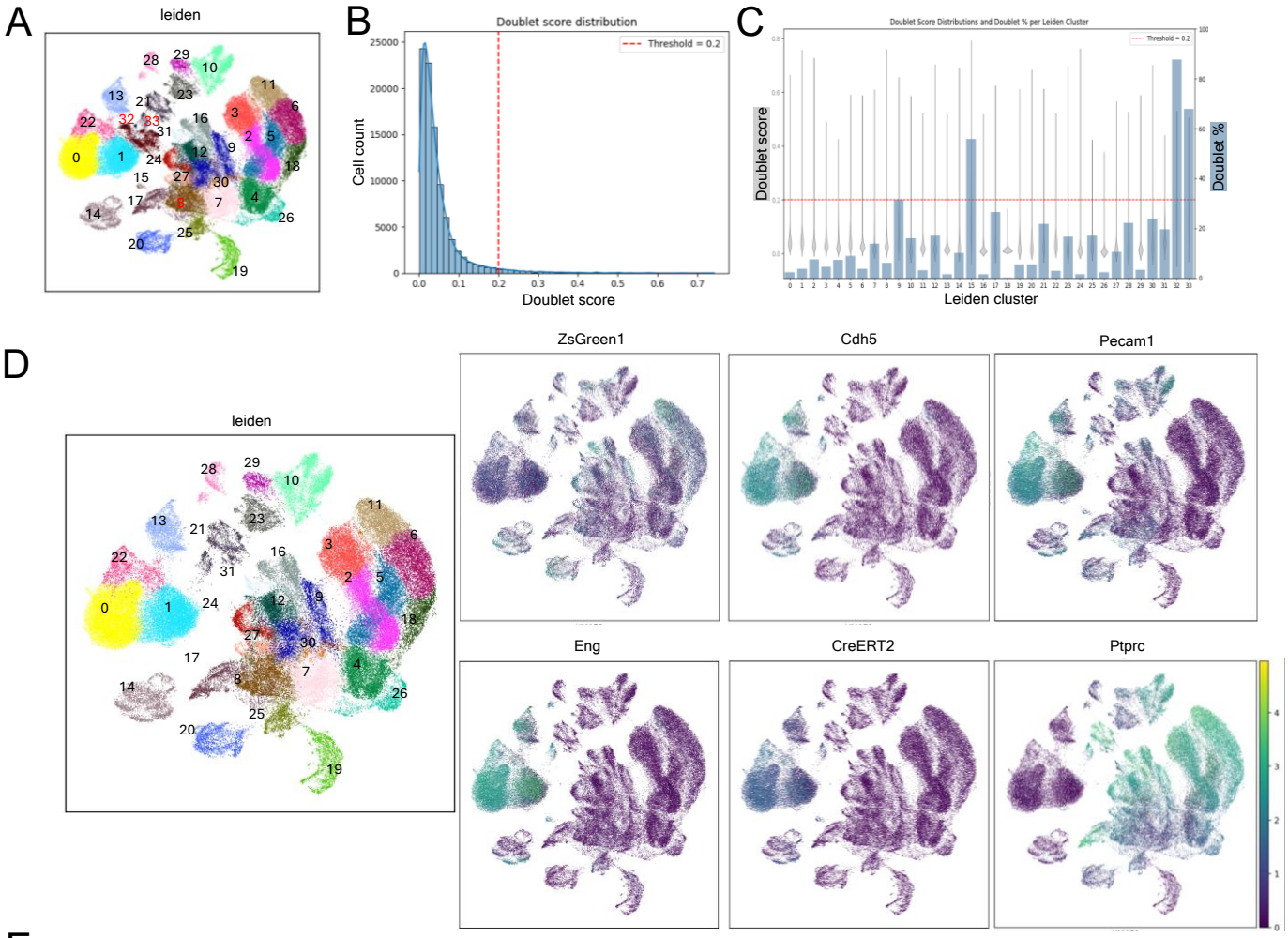
A
leiden
B
Doublet score distribution
Threshold = 0.2
Cell count
Doublet score
C
Doublet Score Distributions and Doublet % per Leiden Cluster
Threshold = 0.2
Doublet score
Doublet %
Leiden cluster
D
leiden
ZsGreen1
Cdh5
Pecam1
Eng
CreERT2
Ptprc

E

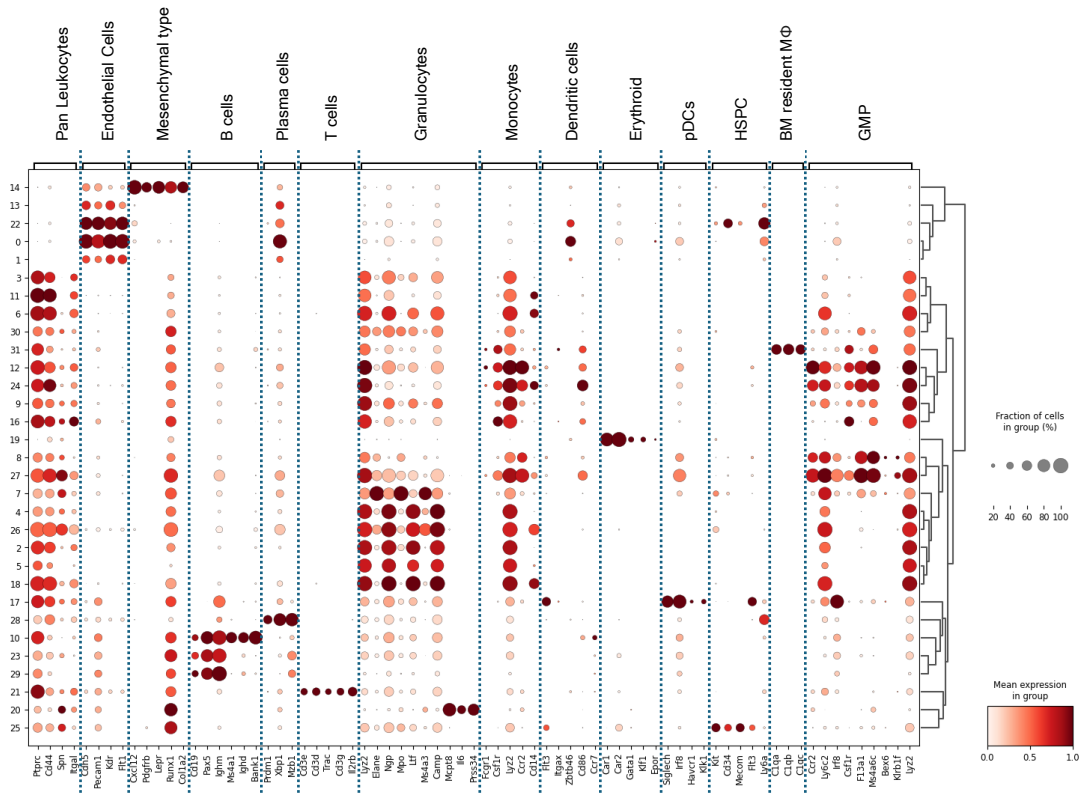
Pan Leukocytes
Endothelial Cells
Mesenchymal type
B cells
Plasma cells
T cells
Granulocytes
Monocytes
Dendritic cells
Erythroid
pDCs
HSPC
BM resident MΦ
GMP
Fraction of cells in group (%)
Mean expression in group

Figure S5

A

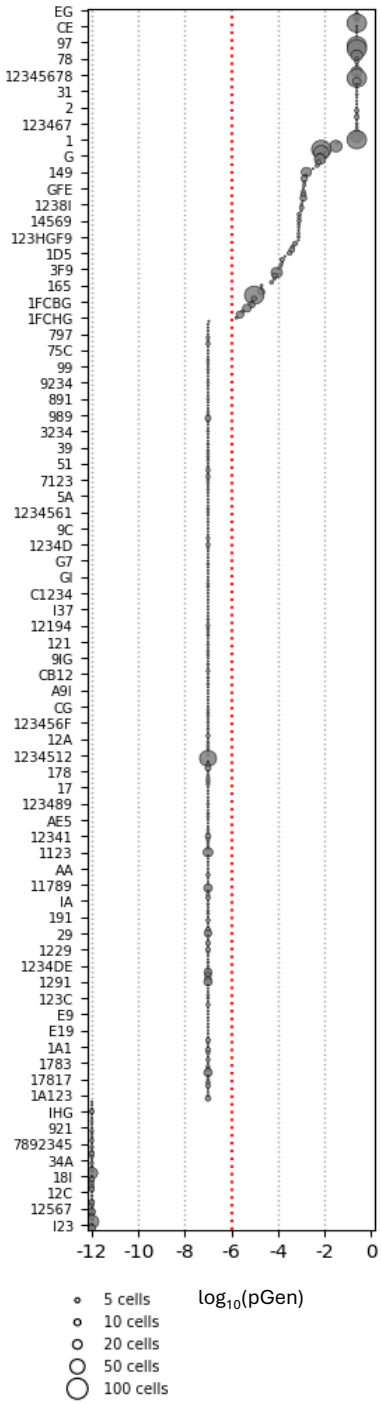

B

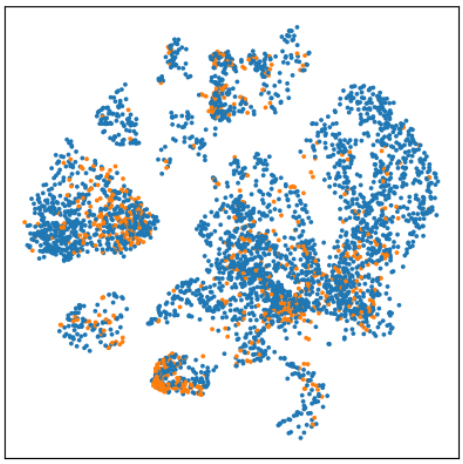

True barcodes: 274 'True' barcodes in 721 cells

Not True barcodes: 125 'Not True' barcodes in 3,348 cells

Total barcodes: 385 in 4,069 cells

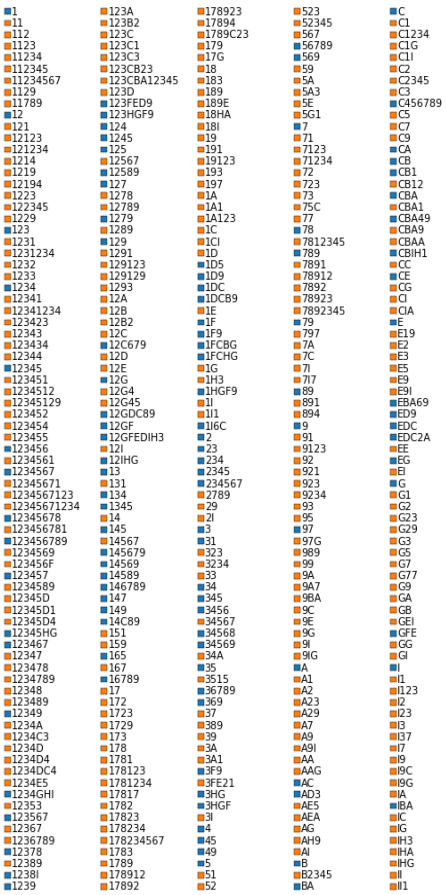

C

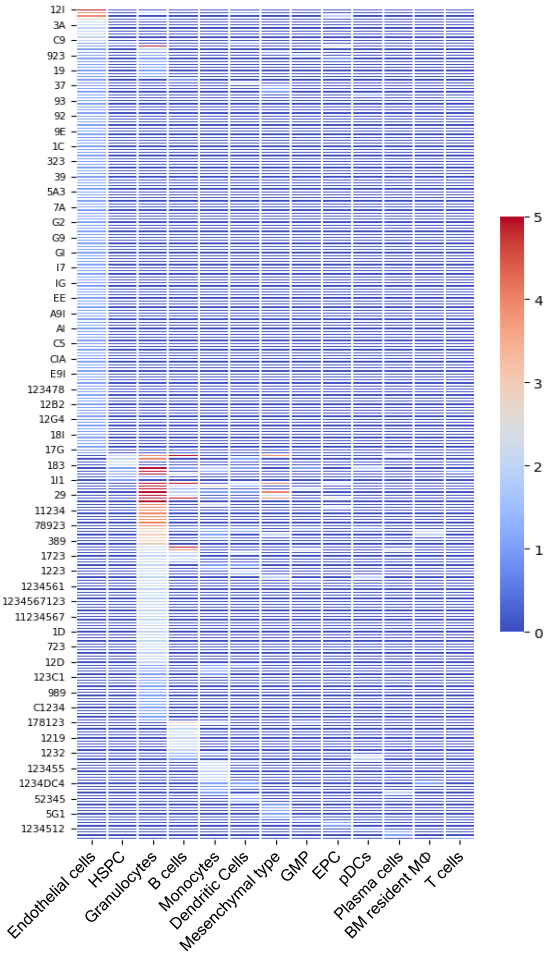

D

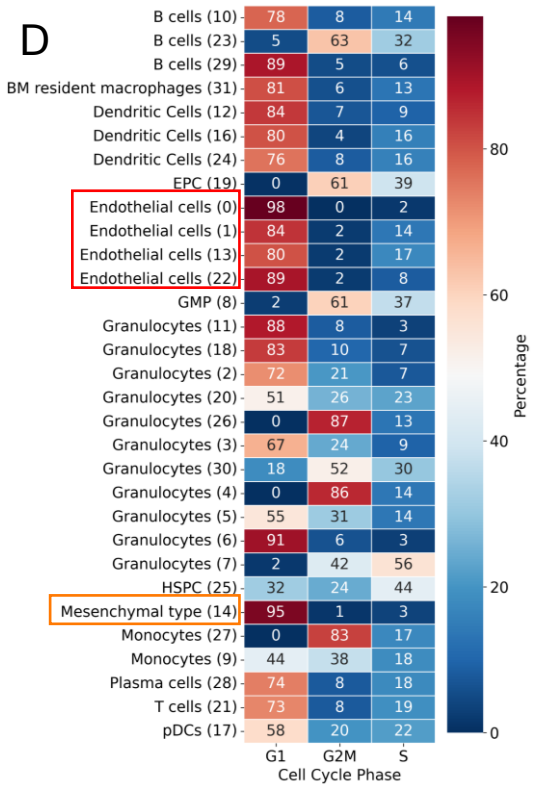

Figure S6

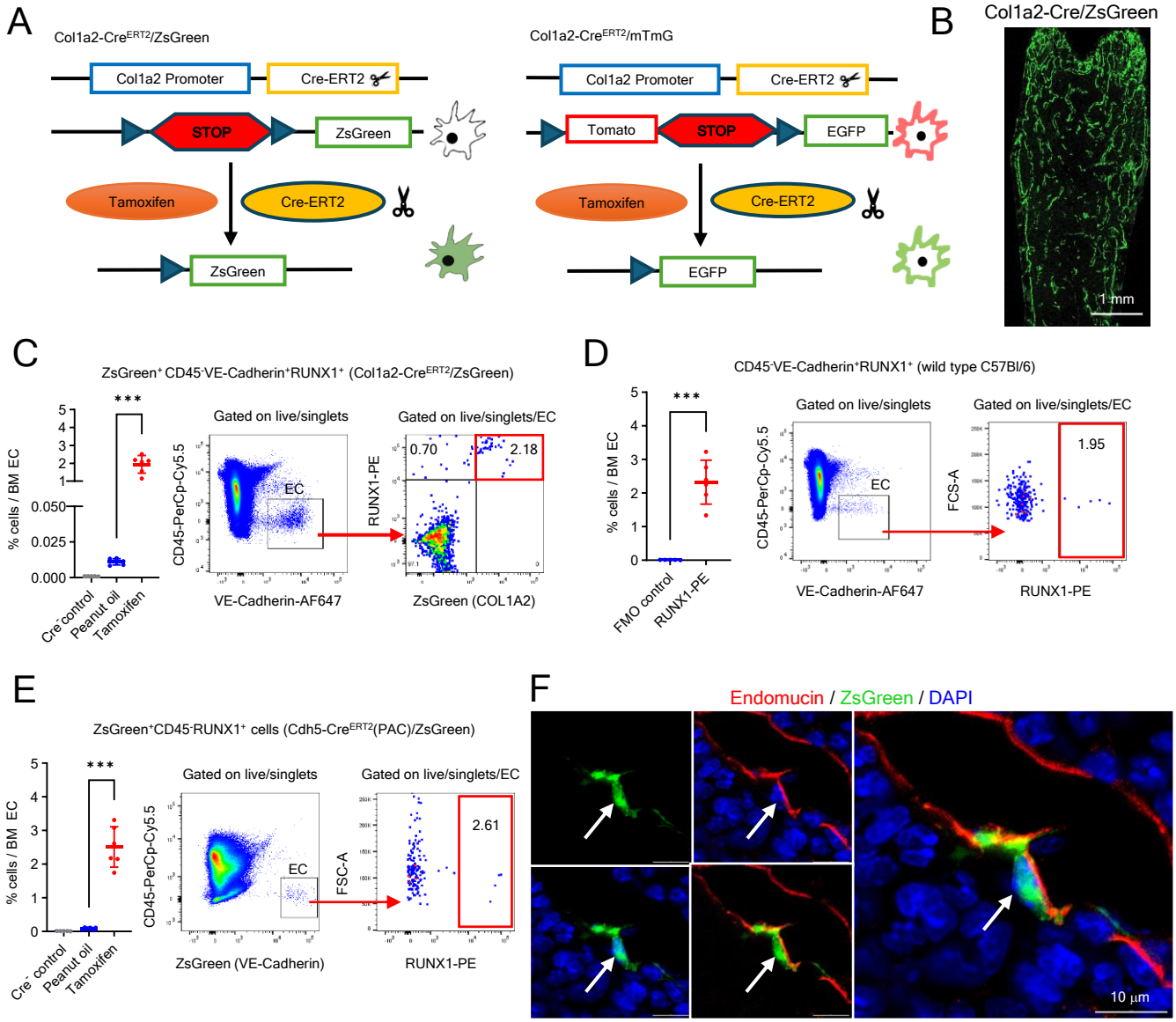
A
Col1a2-CreERT2/ZsGreen
Col1a2 Promoter
Cre-ERT2
STOP
ZsGreen
Tamoxifen
Cre-ERT2
ZsGreen
Col1a2-CreERT2/mTmG
Col1a2 Promoter
Cre-ERT2
Tomato
STOP
EGFP
Tamoxifen
Cre-ERT2
EGFP
B
Col1a2-Cre/ZsGreen
1 mm
C
ZsGreen+ CD45-VE-Cadherin+RUNX1+ (Col1a2-CreERT2/ZsGreen)
% cells / BM EC
***
Cre- control
Peanut oil
Tamoxifen
Gated on live/singlets
CD45-PerCp-Cy5.5
EC
VE-Cadherin-AF647
Gated on live/singlets/EC
RUNX1-PE
0.70
2.18
ZsGreen (COL1A2)
D
CD45-VE-Cadherin+RUNX1+ (wild type C57Bl/6)
% cells / BM EC
***
FMO control
RUNX1-PE
Gated on live/singlets
CD45-PerCp-Cy5.5
EC
VE-Cadherin-AF647
Gated on live/singlets/EC
FCS-A
1.95
RUNX1-PE
E
ZsGreen+CD45-RUNX1+ cells (Cdh5-CreERT2(PAC)/ZsGreen)
% cells / BM EC
***
Cre- control
Peanut oil
Tamoxifen
Gated on live/singlets
CD45-PerCp-Cy5.5
EC
ZsGreen (VE-Cadherin)
Gated on live/singlets/EC
FSC-A
2.61
RUNX1-PE
F
Endomucin / ZsGreen / DAPI
10 µm
G
CD45
DAPI
ZsGreen
Merged
50 µm
H
CD45
DAPI
EGFP
mT (Tomato)
Merged
50 µm

Figure S7

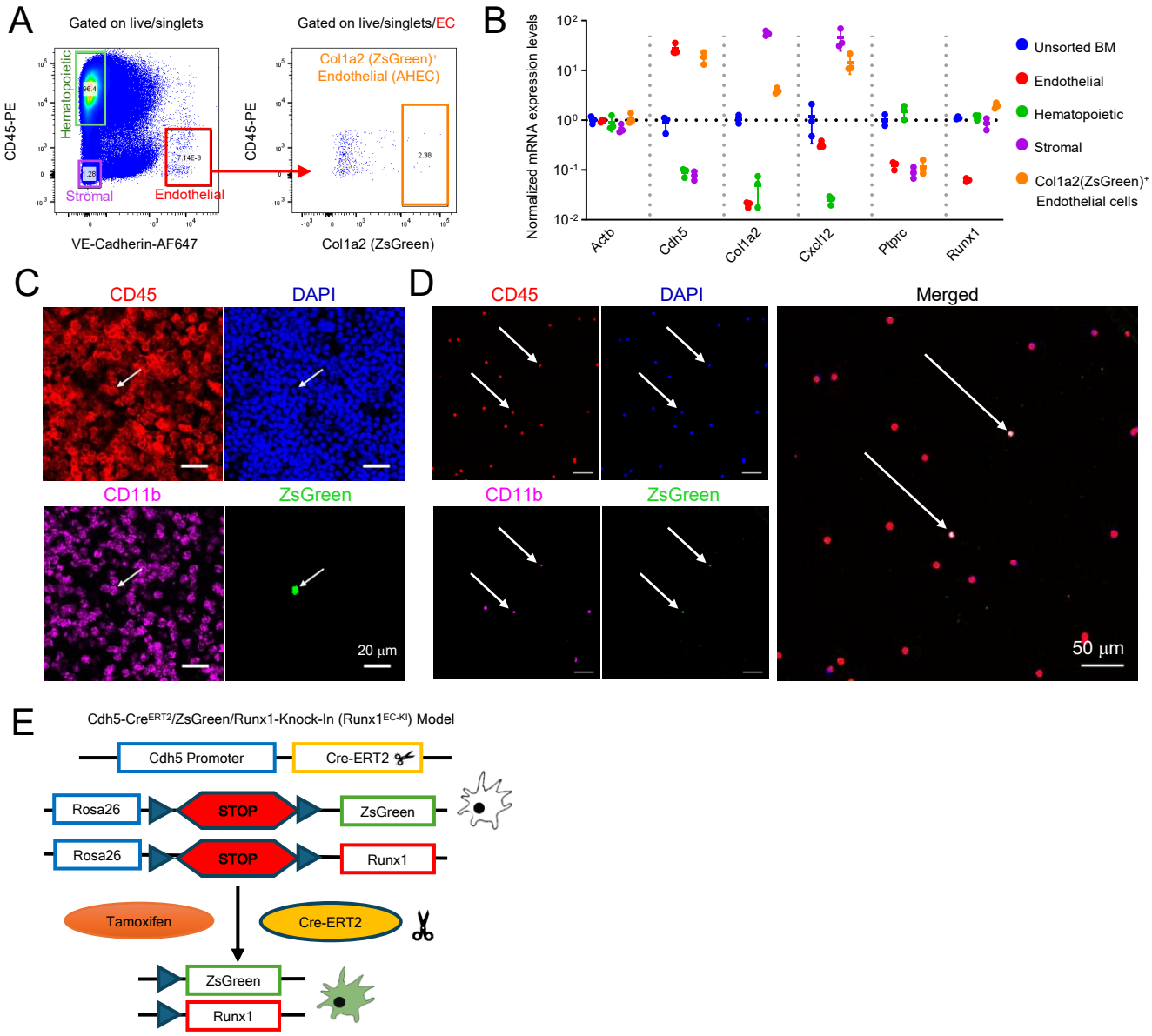
A
Gated on live/singlets
Gated on live/singlets/EC
Hematopoietic
Stromal
Endothelial
CD45-PE
VE-Cadherin-AF647
Col1a2 (ZsGreen)+
Endothelial (AHEC)
Col1a2 (ZsGreen)
B
Normalized mRNA expression levels
Actb
Cdh5
Col1a2
Cxcl12
Ptprc
Runx1
Unsorted BM
Endothelial
Hematopoietic
Stromal
Col1a2(ZsGreen)+
Endothelial cells
C
CD45
DAPI
CD11b
ZsGreen
20 µm
D
CD45
DAPI
Merged
CD11b
ZsGreen
50 µm
E
Cdh5-CreERT2/ZsGreen/Runx1-Knock-In (Runx1EC-KI) Model
Cdh5 Promoter
Cre-ERT2
Rosa26
STOP
ZsGreen
Rosa26
STOP
Runx1
Tamoxifen
Cre-ERT2
ZsGreen
Runx1

Supplemental Figure Legends

Figure S1. Contribution of ECs to hematopoiesis in adult BM is revealed by Cdh5-Cre^{ERT2} mouse tracking lines. Related to Figure 1.

(A) Cdh5-tracking mouse lines. Tamoxifen switches-on green fluorescence in cells that express the Cre-recombinase and their cell progeny.

(B and C) Confocal microscopy images of representative BM sections from Cdh5-Cre^{ERT2}(PAC)/ZsGreen (B) and Cdh5-Cre^{ERT2}(BAC)/ZsGreen (C) adult mice showing tamoxifen-induced ZsGreen fluorescence co-staining of most Endomucin^{+} cells. Control BM sections from representative Cre^{+} mouse treated with peanut oil (no tamoxifen) display occasional ZsGreen^{+}Endomucin^{+} cells but no tamoxifen-independent ZsGreen fluorescence is detected in representative Cre^{-} mice.

(D) Flow cytometry analysis of adult BM cells from Cdh5-Cre^{ERT2}(PAC)/ZsGreen (n = 6-8) and Cdh5-Cre^{ERT2}(BAC)/ZsGreen mice (n = 10) shows that ZsGreen fluorescence identifies most ECs four weeks after tamoxifen administration but also tracks a small proportion of EC expressing tamoxifen-independent fluorescence in Cre^{+} but not Cre^{-} mice.

(E) Percent CD45^{+}ZsGreen^{+} cells of viable BM cells from Cre^{-} control (n=6), Cre^{+} control (peanut-oil treated, no tamoxifen; n= 8) and Cre^{+} tamoxifen-treated Cdh5-Cre^{ERT2}(PAC) /ZsGreen (n=6) or Cdh5-Cre^{ERT2}(BAC)/ZsGreen mice (n=9). Mice were 8 to 12 weeks old at the time of tamoxifen administration.

(F) Percent ZsGreen^{+} cells of PBMC from Cre^{-} control, Cre^{+} control (peanut-oil treated) and Cre^{+} tamoxifen-treated Cdh5-Cre^{ERT2}(PAC)/ZsGreen and Cdh5-Cre^{ERT2}(BAC)/ZsGreen mice (n=9/group). Mice were 8 to 12 weeks old at the time of tamoxifen administration.

23 (G–H) Representative flow cytometry gating of $CD45^+EGFP^+$ cells from BM and blood of Cdh5-
24 CreERT2/mTmG mice (G, relates to Figure 1 C, D), and $CD45^+ZsGreen^+$ cells from BM and
25 blood of Cdh5-Cre^{ERT2}/ZsGreen mice (H, relates to Figure S1 E, F).
26 (I) Representative confocal images showing a nucleated ($DAPI^+$) BM $ZsGreen^+CD45^+$ cell in the
27 BM from a Cdh5-Cre^{ERT2}(PAC)/ZsGreen mouse treated with tamoxifen.
28 (J) Percent $ZsGreen^+$ cells of PBMC in individual Cdh5-Cre^{ERT2}(BAC)/ZsGreen mice before or
29 four weeks after tamoxifen administration. Each dot represents the results from 50-250µl
30 blood/mouse. The lines link results from individual mice (n=15, 8-12 weeks old).
31 (K) Percent B and T-lymphocytes, granulocytes, and monocytes among $EGFP^+$ PBMC of Cre^+
32 tamoxifen-treated Cdh5-Cre^{ERT2}(PAC)/mTmG mice (n=15, 8-12 weeks old).
33 (L) Percent $EGFP^+$ cells in peripheral blood cell populations of Cre^+ peanut oil-treated (n=9) and
34 tamoxifen-treated (n=16) Cdh5-Cre^{ERT2}(PAC)/mTmG mice (8-12 weeks old).
35 Dots represent individual mice. Data are shown as mean ± SD. *$p<0.05$, **$p<0.01$, ***$p < 0.001$
36 by Student's t test.

37 **Figure S2. Characterization of tracked hematopoietic progenitors and mature cells in adult**

38 **BM and peripheral blood of Cdh5-Cre reporter mice. Related to Figure 1, 2, or 3.**

39 (A and B) Percent B lymphocytes, T lymphocytes, granulocytes, and monocytes of all ZsGreen^{+}

40 cells (A) and percent ZsGreen^{+} cells of total BM LSK, B and T-lymphocytes, granulocytes, and

41 monocytes (B). Each dot reflects results from individual mice (1 femur plus 1 tibia combined,

42 n=11); group means ± SD (error bars) are shown by the horizontal lines.

43 (C and D) Percent B lymphocytes, T lymphocytes, granulocytes, and monocytes of all ZsGreen^{+}

44 PBMC in Cdh5-Cre^{ERT2}(PAC)/ZsGreen mice treated with tamoxifen (C, n=10) and percent

45 ZsGreen^{+} cells of peripheral blood B lymphocytes, T lymphocytes, granulocytes, and monocytes

46 in Cdh5-Cre^{ERT2}(PAC)/ZsGreen mice (D) treated with peanut oil (n=15) or tamoxifen (n=20).

47 (E) Gating strategy for identification of HSPC subsets in bone marrow. Representative flow

48 cytometry plots show sequential gating of lineage negative (Lin^{-}) Sca1^{+} cKit^{+} (LSK) cells into

49 long-term hematopoietic stem cells (LT-HSC), short-term hematopoietic stem cells (ST-HSC),

50 multipotent progenitors (MPP), common lymphoid progenitors (CLP), common myeloid

51 progenitors (CMP), megakaryocyte-erythroid progenitors (MEP), and granulocyte-macrophage

52 progenitors (GMP).

53 (F) Representative cytospin image of floating and low-adherent cells from ex vivo culture of BM

54 cells from a tamoxifen-induced Cdh5- Cre^{ERT2}(PAC)/ZsGreen mouse.

55 (G) Representative image (relates to Figure 2B) showing the appearance of sorted ZsGreen^{+} ECs

56 after 4-week culture on OP9 monolayer.

57 (H) Gating strategy for sorting VE-Cadherin^{+} ZsGreen^{+} ECs from the BM of Cdh5-

58 Cre^{ERT2}(PAC)/ZsGreen mice.

59 (I) Purity analysis of sorted VE-Cadherin^{+} ZsGreen^{+} ECs.

60 (J) Gating strategy used for detecting ZsGreen^{+}CD45^{+} hematopoietic cells in WT C57Bl/6

61 recipients of ECs sorted from the BM of Cdh5-Cre^{ERT2}(PAC)/ZsGreen donors.

62 (K) Percent CD45^{+}ZsGreen^{+} cells recovered from the peritoneal cavity (PerC) of Cre^{+}Cdh5-

63 Cre^{ERT2}/ZsGreen mice treated with peanut oil (n=8) or tamoxifen (n=15). Cre^{-} mice (n=5).

64 (L) Percent ZsGreen^{+} cells within PerC cell populations recovered from mice (n=15) under

65 steady-state conditions. Cell type identification; B1 cells: CD19^{+}, CD3^{-}, CD45R(B220)$^{-}$, CD5^{+},

66 CD43^{+}; B2 cells: CD19^{+}, CD3^{-}, CD45R(B220)$^{+}$, CD5^{-}, CD43^{-}; T cells: CD3^{+}, CD11b^{-};

67 monocytes: CD11b^{+}, CD19^{-}, Ly6G^{-}, Ly6C^{high}; neutrophils: CD11b^{+}, CD19^{-}, Ly6G^{+}, Ly6C^{low};

68 and macrophages: CD11b^{+}, CD19^{-}, F4/80^{+}.

69 Dots represent individual mice. Data are shown as mean ± SD. *p<0.05, **p<0.01, ***p < 0.001

70 by Student's t test.

71

72 **Figure S3 BM pDCs, but not other BM hematopoietic cells, express *Cdh5* and *Ptprc*,**

73 **encoding CD45. Related to Figure 4.**

74 (A) UMAP plot showing unsupervised clustering of sc transcriptomic data from a public dataset

75 of mouse BM hematopoietic cells.

76 (B and C) UMAP plots displaying expression of *Cdh5* (B) and *Ptprc* (encoding CD45, C) in the

77 dataset shown in (A).

78 (D) Dot plot illustrating the expression of selected marker genes across clusters shown in (A).

79 The red rectangle highlights gene expression by cluster 13 cells, identifying pDCs. Dot size

80 represents the percentage of cells expressing the gene within each cluster, and color intensity

81 reflects the mean expression level.

82 (E) Gating strategy for selecting ZsGreen^{-} and ZsGreen^{+} LSK progenitors.

83 (F and G) Analysis of purity of sorted LSK populations enriched for ZsGreen^{+} cells (F) and

84 depleted of ZsGreen^{+} cells (G) from the BM of Cdh5-Cre^{ERT2}(PAC)/ZsGreen mice (not treated

85 with tamoxifen).

86

87

88 **Figure S4. Single-cell RNA-seq analysis of BM ZsGreen^{+} cells from tamoxifen-treated**

89 **Cdh5-Cre/ZsGreen/Polylox mice. Related to Figure 5.**

90 **(**A**)** UMAP plot showing unsupervised clustering of sc RNA-seq data, identifying 34 distinct cell

91 clusters within BM ZsGreen^{+} cells.

92 (B) Histogram of doublet score distribution. A threshold of 0.2 was applied to match the

93 expected doublet rate from 10x Genomics Chromium GEM-X chips.

94 (C) Doublet score distribution (gray violin plots, left Y-axis) and corresponding doublet

95 percentages (blue bars, right Y-axis) across Leiden clusters.

96 (D) UMAP plots of clusters after doublet removal, and expression of *ZsGreen1*, *Cdh5*, *Pecam1*,

97 *Eng*, *CreERT2* and *Ptprc* (CD45).

98 (E) Dot plot showing expression of selected marker genes across Leiden clusters identified in

99 (A). Dot size indicates the proportion of cells expressing the gene; color intensity reflects the

100 average expression level of each cluster.

101

102 **Figure S5. Identification and distribution of 'True' Polylox barcodes across cell types.**

103 **Related to Figure 5.**

104 (A) Bubble plot showing individual Polylox barcodes plotted against their corresponding pGen

105 values ($\log_{10}$ scale). The y-axis indicates representative barcodes (one label is shown for every

106 five barcodes). Bubble size reflects the number of cells harboring each barcode. The red dashed

107 line denotes the $\log_{10}(\text{pGen}) = -6$ cutoff, which was used to define true barcodes retained for

108 downstream analyses.

109 (B) UMAP plot showing the distribution of 'True' Polylox barcodes across the 34 Leiden-

110 defined clusters identified in figure S4A. Cells containing 'True' barcodes (n = 721) are shown

111 in orange; cells with 'Not True' barcodes (n = 3,348) are shown in blue. A total of 388 barcodes

112 were detected, including 274 'True' (orange) and 125 'Not True' (blue), as listed below the

113 UMAP plot.

114 (C) Heatmap displaying the distribution and abundance of 'True' Polylox barcodes across

115 annotated cell types. Each row corresponds to a unique barcode (1 out of every 5 barcodes

116 shown); color intensity represents the number of cells carrying that barcode within each listed

117 cell type.

118 (D) Heatmap showing cell cycle phase distribution (G1, G2/M, S) across Leiden clusters

119 identified in figure S4A. Color intensity and numerical values represent the percentage of cells in

120 each phase within the indicated cell type.

121

122 **Figure S6. Characterization of Col1a2-tracked cell populations in BM and blood. Related**

123 **to Figure 7.**

124 (A) Schematic representation of the Col1a2 tracking lines.

125 (B) Representative confocal image of a BM section from a tamoxifen-treated Col1a2-

126 Cre^{ERT2}/ZsGreen mouse, showing widespread distribution of ZsGreen^{+} cells.

127 **(**C to E**)** Flow cytometric identification of RUNX1^{+}VE-Cadherin^{+}CD45^{-} ECs in the BM of

128 peanut oil-treated (n=6) and tamoxifen-treated (n=6) Col1a2-Cre^{ERT2}/ZsGreen adult mice; Cre^{-}

129 mice (n=5) (C); WT C57Bl/6 mice (n= 6) and Fluorescence Minus One (FMO) control (n=5)

130 (D); and Cdh5-Cre^{ERT2}(PAC)/ZsGreen mice treated with peanut oil (n=6) or tamoxifen (n=6);

131 Cre^{-} mice (n=5)(E). Left panels: quantification of cells identified by the indicated gates as a

132 percentage of total BM ECs; each dot represents one mouse (1 femur + 1 tibia). Middle and right

133 panels: representative gating strategies.

134 (F) Representative confocal microscopy image of a BM section from a tamoxifen-treated

135 Col1a2-Cre^{ERT2}/ZsGreen adult mouse showing a ZsGreen^{+} Endomucin^{+} cell lining a vascular

136 structure (white arrows).

137 (G) Representative confocal image of a blood smear from a Col1a2-Cre^{ERT2}/ZsGreen mouse

138 treated with tamoxifen showing the presence of a nucleate CD45^{+} cell tracked by

139 ZsGreen/Col1a2 fluorescence (pointed by the arrow).

140 (H) Representative confocal image of a blood smear from a Col1a2-Cre^{ERT2}/mTmG mouse

141 treated with tamoxifen showing the presence of a nucleated CD45^{+} cell tracked by EGFP/Col1a2

142 fluorescence (pointed by the arrow).

143 Dots represent individual mice. Data are shown as mean ± SD. ***$p < 0.001$ by Student's t test.

144

145 **Figure S7. Analysis and hemogenic potential of Col1a2-tracked adult BM ECs. Related to**

146 **Figure 7.**

147 (A) Representative FACS gating strategy used to isolate BM hematopoietic cells, ECs, stromal

148 cells, and Col1a2-tracked ECs from tamoxifen-treated Col1a2-Cre^{ERT2}/ZsGreen mice.

149 (B) Gene expression profiling of unsorted BM and sorted BM populations defined in (A).

150 Results from qRT-PCR are normalized by *Gapdh* and unsorted BM. Dots reflect experimental

151 triplicates.

152 (C) Representative confocal image of a BM section from a transplant recipient showing a

153 CD45^{+}CD11b^{+}ZsGreen^{+} cell (arrow), indicating hematopoietic derivation from transplanted

154 ZsGreen^{+}VE-Cadherin^{+}CD45^{-} (Col1a2^{+}) cells.

155 (D) Representative image of a blood smear from a WT recipient mouse transplanted with

156 ZsGreen (Col1a2)$^{+}$ BM ECs from Col1a2-Cre^{ERT2}/ZsGreen mice. ZsGreen tracked cells are

157 pointed by the arrows.

158 (E) Schematic diagram of the Cdh5-Cre^{ERT2}/ZsGreen/Runx1-Knock-in (Runx1^{EC-KI}) mouse line

159 used to trace endothelial cells with Runx1 expression induced upon tamoxifen treatment.

160

Supplemental Method

Polylox single-cell lineage tracing and barcode analysis

Polylox single-cell lineage tracing experiments were performed essentially as described previously (Pei et al., 2020), with modifications detailed below.

Mouse treatment and sample collection.
Cdh5-CreERT2/ZsGreen/PolyloxExpress mice were treated with tamoxifen at 10 weeks of age and harvested at 16 weeks of age (approximately 6 weeks post induction). Bone marrow (BM) was collected from three mice (n = 3, 4 long bones from each mouse), separately processed for downstream analyses.

Cell sorting and population mixing.
BM cells were enriched for ZsGreen$^+$ cells by fluorescence-activated cell sorting (FACS). The sorter was set up with 100-micron nozzle, 20psi. Sample rate was set at ~6,000 EPS. Sorting purity was set as 4-way-purity.

Two populations were isolated at >99% purity:
(1) ZsGreen$^+$ VE-Cadherin$^+$ Endomucin$^+$ endothelial cells (ECs), and
(2) ZsGreen$^+$ VE-Cadherin$^-$ Endomucin$^-$ CD45$^+$ hematopoietic cells.

The two sorted populations were mixed at a 1:1 ratio prior to single-cell encapsulation to allow direct comparison of barcode sharing across endothelial and hematopoietic compartments. The six samples from three mice were loaded separately onto 6 different lanes of a 10x GEM-X and processed as individual samples moving forward.

Single-cell capture and sequencing.
A total of 147,446 cells were loaded onto the 10x Genomics Chromium platform, of which 93,553 cells were successfully processed and recovered for single-cell RNA sequencing. Reverse transcription and cDNA amplification were performed according to the manufacturer's protocols. Amplified cDNA was split into two aliquots for parallel transcriptome library preparation and Polylox barcode enrichment.

Transcriptome library preparation and sequencing.
For transcriptome analysis, 25% (10 µL) of the amplified 10x cDNA library was fragmented and processed using Chromium Single Cell 3′ Reagent Kits (v3 and v4). Libraries were sequenced on an Illumina NextSeq 2000 using P3/P4 reagents (28 bp read 1 + 74 bp read 2).

Polylox barcode amplification and long-read sequencing.
Polylox barcodes were enriched from 5–10 ng of amplified 10x cDNA by nested PCR. First-round PCR was performed using primers annealing to the 5′ end of the Polylox cassette and the 10x adaptor sequence, followed by a second round of amplification using internal Polylox primers. PCR products were purified using AMPure beads and used to generate long-read

amplicon libraries, which were sequenced on a PacBio Sequel II platform using SMRTbell library preparation (v3.0).

Barcode recovery and integration with transcriptomes.
Polylox barcodes were extracted using a Snakemake workflow with custom Python scripts (https://github.com/CCRSF-IFX/SF_Polylox-BC). Barcode sequences were linked to single-cell transcriptomes through shared 10x cell indices. A custom mm10 reference genome including ZsGreen1 was used for transcriptome alignment.

Barcode filtering and definition of true barcodes.
Barcode generation probabilities (pGen) were calculated using the published Polylox MATLAB pipeline (https://github.com/hoefer-lab/polylox). "True" barcodes were defined as barcodes with pGen $< 1 \times 10^{-6}$. Using this threshold, 296 true barcodes were retained for downstream lineage analysis.

Clone size and abundance analysis.
Clone sizes and barcode abundances across endothelial, hematopoietic progenitor, mesenchymal-type, and mature blood cell populations were quantified based on the number of cells sharing the same true barcode. These data are visualized as heatmaps (Figure 5C–E) and as intersection plots summarizing barcode sharing across cell types (Figure 5F).

Quality control and downstream analysis.
Doublets were identified using Scrublet, with expected doublet rates estimated based on cell loading numbers. Batch correction was performed using BBKNN. Cell type annotations were assigned based on canonical marker expression and supported by decoupleR, scANVI (ImmGen reference), and CellTypist. All single-cell analyses were performed using Scanpy.

cell_type	Total cells	Cells with barcodes (pGen < 1)	Cells with true barcodes (pGen < 1e-6)	Cells with not true barcodes (1e-6 <= pGen < 1)
B cells	5977	344	73	271
BM resident macrophages	547	18	5	13
Dendritic Cells	6471	235	26	209
Doublets	2607	87	17	70
Endothelial cells	21168	828	169	659
Erythroblasts and erythroid precursors	1809	78	13	65
GMP	3980	121	11	110
Granulocytes	37931	1674	317	1357
HSPC	1257	71	14	57
Mesenchymal type	2544	115	31	84
Monocytes	4840	281	40	241
Plasma cells	824	49	8	41
T cells	1580	52	3	49
pDCs	2018	119	11	108